UNIVERSITÀ DEGLI STUDI DI PARMA

Dottorato di Ricerca in Tecnologie dell'Informazione

XXIII Ciclo

EFFICIENT MULTIHOP WIRELESS COMMUNICATIONS IN VANETS

Coordinatore:

Chiar.mo Prof. Carlo Morandi

Tutor:

Chiar.mo Prof. Gianluigi Ferrari

Dottorando: *Stefano Busanelli*

Gennaio 2011

To my family
For their unconditioned support

Only after knowing the surface of things can one
throw himself into the search for what is underneath
But the surface of things is endless
(Italo Calvino, Palomar)

Contents

List of Figures

List of Tables

Introduction

In the last decades, Intelligent Transportation Systems (ITSs) have attracted the worldwide interest of researchers, automotive companies, and public governments. ITSs promise to hugely improve safety, efficiency and sustainability of our transportation system, by means of a massive introduction of Information Communication Technologies (ICTs). Dedicated Short Range Communications (DSRCs) wireless technologies will be a key component of future ITSs. A vehicle equipped with DSRCs should be able to exchange information with its neighbors, in a totally decentralized and distributed manner, thus yielding to the formation of a Vehicular Ad-hoc NETwork (VANET).

In this thesis, we present a class of innovative multihop broadcast protocols, based on solid mathematical foundations, and tailored for VANETs. Their performance will be extensively analyzed by means of numerical simulations in realistic scenarios, by considering IEEE 802.11b and IEEE 802.11p wireless interfaces. The proposed protocols can be used on a variety of applications, including Vehicle to Vehicle (V2V) communications, distributed data collection, and information dissemination. All these scenarios have been taken into account in this thesis.

After an accurate literature survey and a description of the standards of interest (Chapter 1), this thesis will be structured around the following themes.

- Description of the simulation setup (Chapter 2). In the realm of vehicular communications, the role of numerical simulation is particularly important, due to the extreme difficulty on conducting realistic experiments. In this chapter we present the simulative tools employed during this thesis, discussing their limi-

tations and compliance to the corresponding standards.

- Design of a multihop broadcast protocol for VANETs (Chapter 3). We present an efficient multihop broadcast protocol, denoted as Irresponsible Forwarding (IF), based on the concept of probabilistic forwarding. The IF protocol is extensively evaluated in static V2V scenarios, principally by means of realistic numerical simulations, even if a simple analytical framework has been derived.

- Performance analysis of the IF protocols in mobile scenarios (Chapter 4). In this case we focus on a dissemination application, where a fixed Road Side Unit (RSU) sends its data to the vehicles transiting in its proximity. In particular, we analyze the performance limits of this solution, by means of numerical simulations in realistic mobile environments, comprehensive of highway and urban roads.

- Vehicular decentralized detection of a spatially constant phenomenon (Chapter 5). Nowadays, vehicles are equipped by a large number of sensors, consequently, VANETs can be considered as distributed wireless sensor networks. In this context, we propose a distributed system able to efficiently detect a constant binary phenomenon. The system is composed by a cluster-based distributed detection algorithm, which takes benefit by the presence of an underlying cluster For this reason, we have derived a new protocol, denoted as Cluster-Head Election IF (CHE-IF), for the creation of a cluster-based topology in a VANET. By using this protocol along with a pre-existent detection distributed algorithm, we will able to efficiently monitor a constant binary phenomenon.

- Improvements of the IF protocol (Chapter 6). We present an improved IF protocol, named Silencing Irresponsible Forwarding (SIF), that offers a greater efficiency, without penalizing latency and reliability. In this case, the simulation-based analysis of the protocol performance, is supported by a complete, even if approximated, analytical framework, that offers precious insights about the protocol behavior.

Chapter 1

Literature Analysis and Motivations

1.1 Introduction

In the last decades, Intelligent Transportation Systems (ITSs) have attracted the worldwide interest of researchers, automotive companies, and public governments. ITSs promise to hugely improve safety, efficiency and sustainability of our transportation system, by means of a massive introduction of Information Communication Technologies (ICTs) [1–3]. In order to create an economically sustainable ITS ecosystem, a large number of projects have been conducted by institutions from all around the world [4]. For instance, the Advanced Safety Vehicle (ASV) program in Japan [5], the IntelliDrive project in the United States [6], and, in Europe, the numerous projects coordinated by the Car 2 Car Communications Consortium (C2C-CC) [7], strongly supported by the European Commission [8] and by the European Telecommunications Standards Institute (ETSI) [9].

The future integrated ITSs will be based on vehicles provided by sensorial, cognitive, decision and communication skills. These *smarts* vehicles will be therefore able to perceive the surrounding environment, collecting both public-interest information (e.g., air pollution measurements) or obtaining data needed for the autonomous real-

time management of the vehicle itself [10–13]. In presence of these smartness prerequisites, the vehicles can achieve a higher awareness level, by means of Inter-Vehicular Communications (IVCs), a set of new generation technologies, standards and protocols, that gives networking capabilities to the vehicles. Thanks to IVCs, the smart vehicles can actively cooperate together and exchange relevant information with external entities, for instance, local public authorities, smart grid operators, and road operators.

IVCs can be used by a plethora of services with different exigences, ranging from safety-critical applications [14], with strict latency and reliability requirements, to bandwidth consuming infotainment applications [15, 16]. Hence, does not exist a single technology able to satisfy the needs of a such large spectrum of applications, and a complete IVC system has to rely on multiple technologies at the same time. For this reason, the more important international harmonization effort for IVCs, the Communications Access for Land Mobiles (CALM) [17] family of standards of the International Organization for Standardization (ISO), defines a heterogeneous network architecture. CALM supports many communications technologies, including cellular 2nd Generation (2G), cellular 3rd Generation (3G) [18], satellite, infrared, 5 GHz Dedicated Short Range Communication (DSRC), 60 GHz millimeter-wave, and mobile wireless broadband, such as WiMAX [19].

The DSRCs protocols are certainly the more interesting technology, since they are expressly designated for IVCs and operate within the 5.8-5.9 GHz frequency spectrum, an unlicensed band reserved for vehicular communications in USA, Japan and Europe [4]. The IEEE 802.11p protocol [20] coupled with the IEEE 1609 protocol stack [21], is commonly known as WAVE protocol and it is the *de facto* international DSRC standards and a key component of CALM. The IEEE 802.11p/WAVE technology supports Vehicle-to-Vehicle communications (V2V), where the vehicles are the unique entities involved in the communication process, but also the so-called Vehicle-to-Infrastructure (V2I) and Infrastructure-to-Vehicle (I2V) modes, where at least one of the endpoints of the communication is represented by a fixed Access Point (AP).

DSRCs protocols have been conceived for operate in a decentralized manner without the need of central communication authorities, therefore, the DSRCs nodes

are able to self-organize forming a so-called Vehicular Ad-hoc NETworks (VANETs) [22], a particular type of Mobile Ad-hoc NETworks (MANETs) [23, 24], where the network nodes are vehicles moving in a road infrastructure [4]. Thanks to their decentralized nature, VANETs offer several advantages with respect to traditional centralized approaches (i.e., WiMAX and 2G/3G cellular networks). In particular, they natively support broadcast communications, they work in spatial regions without network coverage (e.g., tunnels), and they exhibit a much smaller latency. One of the peculiarity of VANETs is the co-existence side-to-side of broadcast and unicast transmission techniques. In fact, while in traditional networks the broadcast protocols are typically employed as auxiliary support tools, in VANETs they have a more important role, since they can be used also as data-bearing protocols, even in multihop configurations. For instance, a multihop broadcast protocol fits well the exigences of applications like the diffusion of security-related messages (e.g., warning alerts) or public interest information (e.g., road interruptions).

In this work we present a family of multihop broadcast forwarding protocols suitable for a wide range of VANETs applications, ranging from accident-preventing, to data collection applications. Our protocols can be employed in all the aforementioned scenarios, namely, V2V, I2V and V2I, side to side or in symbiosis with unicast protocols. The proposed protocols were designed in order to conjugate efficiency, reliability and low-latency. Although they can virtually be used with any underlying PHYsical (PHY) and Medium Access Control (MAC) layers, in our opinion the IEEE 802.11 protocol is the ideal choice for deploying VANETs, for several strong reasons. First of all, the IEEE 802.11p protocol is the *de facto* choice for the realization of VANETs all around the world, at least in medium-long term period. Moreover, even if the date of its effective arrival on the market is unpredictable, the IEEE 802.11p protocol has the advantage of being very similar to the pre-existent IEEE 802.11 suite, in particular, with respect to the IEEE 802.11a amendment. Therefore, in the short-term period makes sense deploying a VANETs system based on the traditional IEEE 802.11 standards, especially if we consider the ubiquitous presence of the traditional IEEE 802.11 radio interfaces in residential and commercial buildings, and in every smart mobile device. As a consequence of this choice, the performance of the

proposed broadcast protocols have been extensively analyzed by means of theoretical analysis and numerical simulations performed on top of a IEEE 802.11 protocol stack.

This chapter is structured as follows. In Section 1.2 we introduce the principal characteristics of the IEEE 802.11 standard, since the IEEE 802.11p protocols is defined an amendment of it. The IEEE 802.11p is presented in Section 1.3 together with the IEEE 1609 protocol stack. In Section 1.4, we consider the problem of analyzing, by means of numerical simulations, the performance of routing protocols in VANET, presenting the principal concerns and obstacles, in particular with respect of the problem of modeling the mobility of the vehicles. In Section 1.5, we review the literature related to the role of forwarding protocols in VANETs, in particular with respect to the multihop broadcast protocols. Finally, thanks to the large number of sensors which normally equip the vehicles, VANETs can be naturally considered as a distributed Wireless Sensor Network (WSN), in Section 1.6 we present some techniques which allow to exploit the VANETs as a WSN.

1.2 The IEEE 802.11 Standard

The IEEE 802.11 standard specifies PHY and MAC layer for set up wireless local area networks (WLANs) [25]. Although its first release was published in the far 1997, it is not yet a obsolete technology. In order to accommodate the introduction of new functions the standard has been continuously modified through the release of specific amendments processes. An up-to-date release of the standard aggregating several of these amendments, was released in the 2007 and denoted as IEEE 802.11-2007 [26]. In particular, the *a*, *b*, and *g* amendments were introduced, respectively as the chapter 17, 18, and 19 of [26], while the amendment *e* that has introduced the support for Quality of Service (QoS) at MAC level, has been merged in chapter 9. Two important amendments, IEEE 802.11p [20] and IEEE 802.11n [27], ere released in the last two years and hence, they are not yet included in the standard. The PHY layer aspect that are of interest for our work will be discussed in Subsection 1.2.1, will the relevant MAC layer characteristics will be analyzed in Subsection 1.2.2.

1.2.1 Physical layer

The IEEE 802.11 standard defines several PHY layers differing in terms of modulation format and carrier frequencies [26]. Because of their obsolescence we ignore some of them, namely, the legacy Frequency Hopping Spread Spectrum (FHSS), Direct Sequence Spread Spectrum (DSSS), and InfraRed (IR) modulations, respectively, defined in Chapter 14, 15, and 16 of the standard [26]. We also ignore the IEEE 802.11n amendment [27] that defines an high rate Multiple Input Multiple Output (MIMO) modulation format, because it has not reached yet a sufficient diffusion (especially in handheld devices), and because its distinguish MIMO capabilities are not yet supported by the IEEE 802.11p amendment. We therefore focus on the remaining physical layers, introduced in the amendments *a*, *b*, and *g*.

The IEEE 802.11b amendment (now in the chapter 18 of [26]) has introduced the so-called High Rate Direct Sequence Spread Spectrum (HR/DSSS) modulation, that combines the original DSSS modulation of the legacy standard with a 8-chip Complementary Code Keying (CCK) modulation, providing a maximum data rate of 11 Mbit/s. The IEEE 802.11b defines 14 overlapped channels 22 MHz width centered in the nearby of 2.4 GHz frequency. Being overlapped there is a strong co-channel interference, and therefore the channels cannot be used all together. Thanks to its adaptive rate selection capabilities, a IEEE 802.11b network interface can select the desired data rate among the set $\{1, 2, 5.5, 11\}$ Mbit/s. Obviously, a lower data rate leads to a higher receiver sensitivity, thus allowing to operate in harder channel condition with a lower Signal to Noise Ratio (SNR). As a rule of thumb, downscaling the data rate from 11Mbit/s and 1Mbit/s, allows to improve the sensitivity of approximately 8 dB.

On the opposite hand, the IEEE 802.11a amendment (now in the chapter 17 of [26]) is based on a more robust Orthogonal Frequency Division Multiplexing (OFDM) modulation that offers a greater maximum data rate of 54 Mbit/s. Also in this case, the radio interface can adaptively selects lower data rates, scaling down up to 6 Mbit/s. Differently from IEEE 802.11b, the IEEE 802.11a works in the $[5.2, 5.8]$ GHz frequency band. The number of channels is not fixed since can be used channels of three different size, namely, 5, 10, and 20 MHz. Each channel is sep-

arated into 52 orthogonal sub-carriers. Depending on the modulation scheme each sub-carrier encodes a specific number of bits in each symbol; for example, using the relatively simple Binary Phase Shift Keying (BPSK) modulation scheme, each sub-carrier encodes 1 bit. The signals of all sub-carriers are transformed into the time domain as symbols of fixed length. Subsequent symbols are separated by a guard interval in order to avoid interferences between distinct symbols. The duration of the guard interval is function of the channel bandwidth. In particular, with a channel size equal to, respectively, 5, 10, and 20 MHz, the corresponding guard interval length is equal to 3.2, 1.6, and 0.8 μs.

Finally, the IEEE 802.11g release (now in the chapter 19 of [26]) defines the Extended Rate PHY (ERP), a collection of different PHY partially retro-compatible with the pre-existent modulation formats (especially the HR/DSSS). However, only the ERP-OFDM mode is implemented by almost all the chipset, will the other modulation are not very spread in the market [25]. The ERP-OFDM modulation format is basically a simple transposition of the IEEE 802.11a OFDM modulation in the 2.4 GHz band, with a few minor changes to provide backwards compatibility. It supports the channel bandwidth, data rates and guard intervals of the IEEE 802.11a modulation.

1.2.2 MAC layer

The basic building block of an IEEE 802.11 network is the Basic Service Set (BSS), a group of STAtions (STAs) that can communicate with each other. IEEE 802.11 offers different opportunities to build a BSS, for instance, nodes can form an Independent BSS (IBSS) with no central coordination authority, or, as in environments with infrastructure (i.e., AP) be part of an infrastructure BSS which is identified by an individual identification number.

The IEEE 802.11 standard defines three types of frames, management, control, and data, that share a set of common characteristics. In particular, all the frames include a bit field for frame control, a duration field, several addresses, the frame body and a Frame Control Sequence (FCS) for error detection. Each subtype is derived and adapted from the generic format (i.e., specific fields and data elements are added or

left out).

IEEE 802.11 provides several approaches for medium access control: (i) Point Coordination Function (PCF), that is only applicable if an AP is available; (ii) Distributed Coordination Function (DCF), that can be used also in fully distributed networks; (iii) Hybrid Coordination Function (HCF), defined in the IEEE 802.11e amendment [28]. Within the HCF, there are two methods of channel access, similar to those defined in the legacy 802.11 MAC: HCF Controlled Channel Access (HCCA), and Enhanced Distributed Channel Access (EDCA). In both EDCA and HCCA, every packet has to be assigned to a particular Access Class (AC). In turn, every AC establishes different channel access settings, allowing to assign different priority levels to the packets [4]. Since the PCF and the HCCA mechanism are not of interest in VANETs, in the rest of the section we focus on the DCF mechanism, while greater details about the EDCA mechanism will provided in Section 1.3.

The DCF defines two different channel access mechanisms, both based on a Carrier Sense Multiple Access with Collision Avoidance (CSMA/CA) strategy, that differs for the number of employed control packets:

- the Basic Access;
- the Ready To Send / Clear To Send Access, indicated in the following as "RTS/CTS Access" for sake of conciseness.

Basic Access

The functioning of the Basic Access is represented in Figure 1.1 and is the following. When a STA has a frame ready to be transmitted, its MAC layer invokes the Clear Channel Assessment (CCA) functionality of the PHY layer to determine the status of the channel (e.g., busy or idle). If the channel remains idle for a period of time at least greater than a Distributed InterFrame Space (DIFS), the STA is free to immediately transmit. On the opposite hand, if the wireless medium is busy, the STA shall defer transmission until the medium remains idle for a whole DIFS without interruption. After this period, the STA generates a random backoff period for an additional waiting time before transmitting. The STA transmits when the backoff time reaches

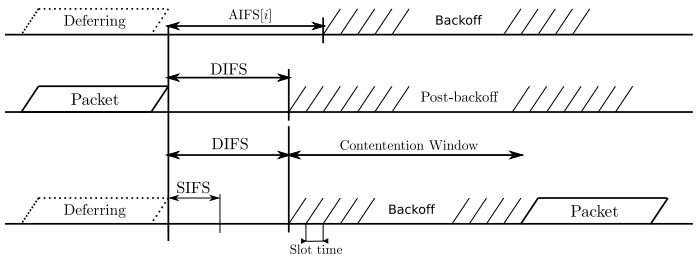

Figure 1.1: Distributed Coordination Function mechanism defined by the IEEE 802.11 standard.

zero. At each transmission, the backoff time is uniformly chosen in the range $[0, \mathrm{CW}]$, where CW is the current backoff window size. The backoff period is slotted and the duration of a backoff slot is defined as T_{SLOT} (dimension: [μs]). The duration of the backoff expressed in terms of number of backoff slots is denoted as Backoff Counter (BC). This number is decremented as long as the medium is sensed idle, and it is frozen when a transmission is detected on the channel. The reactivation can happen when the medium is sensed idle again for more than a DIFS.

In case of unicast transmissions, after a period of time equal to a Short InterFrame Space (SIFS) the destination STA has to send an acknowledgment (ACK) in order to confirm the (hopefully) successful reception of the packet. The SIFS is shorter than the DIFS thus giving a higher priority to the ACK transmission. After the reception of the ACK, the sender STA is forced to begin a backoff period, denoted as *post-backoff*. Otherwise, the sender would "capture" the channel precluding the channel access to the other STAs. So, if another frame is ready for transmission before this post backoff period ends, the STA has to execute it until the end before transmitting the frame. If the original sender does not correctly receive the ACK, and if it has not yet exceed the maximum number of retry, it can re-attempt the packet transmission from the beginning, after having doubled its CW value. We note that the CW is initialized to $\mathrm{CW}_{\mathrm{min}}$, and it cannot never exceed the value $\mathrm{CW}_{\mathrm{max}}$.

In case of a broadcast transmission the use of the ACK is forbidden, determining

a slightly different Basic Access behavior.[1] Without ACKs, the sender cannot known the status of the packet reception at the destination and therefore there are never retransmissions (at least at MAC layer). This leads to several consequences:

- CW is never increased and it is always equal to CW_{min};
- the transmissions are intrinsically less reliable;
- the transmission overhead is smaller.

Because of the less reliable transmissions it is necessary to adopt suitable countermeasures at the upper layers (network and transport).

We finally observe that, when the last received packet by a certain node was corrupted,[2] the DIFS period shall be replaced by a longer Extended IFS (EIFS) period. If we define the duration of a SIFS, DIFS and EIFS, as respectively, T_{SIFS}, T_{DIFS}, and T_{EIFS} (dimension: [μs]), we relationships among them are the following:

$$\begin{aligned} T_{\text{DIFS}} &= T_{\text{SIFS}} + 2T_{\text{SLOT}} \\ T_{\text{EIFS}} &= T_{\text{SIFS}} + T_{\text{DIFS}} + T_{\text{ACK}}, \end{aligned}$$

where T_{ACK} (dimension: [μs]) is the time required to transmit an ACK frame.

RTS/CTS Access

The RTS/CTS Access mechanism envisions two additional control frame, respectively, the Ready To Send (RTS) and the Clear To Send (CTS) packets, introduced for coping with the well known hidden terminal problem that affects MANETs and VANETs. In particular, the exchange of these small size control packets leads to the creation of a second *virtual* contention channel, commonly denoted as Network Allocation Vector (NAV), superposed over the real physical channel. As a consequence of that, the STA can transmit only and only if both the real and the NAV channel

[1] The use of the ACK is forbidden since the ACKs sent by distinct destination nodes will inevitably collide at the original sender.

[2] A received packet is considered corrupted if the corresponding FCS field is wrong.

Table 1.1: Main parameters of IEEE 802.11a and IEEE 802.11b standards.

Parameter	IEEE 802.11b	IEEE 802.11a (20 MHz)
Carrier Frequency [GHz]	2.4	5.8
Bandwidth [MHz]	22	20
OFDM Guard Time [μs]	-	0.8
CW_{min}	31	15
CW_{max}	1023	1023
T_{SLOT} [μs]	20	9
T_{SIFS} [μs]	10	16
Data rates [Mbit/s]	1,2,5.5,11	6, 9, 12, 18, 24, 36, 48, 54

are idle, otherwise it has to defer its transmission. It is important to point out that broadcast transmissions cannot use the RTS/CTS mechanism, for the same reason for which they cannot use ACKs

1.2.3 Main IEEE 802.11 parameters

In Table 1.1 we have summarized the main default parameters defined in [26] for the IEEE 802.11a and IEEE 802.11b standards.

1.3 The WAVE Protocol Stack

The IEEE has realized a totally new protocol stack (commonly denoted as WAVE) that covers the specifics of IVCs: highly dynamic and mobile environment, message transmission in an ad-hoc manner, low latency, and operation in a reserved multi-channel frequency range. As shown in Figure 1.1, WAVE maintains the traditional ISO/OSI protocol stack [29] and is composed a collection of standard, namely, IEEE 802.11p the IEEE 1609 standards family [30]. The latter defines higher layer services, such as system architecture, security, resource management and the communication model [21], while IEEE 802.11p is focused on PHY and MAC layer.

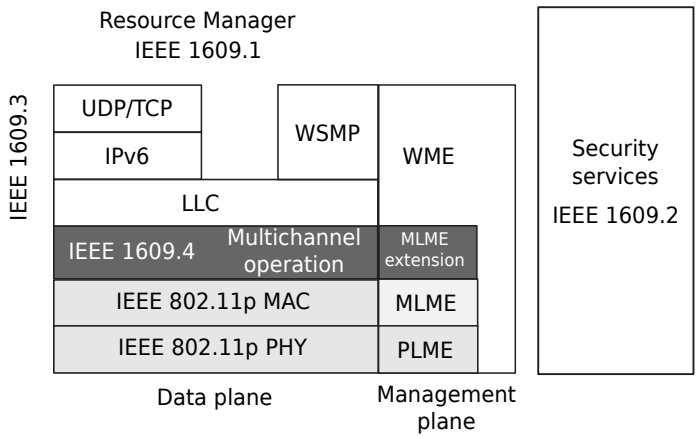

Figure 1.2: Protocol stack jointly defined by the IEEE 1609 and the IEEE 802.11p standards.

IEEE 1609

IEEE 1609 is defined by 4 sub-protocols, with different functions and a different grade of maturity.

More specifically, IEEE 1609.1 is a sufficiently mature standard (it dates 2006) and it basically defines a resource manager [31] acting as an “outsourcing” manager. In other words, it allows to physically separate the applications from the physical radio interfaces, either Road Side Units (RSUs) or On-Board Units (OBUs). For example, an application can run on an external device, such as a smarthphone or a Global Positioning System (GPS) [32] navigator, without adding computational load and complexity to the OBU. This should allow to reduce the cost and increase the reliability of the OBU and RSUs.

The IEEE 1609.2 standard [33] defines security services for the WAVE networking stack and for applications that are intended to run over the stack, such as authentication of STAs and encryption of messages. IEEE 1609.2 provides mechanisms to authenticate WAVE management messages, to authenticate messages that do not require anonymity, and to encrypt messages to a known recipient.

The IEEE 1609.3 defines the networking services for IVCs, but its specifications are still in draft form [34]. The WAVE networking services can be divided into two sets: (i) data-plane services, with data-bearing functions; (ii) management-plane services, charged of the system configuration and maintenance. WAVE supports both two network-layer protocols: (i) the traditional IPv6 routing protocol [35], together with the transport protocols associated with it; (ii) the new WAVE Short Message Protocol (WSMP), expressly designated for accommodate high-priority, time-sensitive communications [30].

The IEEE 1609.4 specification, that is still a draft, defines the organization of multiple channels operations [36], and therefore it has a strong relation to the EDCA mechanism, described in Paragraph 1.3. IEEE 1609.4 envisions the presence of a single Control CHannel (CCH), reserved for system control and safety messages, and up to 6 Service CHannels (SCHs) used to exchange non-safety data packets (e.g., IP traffic) and WAVE-mode Short Messages (WSM). According to the multi-channel operation, all vehicular devices have to monitor the CCH during common time intervals (the CCH intervals), and to (optionally) switch to one SCH during the SCH intervals. The described operation allows the safety warning messages to be transmitted on CCH using the WSM protocol, while non-safety data applications, either running over IP or WSM packets, use the SCHs.

IEEE 802.11p

The IEEE 802.11p standard differs form the existing IEEE 802.11a standard in three main aspects [37]: (i) the definition of BSS; (ii) some details of the PHY; (iii) the MAC layer.

In the WAVE mode, data packets transmission is only allowed to occur within a IBSS, which is established in a fully ad-hoc manner, without any need for active scanning, association or authentication procedures. A node that initiates a IBSS is called provider, while a node that joins a IBSS is called user. To establish a IBSS, the provider has to periodically broadcast on CCH a IBSS announcement message, which includes the WAVE Service Advertisement (WSA). The latter message contains all the information identifying WAVE applications and associated network parameters,

necessary to join a IBSS (e.g., the ID, the SCH index, and timing information). A node should monitor all WSAs on CCH to learn about the existence and the operational parameters of available IBSSs.

The IEEE 802.11p physical layer is an amended version of the IEEE 802.11a specifications, and it is thus based on a OFDM modulation. It mandates the use of 10 MHz channels that offers a greater resistance with respect to the channel delay spread, thanks to its double guard time (1.6 μs). The 10 MHz leads to halved data rates, and the maximum sustainable data rate becomes 27 Mbit/s. We remark that, differently from the IEEE 802.11a whose use was forbidden for several years in Europe, the use of IEEE 802.11p is already allowed since regulated by the ETSI European Standard 202 663 [38].

The IEEE 802.11p MAC layer has the same core mechanism of EDCA introduced in the IEEE 802.11e amendment [28], and already mentioned in Section 1.2. EDCA maintains the distributed approach of the CSMA/CA protocol as in legacy DCF, but introduces four Access Categories (ACs), each one defining a priority level for channel access and having a corresponding transmission queue at the MAC layer. Each AC in the queue behaves like a virtual STA, and it follows its own DCF algorithm, independently contending with the others to obtain the channel access. Each i-th AC has a set of distinct channel access parameters, including Arbitration Inter-Frame Space (AIFS) duration and contention window size ($\mathrm{CW}_{\min}[i]$ and $\mathrm{CW}_{\max}[i]$). The AIFS has the same meaning of DIFS parameter in the DCF algorithm but the different duration, and it is defined as:

$$T_{\mathrm{AIFS}}[i] = T_{\mathrm{SIFS}} + \mathrm{AIFSN[i]} \cdot T_{\mathrm{SLOT}},$$

where AIFSN[i] is an adimensional parameter different for every AC. Clearly, when $\mathrm{AIFSN[i]} = 2$, $T_{\mathrm{AIFS}}[i]$ becomes identical to T_{DIFS}. The amendment [28] has also introduced the possibility of sending a train of consecutive frame by the concept of Transmission Opportunity (TXOP), but this feature is not exploited by the IEEE 802.11p amendment.

In the IEEE 802.11p standard the access mechanism is properly modified to work in the multi-channel WAVE environment, by implementing two separate EDCA func-

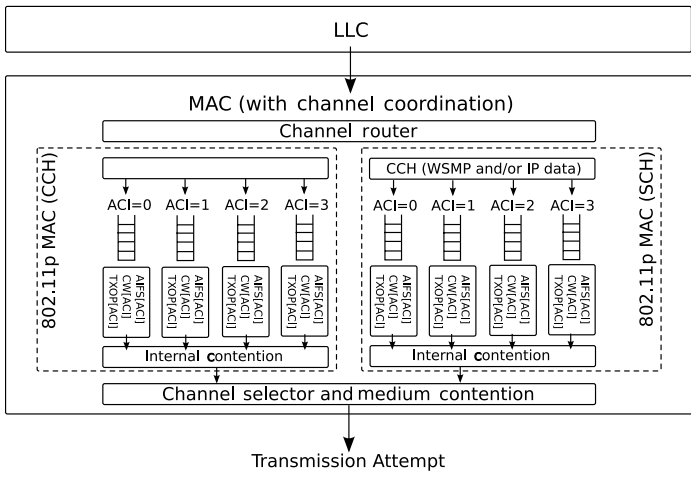

Figure 1.3: Enhanced Distributed Channel Access mechanism defined by the IEEE 802.11p standard.

tions, one for CCH and one for SCH, which handle different sets of queues for packets destined to be transmitted on different channel intervals, as shown by Figure 1.3. In Table 1.2 are summarized the more interesting parameters of the PHY and MAC layers of IEEE 802.11, with the exception of the EDCA parameters that are listed in Table 1.3. From Table 1.3 we observe that IEEE 802.11p uses the same CW_{min} and CW_{max} values of the original IEEE 802.11e specification [28], but slightly modified AIFSN values. While in standard WLAN the AC_VI and AC_VO means, respectively, Video and Voice, in the case of IEEE 802.11p, AC_VI and AC_VO have to interpreted as ACs reserved for prioritized messages (e.g., critical safety warnings).

1.4 Simulative Analysis of VANETs

According to [39] VANET simulation software can be classified into three categories: (a) vehicular mobility generators; (b) network simulators, and (c) VANET simulators. A mobility generator software simulates the dynamic behavior of the vehicles in a given road infrastructure, producing mobility traces containing a sequence of the

Table 1.2: Main parameters of the IEEE 802.11p standard.

Parameter	IEEE 802.11p
Carrier Frequency [GHz]	5.9
Bandwidth [MHz]	10
OFDM Guard Time [μs]	1.6
CW_{min}	See Table 1.3
CW_{max}	1023
T_{SLOT} [μs]	13
T_{SIFS} [μs]	32
Data rates [Mbit/s]	3, 4.5, 6, 9, 12, 18, 24, 27

Table 1.3: EDCA parameters of the IEEE 802.11p standard.

AC	CW_{min}	CW_{max}	AIFSN
AC_BK	15	1023	9
AC_BE	15	1023	6
AC_VI	7	15	3
AC_VO	3	7	2

spatio-temporal coordinates of each vehicle involved in the simulation.

There are several types of mobility generator [40], some are based on measurement campaign of real road traffic, while others are synthetic, in the sense that are generated according to a mathematical model. A partial list of synthetic models includes [41]: (i) stochastic models, the vehicles movement is constrained to the road topology but it is random; (ii) traffic stream models, vehicular mobility is treated as a hydrodynamic phenomenon; (iii) car-following models, the behavior of each driver is computed on the base of the dynamic state of the surrounding vehicles; (iv) flows-interaction models, built upon an instance of one of the previous categories; (v) cellular automata approaches [42]; (vi) behavioral models [43]. According to the results of the extensive analysis conducted on [41], the flows-interaction models based on car-following models represent the best tradeoff between complexity and fidelity to the reality. The car-following models were first employed in the 50's and are continuous-in-time microscopic models, able to determine the behavior of each vehicle on the basis of the states (in terms of position, speed, acceleration) of the surrounding vehicles. A list of mobility generator software comprehends, Simulation of Urban MObility (SUMO) [44], VanetMobiSim [45], FreeSim [46], CityMob [47].

Network simulators perform detailed packet-level simulation of source, destinations, data traffic transmission, reception, background load, route, links, and channels. The mobility traces generated by the mobility generator are provided as input to the network simulator. The principal up-to-date open source software with a large base of user are Network Simulator 2 (ns-2) [48], his successor Network Simulator 3 (ns-3), and OMNeT++ [49].

Finally, the third category, which of VANET simulator, it encompasses software that integrates both the mobility generator and the network simulators, potentially allowing to exchange data bidirectionally between the two components of the simulator. The most representative software in this category are GrooveSim [50], NCTUns [51], Traffic and Network Simulation Environment (TraNS) [52], and the recently released Veins [53].

1.5 Multihop Broadcast Protocol in VANETs

Being a subset of MANETs, the VANETs share a lot of characteristics with them, but VANETs are different in several aspects: (i) the nodes mobility is much higher; (ii) the wireless channel in VANETs has worse propagation condition than MANETs, with more severe fading effects; (iii) the network shape of VANETs can be approximate by a series of nodes lying in the same one-dimensional line [54]. The latter linearity assumption can be motivated as follows. The width of a multi-lane road is much smaller than the transmission range of a IEEE 802.11p radio interface (hundreds of meters), therefore a single road can be modeled as a unidimensional space. Vehicles moving in distinct roads cannot communicate together, with the exception of short temporal windows in correspondence of road junctions. In fact, while in urban scenarios, the presence of buildings inevitable blocks the communication between different roads, in non-urban scenarios roads are typically separated by too large distance with respect to the transmission range of a IEEE 802.11 radio interface.

The purpose of a multihop broadcast protocol is which of delivery a packet from a source to the all the nodes within a certain spatial region. In centralized network such as cellular networks and in low-mobility MANET, the broadcast communications are mostly used for finding the route for a particular set of destinations. On the contrary, in VANETs broadcast protocols play a major role. In this field there are several applications relying on broadcast transmissions. For example, in safety-related applications where the main goal is which of preventing vehicles collisions, the messages are useful only if sent with a latency smaller then 100 ms to all the surrounding vehicles. This result cannot be achieved by traditional unicast and multicast protocols, since because of the high vehicles mobility multicast protocols, they have an extremely elevated overhead [55].

In sparse VANETs, with a few vehicles for kilometer, an effective multihop broadcast protocol can be realized by simply adopting the flooding policy, according with, every network node is a broadcaster. However, the validity of the flooding solutions is limited by the intrinsically broadcast nature of the wireless medium. In fact, in VANETs with a high vehicle density (e.g., dozens of vehicles in the node transmis-

sion range), the flooding approach inevitably leads to numerous contentions and collisions. This phenomenon in known in literature as the broadcast storm problem [56].

In order to increase the effective throughput is necessary to reduce the number of transmissions. This problem has been deeply investigated by the MANET research community, and it is possible to find a theoretical optimal solution. Let model a MANET as a graph $G(V,E)$, whose vertexes represent the nodes of the network. The number of nodes in the network, denoted as N, coincides with the cardinality of the set V, $N = |V|$. An edge between a pair of vertexes marks the existence of a valid wireless link between these nodes. The cost associated with the graph $G(V,E)$ is defined as the number of transmissions needed to reach all the vertexes. It is well known that the so called Minimum Connected Dominant Set (MCDS) of $G(V,E)$, corresponds to the set of nodes guaranteeing the minimum number of transmissions [57]. Given a graph $G(V,E)$, the MCDS problem is to find a minimum connected subset $S \subset V$, in which all elements in $V - S$ are adjacent to at least one node in S. Once defined the MCDS of $G(V,E)$, $N^{\min} = |S|$ is the source belong to the MCDS, or $N^{\min} = |S| + 1$ on the opposite case [58]. In bi-dimensional network topology, the MCDS is a NP-complete problem, only solvable in a polynomial time by adopting some approximations [57–59]. In one-dimensional network, as in VANETs, the MCDS is a significantly easier task that can be accomplished by simply selecting the last reachable node at every hop. However, because of their high mobility, in VANETs the MCDS solution remains valid for a short time and it cannot be efficiently exploited.

As a consequence of that, VANETs broadcast protocols, with the exception of some cluster-based approaches [60,61], typically act in a distributed manner, without keeping trace of the network state. There are a multitude of multihop broadcast protocols, based on different techniques, but with the common goal of selecting a single node in every transmission domain, ideally the furthest from the previous transmitter.

In [56, 62], the authors have proposed several distributed and simple protocols, known as counter-based, distance-based, and location-based, where the node compares an adaptively set threshold with the corresponding local information (number of packet receptions, distance, or position). Among them, the location-based protocols is resulted to be effective and reliable. The position-based broadcast protocols

(see [63] and references therein), are a class of protocol exploiting the knowledge of some geographical characteristics of the network, to improve the retransmission efficiency. For example, the Geographic Random Forwarding (GeRaF) [64] protocol takes advantage of the knowledge of the positions of source and destination, while the Emergency Message Dissemination for Vehicular environments (EMDV) protocol [65] achieves remarkable performance by using both geographical information and information concerning the local network topology. However, position-based protocols have a major shortcoming, the need of having information about the network topology and the geographical characteristics of the environment where the nodes are located [65], that have to be obtained by periodic beacon messages. The EMDV protocol obtains the best results when it can effectively to elect a pre-designated node forwarder node, while in other cases he acts as a distance-based IEEE 802.11 protocol, that has been demonstrated to be suboptimal [22].

Since collecting this kind of information may be very expensive in terms of overhead, several probabilistic broadcast protocols have been recently proposed with the goal of achieving the same performance level of position-based protocols without the need for major information exchange [66–71]. These protocols are designed around the idea that each node forwards the packet with a certain probability $p < 1$, computed according to local information a-priori owned by the node, or inserted in the packet itself. An entire class of probabilistic protocols was proposed and analyzed in [54].

Besides the probabilistic-approaches, there are other solutions allowing to have good performance without the exigence of exchange auxiliary messages. An efficient IEEE 802.11-based protocol, denoted as Urban Multihop Broadcast (UMB), was proposed in [22] and further extended in [72]. The main contribution of UWB is which of suppressing the broadcast redundancy by means of a black-burst (channel jamming signal) contention approach [73], followed by a RTS/CTS-like mechanism. According to this protocol, a node can broadcast a packet only after having got the channel control. In particular, the transmission range of the source is partitioned in distinct region. Each region is associated to a different duration of the jamming periods, and this allows to select a single node. The UMB approach can effectively obtain a high

penetration rate, but at the price of a high latency [74].

A different approach is adopted by another 802.11-based protocol, the Smart Broadcast (SB) protocol proposed in [74]. Similarly to UMB, SB partitions the transmission range of the source, associating non-overlapping contention windows to different regions. Moreover, it uses a RTS/CTS-like mechanism for selecting the forwarders. Albeit these similarities, the main goal of SB is the minimization of the time to perform a hop. For this reason it does not necessarily select the relay in the region that provides the largest progress, and it does not spend time to resolve collisions. For this reason SB has worse penetration than UMB but a much smaller latency [74].

Finally, the Binary Partition Assisted Protocol (BPAB) [75] takes concepts from both UMB and SB, and it denotes therefore similar performance, while the authors shown a performance gain with respect to the SB protocols, in low-density and irregular topologies.

1.6 VANETs as a Distributed Wireless Sensor Network

An overview of vehicular sensor network technologies and trends has been recently carried out in [76], where vehicles continuously gather, process, and share location-relevant sensor data (e.g., road condition, traffic flow). The information collection and dissemination can be performed using IVCs [11, 77] as well relying on the presence of the infrastructures [78]. The increasing popularity of smartphones, with onboard sensor capabilities and Internet data connections (e.g., 3G cellular networks), is another key factor for rapid development of vehicular technologies. In [79], the problem of monitoring road and traffic conditions in a city is taken into account and a novel system, called Nericell, is presented. In particular, Nericell is based on sensing by piggybacking on smartphones carried by users and its effectiveness is evaluated on the basis of experiments conducted on the roads of Bangalore, India. In order to satisfy the requirements of the aforementioned applications, several authors have proposed broadcast transmission techniques, but the design of an efficient and reliable broadcasting forwarding protocol is not an easy challenge [55]. From pioneering works, such as [80], cluster-based networks have found a fertile application ground in the

field of wireless sensor networking, since they allow to reduce network congestion, to increase the spectral efficiency, to simplify routing issues, data aggregation, and dissemination. Data aggregation and decentralized detection aim to detect, through a sensor network, a physical event of interest in an energy-efficient manner [81]. The advantages of clustering have also been exploited in the realm of decentralized detection [82, 83], e.g., to determine optimum clustering and MAC configurations. In particular, in [82] the authors provide a generic framework for the computation of the probability of decision error when a spatially constant binary phenomenon is detected through a (possibly) multi-level sensor network.

One of the strongest motivation for the design of cluster-based vehicular networks is provided by [41], where the authors show that, according to realistic mobility models, VANETs naturally evolve to clustered configurations. Among the more recent cluster-based protocol proposed in VANETs, some interesting approaches can be found in [60, 61]. In the latter work, communications are typically broadcast but, when possible, short-lived clusters are created in order to constitute a backbone. It is then possible to employ unicast communications among the nodes of the backbone, leading to a higher reliability without sacrificing network performance.

In [84], the authors derive an innovative broadcasting technique, which integrates the probabilistic approach of a previously proposed protocol (denoted as Irresponsible Forwarding, IF) with a cluster-based structure, in order to improve its performance. This new protocol is referred to as Cluster-based Irresponsible Forwarding (CIF). The key characteristics of CIF is that a clustered structure is not imposed. Rather, CIF opportunistically exploits the “ephemeral” clusters which appear in a VANET. In this work, we present a slightly modified version of CIF, denoted as Cluster-Head Election IF (CHE-IF), well suited for efficient data dissemination with cluster-head (CH) election.

Chapter 2

VANETs Simulative Tools

The best material model of a cat is another, or preferably the same, cat.

– Norbert Wiener

2.1 Introduction

According to the analysis carried out in Section 1.4, there are two different ways for studying VANETs by means of numerical simulations: (i) using two distinct pieces of software, one generating the mobility traces and the second performing the effective network simulation; (ii) using an integrated *VANET simulator* performing both the tasks at the same time and therefore providing a bidirectional coupling between the network simulator and the mobility generator. The second solution is certainly the most powerful and attracting, but it is really useful only for testing complete applications and services, where the vehicles react consequently to the reception of significant information. For instance, the path followed by the vehicles can be determined by a shortest path algorithm periodically executed on the basis of the effectively received information. In our case, we are not interested in studying applications but forwarding protocols, and for this reason we have selected the simpler solution: us-

ing a mobility generator for produce mobility traces and using them in the network simulator.

As a network simulator we have chosen Network Simulator 2 (ns-2) [48], a discrete event simulator developed by the VINT project research group at the University of California at Berkeley [85]. Our choice was motivated by the following considerations:

- ns-2 is one of the most widespread software among MANETs/VANETs researchers;
- it natively implements the IEEE 802.11p protocol (since version 2.33);
- it can be easily integrated with several mobility generator software;
- it is an open-source software already used in our laboratory.

On the other hand, ns-2 has also several well-known shortcomings: (i) it offers a scarce support for VANETs, since it does not allow to define real vehicular scenario, comprehensive of roads and obstacles; (ii) the source code of ns-2 is not well written and its complex structure slows down the development process and facilitates the insertion of unwanted bugs; (iii) the IEEE 802.11 implementation is not perfectly compliant to the standard [86, 87], leading to the proliferation of patches not always coherent with respect to each other. Our simulations were conducted using the latest release of the ns-2 simulator, namely the 2.34 [48].

For which concerns the mobility generators software, we have selected two open-source software, namely, VanetMobiSim [45] and SUMO [44], both able to generate mobility traces compatible with ns-2, and supporting flows-interaction mobility models derived from car-following models.

VanetMobiSim [45] is an extension of the CANU Mobility Simulation Environment (CanuMobiSim) [88] which focuses on vehicular mobility, and features realistic automotive motion models at both macroscopic and microscopic levels. At the macroscopic level, VanetMobiSim can import maps from suitable databases, or randomly generate them using tessellation. At the microscopic level, it supports mobil-

ity models derived from the Intelligent Driving Model (IDM), a car-following model originally introduced here [89].

SUMO [44] is an open source, highly portable, microscopic road traffic simulation package designed to handle large road networks. Its main features include collision free vehicle movement, different vehicle types, single-vehicle routing, multi-lane streets with lane changing, junction-based right-of-way rules, hierarchy of junction types,and dynamic routing [40].

In Section 2.2 we describe the mobility models implemented in SUMO and VanetMobiSim. In Section 2.3 we first present the problem of the statistical characterization of the property wireless channel in VANET. Then we briefly analyze the channel available in ns-2, motivating our choice of using a deterministic channel. In Section 2.4 we discuss the accuracy and the shortcomings of the ns-2 implementation of the MAC layer of the IEEE 802.11 standard

2.2 Mobility Models

SUMO supports several car-following models including IDM [44], but the latter is not correctly implemented in the release of the software used in this work (the 0.12.1). Specifically, the IDM model does not work together with the lane-change decision algorithm used by SUMO for manage the movements of the vehicles between parallel lanes running in the same direction. On the opposite hand, VanetMobiSim supports several car-following models but all derived from IDM, therefore the two software do not have any common car-following model. For this reason, in VanetMobiSim we employed the Intelligent Driving Model with Lane Changing (IDM/LC), a combination of IDM with the overtaking model known as MOBIL [90], while in SUMO we have used the default model. The latter was a slightly different car-following model originally introduced by Krauss et. al in [91], and we indicate it with the acronym KWG deriving from the initial of the authors.[1] The IDM/LC model is described in Subsection 2.2.1, while the KWG model is presented in Subsection 2.2.2.

[1] The model is also known in literature as *Krauss* model.

2.2.1 IDM/LC Model

The IDM model is defined as follows. Each i-th vehicle ($i \in \{1,2,\dots N\}$) randomly selects a fixed target speed $v_i^{\text{target}} \in [v^{\min}, v^{\max}]$, where $v^{\min}$ and $v^{\max}$ are, respectively, the minimum and maximum speeds. Once its target speed has been selected, the vehicle tries to make its own speed $v_i(t)$ reach the target speed. The achievement of this goal is impaired by the road topology and by the presence of other vehicles that accelerate and decelerate. The speed evolution can be analytically characterized by the following equation [92]:

$$\frac{\mathrm{d}v_i(t)}{\mathrm{d}t} = a\left[1 - \left(\frac{v_i(t)}{v_i^{\text{target}}}\right)^4 - \left(\frac{\delta}{\Delta_{x_i}(t)}\right)^2\right] \tag{2.1}$$

where

$$\delta \triangleq \Delta_{x_{\min}} + v_i(t)T + \frac{v_i(t)\left[v_i(t) - v_{i+1}(t)\right]}{2\sqrt{ab}}. \tag{2.2}$$

Equation (2.1) shows that the local acceleration depends on two contributions: (i) the acceleration needed to reach the target speed v_i^{target} and (ii) the deceleration induced by the preceding vehicle. The term δ defined in (2.2) determines the desired dynamic distance from the preceding vehicle. This term depends on the following parameters [92]: the safe time headway (T), the maximum acceleration of movement (a), and the comfortable deceleration of movement (b).

Moreover, thanks to the integration of the MOBIL lane changing model [41], the IDM-LC mobility model takes also into account possible overtakings between vehicles. In particular, according to a game-theoretic approach considered by the MOBIL model, a vehicle (say i) moves to an adjacent lane if its advantage, in terms of acceleration, is greater than the disadvantage of the preceding vehicle (say j) in the new lane. This condition can be expressed as

$$\frac{\mathrm{d}v_i'(t)}{\mathrm{d}t} - \frac{\mathrm{d}v_i(t)}{\mathrm{d}t} \geq P\left(\frac{\mathrm{d}v_j(t)}{\mathrm{d}t} - \frac{dv_j'(t)}{\mathrm{d}t}\right) + a_{\text{thr}}$$

where the superscript $'$ refers to the speed values after the potential overtake. The parameter P models the drivers' politeness and the acceleration threshold a_{thr} prevents

lane hopping phenomena in borderline conditions. In order to prevent collisions between the back vehicle j and the overtaking vehicle i, there is also the following safety condition on the deceleration of vehicle j, based on an arbitrary parameter b_{safe}:

$$\frac{dv'_{j-i}(t)}{dt} \geq -b_{\text{safe}}.$$

2.2.2 KWG Model

The KWG model takes five input variables, $v^{\max}$, a, and b having the same meaning of the homonymous parameter of IDM (maximum speed, maximum acceleration, comfortable deceleration) and two new parameters, τ (dimension: [s]), and $\sigma \in [0,1]$ (adimensional), denoting the driver's reaction time and the dawdling parameter [93]. Let us consider the i-th vehicle, then, the KWG model can be built up by the following set of equations:

$$\begin{aligned} v_i^{\text{s}}(t+\Delta t) &= v_{i+1}(t) + \frac{\Delta x_i(t) - v_{i+1}(t)\tau}{\tau + (v_i(t)+v_{i+1}(t))/2b} \\ v_i^{\text{d}}(t+\Delta t) &= \min\left[v^{\max}, v_i(t)+a\Delta t, v_i^{\text{s}}(t+\Delta t)\right] \\ v_i(t+\Delta t) &= \max\left[0, v_i^{\text{d}}(t+\Delta t) - \sigma\, a\Delta t\, \eta\right], \end{aligned}$$

where v_i^{s} is the speed required to maintain a safety distance from its leading vehicle, v_d^{s} is its desired target speed, and v_i^{s} is its actual speed. The random variable η is uniformly distributed in the interval $[0,1]$ thus introducing a stochastic behavior, whose effect is scaled by the factor $\sigma\, a\Delta t$.

2.3 Physical Channel Consideration

2.3.1 The Wireless Channel in VANETs

The statistical characterization of the physical channel of V2V communications is a complex task. According to [94], a general consensus on a specific model has not been yet attained, due to two main causes.

First of all, it is difficult to define a common reference scenario, because of the extreme variety of environments of interest for IVCs. Roads can run in a desert countryside, inside a tunnel, or in a urban canyon studded with skyscrapers. Furthermore, because of its metallic nature, the density and the type of surrounding vehicles have a huge impact on the number of multi-path reflections experienced by the receiver. Also the antenna radiation pattern is highly influenced by its placement with respect to the vehicle (i.e., inside, on the roof). The impact of the different reference models on the Bit Error Rate (BER) and Frame Error Rate (FER) have been analyzed in [95].

The second, but not less important, reason is the lack of statistically meaningful empirical models [94]. In [96] the authors have focused on a single and relatively simple scenario, an expressway, and on a very simple metric, the delay spread. They have then compared the results generated using several empirical models obtained from independent measurement campaigns [97–100], showing that, even in this easy situation, this set of representative models provides discordant results.

From the point of view of the network layer, a physical wireless channel behaves as ON-OFF system, since the packet can be either successfully received or discarded. Typically, a checksum is used to determine the reception status of the channel (e.g., the FCS in the IEEE 802.11 model). In network simulator, a common approach is which of defining a hard threshold, the receiver sensitivity, denoted as $\mathrm{RX_{TH}}$ (dimension: [dB], according which, a packet is successfully received (with probability 1), only and only if the received power P_r (dimension: [W] is greater then the sensitivity. On the other hand, the packet is discarded with probability 1 when $P_\mathrm{r} < \mathrm{RX_{TH}}$. Thanks to this assumption, in order to know if a packet is correctly received or not, it is only necessary to derive P_r and compare it to $\mathrm{RX_{TH}}$.

Once fixed the transmit power, denoted as P_t (dimension: [W]), the value of P_r depends only on the inner characteristics of the wireless channel, and the distance between the transmitter and the receiver. There are two family of physical channel model, deterministic and stochastic. With a deterministic path-loss model, such as Friis and Two Ray Ground (TRG) models [101], once setting the transmit power and the receiver sensitivity, it is possible to calculate the transmission range, defined in this work with the symbol z (dimension: [m]). When the distance is grater then the

transmission range, the packet is never received, conversely it is always correctly detected for distance smaller than the transmission range. On the opposite hand, in stochastic models the instantaneous power is a random variable [101], and it is only possible to derive the *average* received power. In this case we cannot defined a finite transmission range, since it is not possible to a-priory predict if a packet will be successfully decoded knowing the distance from the source. However, we will define the transmission range with respect to the average received power. Depending on the characteristic of the channel, there are several types of stochastic model, such as the Shadowing, Rayleigh, Weibull, or Nakagami models [102, 103].

Because of the aforementioned lack of consensus, in recent years the researchers have used many different path loss models, either deterministic or stochastic. A non exhaustive list comprehend: Friis [54,104], TRG [16], Shadowing [105], Rayleigh [106], and Nakagami adopted in [65, 107], on the basis of empirical measurements [108, 109]. Moreover, even if not yet used in practice, there are several studies [110, 111] showing that the path loss follows a Weibull distribution [112]. In our work we have considered both a deterministic (Friis, TRG) and stochastic (Nakagami) channel models.

The Friis model is valid in quite unrealistic scenarios, without any obstacles, while the TRG can be used where the transmitter and receivers antennas are near to the ground. In particular, according to the Friis model, the received power can be expressed as follows:

$$P_{\mathrm{r}}(d) = P_{\mathrm{t}} G_{\mathrm{t}} G_{\mathrm{r}} \left(\frac{\lambda}{4\pi d} \right)^2,$$

where G_{t} and G_{r} denote the antenna gain of, respectively, the transmitter and the receiver, while λ (dimension: [m]) is the wavelength corresponding to the used the carrier frequency, denoted with f_{c} (dimension: [Hz]) (e.g., $\lambda = c/f_{\mathrm{c}}$, where c represents the speed of light).

The TRG model is defined by the following equations:

$$P_{\mathrm{r}}(d) = \begin{cases} P_{\mathrm{t}} G_{\mathrm{t}} G_{\mathrm{r}} \left(\frac{\lambda}{4\pi d} \right)^2 & d \leq d^* \\ P_{\mathrm{t}} G_{\mathrm{t}} G_{\mathrm{r}} \left(\frac{h_{\mathrm{t}} h_{\mathrm{r}}}{d^2} \right)^2 & d > d^*, \end{cases} \tag{2.3}$$

where h_{t} and h_{r} are the heights of the the transmitter and the receiver antenna, while d^* is a threshold defined as

$$d^* = \frac{4\pi h_{\mathrm{t}} h_{\mathrm{r}}}{\lambda}.$$

It is trivial to observe that in the interval $[0, d^*]$ the Friis and the TRG models are identical.

According to a m-Nakagami distribution the signal amplitude is distributed as follows [103]:

$$f_{\mathrm{x}}(x) = \frac{2m^m x^{2m-1}}{\Gamma(m)\Omega^m} \exp\left(-\frac{mx^2}{\Omega}\right), \qquad x \geq 0, \Omega > 0, m > 0.5,$$

where m and Ω are suitable parameters, in particular Ω is the average received power. The corresponding Probability Density Function (PDF) of the received power P_{r} it is therefore given by a gamma distribution of the following form:

$$f_{\mathrm{Y}}(y) = \left(\frac{m}{\Omega}\right)^m \frac{y^{m-1}}{\Gamma(m)} \exp\left(-\frac{my}{\Omega}\right), \qquad y \geq 0.$$

In order to use the Nakagami model it is necessary to specify the average received power (Γ). In [113], the authors define Ω (expressed in dB) as a piecewise constant function of d:

$$\Omega(d)[dB] = \begin{cases} 10\gamma_0 \log(d/d_{\mathrm{ref}}) & 0 < d \leq d_0 \\ 10\gamma_0 \log(d_0^\gamma/d_{\mathrm{ref}}) + 10\gamma_1 \log(d/d_0^\gamma) & d_0 < d \leq d_1 \\ 10\gamma_0 \log(d_0^\gamma/d_{\mathrm{ref}}) + 10\gamma_1 \log(d_1^\gamma/d_0^\gamma) + 10\gamma_2 \log(d/d_1^\gamma) & d_1^\gamma < d, \end{cases} \tag{2.4}$$

where d_{ref} represents a reference distance that can be freely chosen (we set $d_{\mathrm{ref}} =$ 1 m), while γ_0, γ_1, γ_2, d_0, and d_1 have been set according to the empirical values obtained by measurements on highway [113]. Obviously, by setting $gamma_i = 2$ for $i = 0, 1, 2$ in equation (2.4), we have the same attenuation of the Friis model.

Also the parameter m has a huge impact, since it determines the shape of the PDF. For example, when $m = 1$ the Nakagami PDF coincides with a Rayleigh distribution, when $m < 1$ the Nakagami distribution determines a severe fading (worse than Rayleigh), while with $m > 1$ we have a Ricean model, less sever than Rayleigh

Table 2.1: Main parameters of Friis, TRG, and Nakagami propagation models.

Parameters	Values
f_c	5.9 GHz
G_t, G_r	1
h_t, h_r	2 m
γ_0, γ_1, γ_2	1.9, 3.8, 3.8
d_0^γ, d_1^γ	200, 500 m
m_0, m_1, m_2	1.5, 0.75, 0.75
d_0^m, d_1^m	80, 200 m

(e.g., if $m \to \infty$ the Nakagami distribution reduces to deterministic model). In [113] the authors define m as a piecewise constant function of d:

$$m(d) = \begin{cases} m_0 & d < d_0^{\mathrm{m}} \\ m_1 & d_0^{\mathrm{m}} \leq d < d_1^{\mathrm{m}} \\ m_2 & d_1^{\mathrm{m}} \leq d, \end{cases}$$

where m_0, m_1, m_2, d_0^{m}, and d_1^{m} have been set according to the empirical values presented in [113].

2.3.2 Effects on the Performance of Physical Channel Characteristics

We now analyze the performance obtained using the Friis, TRG, and Nakagami model in a typical VANETs environment, characterized by having $f_c = 5.9$ GHz, as established by the IEEE 802.11p specification, and by $h_t = h_r = 2$ m, by considering the typical distance from the ground and an antenna mounted on the roof of a car. These parameters along with these used for the Nakagami model are summarized in Table 2.1.

In Figure 2.1 we show $P_r(d)$ as a function of the distance, obtained with the Friis, TRG, and Nakagami propagation models and using the parameter of Table 2.1. The transmit power is set to 100 mW (20 dBm), that is the maximum value allowed in

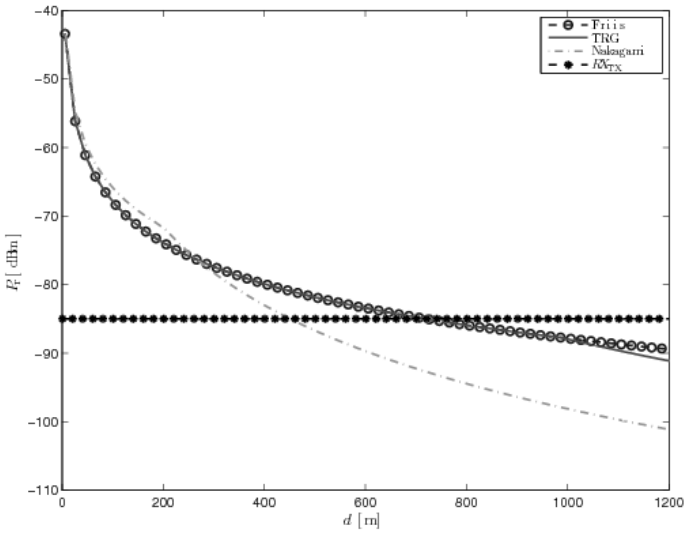

Figure 2.1: Received power obtained with the Friis, TRG, and Nakagami propagation models, using the parameters summarized in Table 2.1, and $P_t = 100$ mW.

Europe in the 5.9 GHz frequency band. In Figure 2.1 it is also shown the minimum sensitivity mandated by the IEEE 802.11p standard (85 dBm) [20]. In Figure 2.1 we observe that in the considered range ([0, 1200] m), the Friis and TRG models lead to identical results. This can be motivated by observing that using the values of Table 2.1 $d^* \approx 990$ m. For this reason, in the rest of the paper we will only consider the Friis model. Putting the values in Table 2.1 in equation (2.4), the Nakagami propagation model leads to a significantly smaller transmission range, namely $z \approx 420$ m, then the value $z \approx 700$ m achieved with the deterministic models.

Therefore using the Nakagami model it is necessary to use a higher transmit power than in deterministic model, to have the same average transmission range. For instance, using the Friis model a transmission range $z = 500$ m can be obtained by setting $P_t = 16.7$ dBm, while using the Nakagami propagation model the same result is obtained by setting $P_t = 21.5$ dBm. However, in the case of Nakagami we talk of average received power, but the real value experienced by a node at a given distance d from the destination, as shown by Figure 2.2, where it is represented the distribution

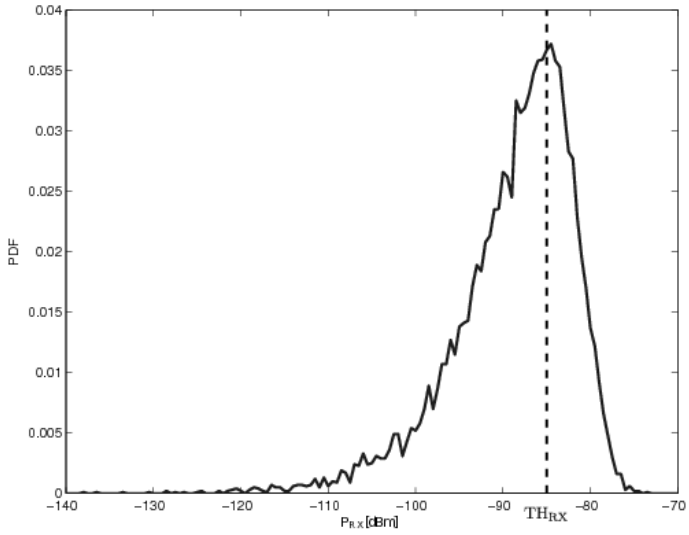

Figure 2.2: Distribution of $P_r(d)$ at the distance $d = 500$ m, obtained with the Nakagami propagation model, using the parameters summarized in Table 2.1, and $P_t = 21.5$ dBm.

of $P_r(d)$ at the distance $d = 500$ m, obtained with the Nakagami propagation models using the parameters summarized in Table 2.1, and $P_t = 21.5$ dBm. In Figure 2.2 we observe that the mode of the PDF is in TXRX, but the are a significant probability of having larger or smaller received power thus yielding to a high variability on the effective communication range. Because of this large fluctuations, also the FER experienced by a node is not a step-wise function as in the case of the Friis model, but it is a continuous function, as visible in Figure 2.3, where it is shown the FER as a function of the distance, obtained with the Friis and Nakagami propagation model, after having setting the respective P_t at a value that leads to a transmission range of respectively, 200 m and 500 m.

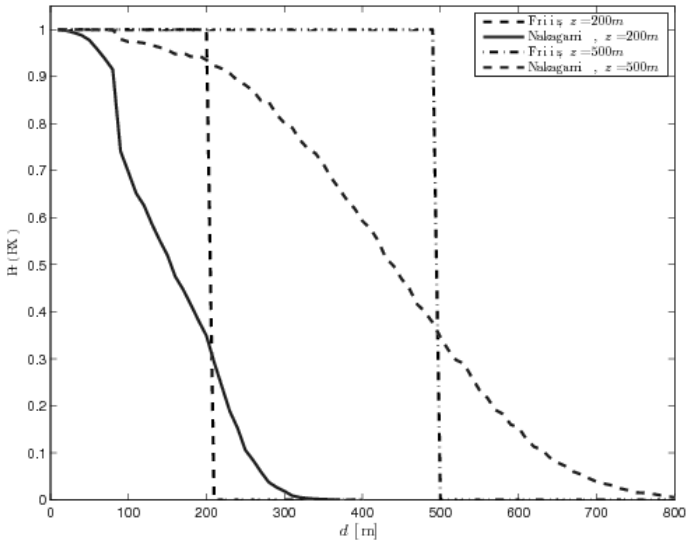

Figure 2.3: FER obtained with the Friis, and Nakagami propagation models, using the parameters summarized in Table 2.1. In both cases, we impose *z*, 200 m and 500 m, setting P_t accordingly.

2.4 IEEE 802.11 Implementation in ns-2

The last release of ns-2 (ns-2.34) contains two implementations of the IEEE standard, the default IEEE 802.11b module and a new IEEE 802.11p module, which differ in several aspects.

The default IEEE 802.11b module of ns-2 is not well coded and rich of bugs. In particular, in [87], the authors have found several issues, not entirely fixed in the subsequent releases. In the current version there are still two main problems, both described in [87]. The first is an incorrect management of the EIFS inter-frame after a collision, that leads to slightly better performance in congested networks. The second problem is related to the standard interpretation. As explained in Section 1.2.2, according to the IEEE 802.11 specifications a node should not enter in pre-backoff state if the channel is idle and it is sending the first frame of a burst or an isolated frame. The default IEEE 802.11b module of ns-2 acts differently. In particular, the sender

always perform the pre-backoff wait even in sending an isolated packet and the channel is idle. This waste of time leads to slightly worse performance in not-congested scenario, but it does not affect the saturated scenarios. On the other hand, it is beneficial in broadcast communications, since it avoids collisions in the first frames of the communication. We also note that this approximation was also widely adopted in many theoretical studies [114].

The IEEE 802.11p module has been designed from the scratch and it is a completely revised architecture for the PHY and MAC modules [113]. More precisely, the MAC layers models the basic DCF IEEE 802.11p mechanism, but without supporting the EDCA mechanism foresees by the IEEE 802.11p amendment. Therefore. using the IEEE 802.11p module is not possible to simulate the multi-channels features of the IEEE 802.11p/WAVE stack protocol. We observe that in this implementation, the authors have correctly interpreted the standard, and hence, a node does non enter in the pre-backoff when sending the first frame of a burst. However, from the point of view of broadcast communications, the new implementation of the MAC behaves as the default IEEE 802.11 module. In fact, the reception of a frame is followed by a DIFS period, during which the receiver sees a busy channel. Therefore, in the case of a broadcast multihop protocol, all the retransmissions by the forwarder node sees a busy channel, and hence the always experiences a pre-backoff. We observe that this happen as long the delay introduced by the higher layers is smaller than DIFS.

The PHY component of IEEE 802.11p module introduces a more advanced management of the interference, and of the phenomenon of the packet capturing. In particular, the PHY modules continuously tracks the cumulative received power comprehensive of both noise and signal(s), thus computing the Signal to Interference plus Noise Ratio (SINR) for every packet. A packet can be successfully decode if its SINR remains over a suitable threshold, associated to the used modulation format (i.e., 5 dB for the BPSK modulation), for all the packet duration. Differently from the standard module, the PHY module ignores the concept of receiving threshold, without assessing if the cumulative received power is over the carrier sense threshold, which is used to determine the status of the channel. done in the IEEE 802.11b module. We by-pass the problem by imposing that the carrier sense threshold value is

identical to the sum of the modulation threshold (i.e., 5 dB for the BPSK modulation) and the noise power.

Now it is interesting to assess the impact of these different IEEE 802.11 implementation on the performance of the most traditional multihop broadcast protocol, the naive flooding protocol. We utilize the same reference scenario that will be described in Section 3.2, with $\rho_s = 0.04$ veh/m, and $z = 500$ m (e.g., on average, there are on 20 nodes in the forward transmission range of a node). As reference metric we consider the number of transmissions and the REachability (RE), defined as the ratio between the number of nodes that have received the sent packet, with respect to the number of nodes in the network [2]. There is a single source sending packet of 300 bytes, generated according to a Poisson distribution of parameter λ (dimension: [pck/s]). We have considered 4 different MAC module, all transmitting with a data rate of 3 Mbit/s:

- the legacy ns-2.34 implementation, indicated as 802.11b;
- the ns-2.34 implementation patched according to [87], denoted as "802.11b [87], wo BO", since in this case there is no backoff if the channel is free;
- the ns-2.34 implementation patched according to [87], with the insertion of the pre-backoff as in the original implementation, and thus denoted as "802.11b [87], w BO"; it is important to note that this is the version effectively used in our work;
- the IEEE 802.11p module present in the ns-2.34 release, indicated as 802.11p. This implementation has slightly different values of slot time duration, SIFS and DIFS duration, but we set the save values $CW_{min} = 31$ as in the IEEE 802.11b standard.

In all cases the data rate of is equal to 3 Mbit/s and $CW_{min} = 31$.

In Figure 2.4 are depicted the RE and the number of transmissions. as a function of the hop index, obtained considering a fixed packet size of 300 bytes, and two values of λ, respectively, 1 pck/s and 385 pck/s. Figure 2.4 offers to us several precious

[2] The RE which will be more precisely defined in Section 3.2

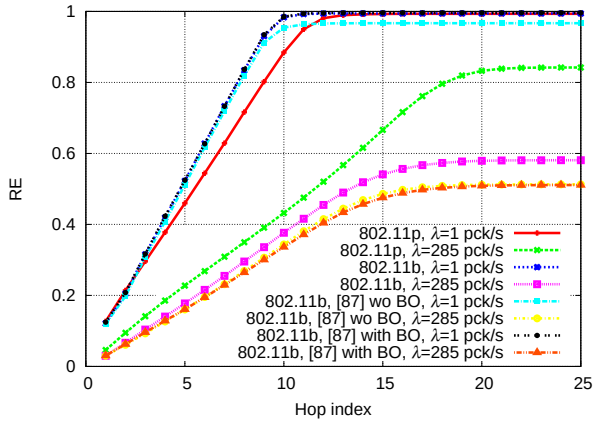

(a) RE

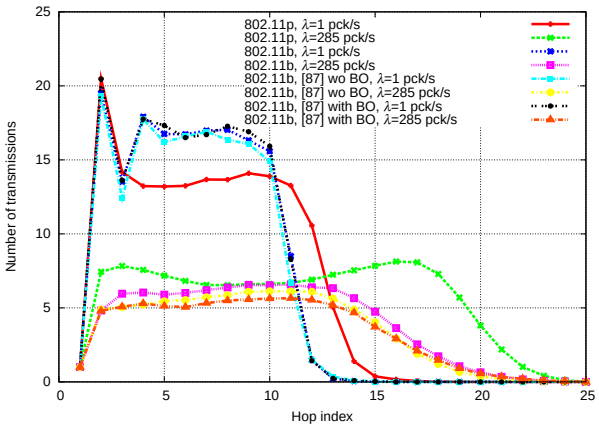

(b) Number of transmissions

Figure 2.4: RE (a), and (b) number of transmissions, as a function of the hop index i, obtained using the flooding protocol coupled with several implementations of the IEEE 802.11 standard. Results are obtained by setting: $\rho_s z = 20$ veh, a packet size of 300 bytes, a data rate of 3 Mbit/s, and two values of λ, respectively, 1 pck/s and 385 pck/s.

insights:

- When $\lambda = 1$ pck/s, the traffic load is scarce (2.4 Kbit/s) with respect to the data rate, hence, the EIFS is never used, the interference is limited, while the pre-backoff has a certain importance. In fact, because of the lack of the pre-backoff the "802.11b [87], wo BO" is the unique module not achieving RE=1. We also observe that while the IEEE 802.11p module offers RE=1, but in a larger number of hops than the 802.11b modules.

- When $\lambda = 285s$ pck/s, the traffic load is 685 Kbit/s, approximately the 25% of the available data rate, thus representing a saturation condition. In this case, the EIFS is therefore frequently employed, the interference is high, while the pre-backoff has no importance. The flawed EIFS management of the legacy IEEE 802.11b guarantees a slightly advantage with respect to the patched releases. At the same time, we observe that the improved interference management of the IEEE 802.11p module, yields to a huge performance boost. In fact, in this case the packets are correctly received by a number of nodes 30% higher than in the IEEE 802.11b implementations.

- By observing Figure 2.4 it emerges clearly that the IEEE 802.11p could obtain a much higher RE, thanks to a more homogeneous distribution of the transmissions across the hops. More precisely, it seems that the PHY module limits the number of transmissions and thus the number of collisions, by reducing the effective transmission range of a node. This can also motivate the larger number of hops.

From this analysis it is emerged that the IEEE 802.11b modules offer comparable performance in both low and high traffic load conditions. On the contrary, the IEEE 802.11p has a radically different behavior, especially at high traffic load, where it is good antidote for the broadcast storm problem, limiting the need of refined multihop broadcast schemes. Finally, it is important to point out that in our simulations we have used the so-called "802.11b [87], wo BO" implementation.

Chapter 3

The Irresponsible Forwarding Broadcast Protocol

3.1 Introduction

As shown in Section 1.5, in literature there are many multihop broadcast protocols, with good characteristics and quasi-optimal performance. However, in our opinion, the existing protocols are still not satisfactory, and we feel it is possible to obtain better results. First of all, most the proposed protocols are empirical, in the sense they are not supported by a theoretical background proving their efficiency. One remarkable exception is constituted by the SB protocol, whose design is derived from an analytical latency optimization [74]. Furthermore, with the exception of the EMDV [65], that has been designed targeting physical channels affected by fading, all the proposed approaches ignores the underlying nature of the VANETs' physical channel, that has been proved to be affected by severe fading, as shown in Section 2.3. For instance, we are doubtful about the effectiveness in a vehicular environments, where the nodes experience severe and uncorrelated fading, of the protocols based on the black-burst technique, such as UMB [22] and BPAB [75]. An additional problem is constituted by the scarce reliability of the simulative tools commonly employed for analyzing the protocol performance, as shown in Section 2.4, even different releases

of the same simulator can lead to very different performance. This problem is rarely taken into account, with the remarkable exception of EMDV [65].

For these reasons, in this chapter we propose a probabilistic-based multihop broadcast scheme, denoted as Irresponsible Forwarding (IF), designated with the goal of guaranteeing both the minimum latency and the minimum channel occupancy. The IF protocol does not introduce overhead, is extremely simple and it only requires the presence of a GPS receiver in the vehicle. Furthermore, it has shown to to successfully operating also in channel affected by fading. The remainder of this chapter is organized as follows. In Section 3.2, we describe the reference scenario. In Section 3.2 we accurately describe the IF protocol, while in Section 3.4 we present an analytical framework that offers some insights about the behavior of IF. The performance of the IF protocol in realistic IEEE 802.11b multi-hop linear networks is investigated in Section 3.5. It is important to underline that the simulative results shown in this chapter have been obtained using the IEEE 802.11b module of the ns-2 simulator. As emerged in Section 2.4, by using the IEEE 802.11p module we would probably obtain different performance, especially in saturation conditions. However, we can anticipate that simulation results obtained with the IEEE 802.11p standard are present in Chapter 6. Finally, conclusions are drawn in Section 3.6.

3.2 The Reference Scenario

Figure 3.1 shows the linear network topology of reference. We consider a static one-dimensional wireless network with N (receiving) nodes. Each node is uniquely identified by the indices $j \in \{1, 2, \ldots, N\}$. The assumption of static nodes is not restricting and, in Chapter 5, we will provide more details on the applicability of the obtained results to mobile networks. The source node, denoted as node 0, is placed at the west end of the network, therefore there is a single propagation direction (eastbound). The following preliminary assumptions are introduced to derive simple, yet significant, insights. The inter-vehicle spacing is distributed according to an exponential distribution with mean $1/\rho_s$, where ρ_s is the vehicle spatial density (dimension: [veh/m]). In other words, the nodes' positions are generated according to a one-dimensional Pois-

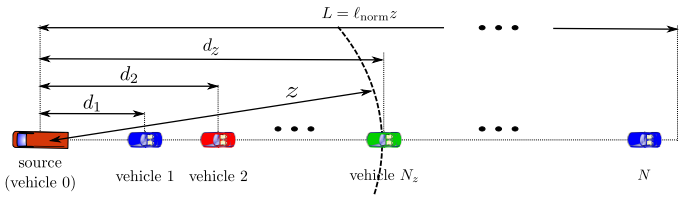

Figure 3.1: A typical linear network topology of a VANET.

son distribution with parameter ρ_s—the validity of this assumption is confirmed by empirical traffic data [115]. Each vehicle has a fixed transmission range, denoted as z (dimension: [m])—the transmission range depends, obviously, on the transmit power P_t (dimension: [W]). The model presented in this chapter are based on the assumption of a Friis propagation model, leading to a deterministic one-to-one relationship between the transmission range and the transmit power, as illustrated in Section 2.3. Each vehicle is equipped with a Global Positioning System (GPS) receiver. As a result, each vehicle knows its own position at any given time. The network size (the line length) is set to L (dimension: [m]). For generality, we denote as *normalized network size* the positive real number $\ell_{\text{norm}} \triangleq L/z$, and we observe that $\rho_s z$ (dimension: [veh]) represents the average number of vehicles within a transmission range.

Each topology realization, consistent with the previous assumptions, is obtained by iteratively generating the positions of consecutive nodes (with exponentially distributed distance between a pair of consecutive nodes). The generation process stops as soon as $d_{0,N+1} > L$, where $d_{0,N+1}$ is the (positive) distance between the source node and the $N+1$-th node. Therefore, N is the random variable denoting the index of the last generated node. In general, $d_{j,k}$ denotes the distance between the two nodes j and k ($j,k \in \{1,\ldots,N\}$). In order to guarantee the significance of every scenario, we impose that the 1-st node has to lie in the interval $[0,z]$, i.e., $d_{0,1} < z$, so that $N > 1$. Apparently, these requirements break the Poissonianity of nodes' position process. However, conditionally on $d_{0,1}$, the remaining nodes in the set $\{2,\ldots,N\}$ are still distributed according to a Poisson point process of parameter ρ_s. Considering that[1] $\mathbb{E}[d_{0,1}] \simeq 1/\rho_s$, it is accurate to assume that the number of nodes, denoted as

[1]Given that $d_{0,1} < z$, it follows that $d_{0,1}$ has the truncated exponential probability density function

$N' \triangleq N-1$, in the network region $[d_{0,1}, L]$ (i.e., after the first node) has a Poisson distribution with parameter $\rho_s(L-1/\rho_s) = \rho_s L - 1$. On the basis of the previous assumptions, we want to preliminary investigate the network connectivity (which does not depend on the chosen broadcasting protocol). To this end, we introduce the concept of *last reachable node* (identified by the index n_{reach}). Given that there are N nodes in the network, for every pair of consecutive nodes, say $(j, j+1)$, $j \in [1,2,\ldots,N-1]$, since the distribution of $d_{j,j+1}$ is well approximated by an exponential distribution with parameter ρ_s, there is (approximately) a probability $e^{-\rho_s z}$ that $d_{j,j+1} > z$. We denote as j^* the minimum node index such that $d_{j^*,j^*+1} > z$. Clearly, if j^* exists, than the (j^*+1)-th node is unreachable from any node $j < j^*+1$. Therefore, the network is said topologically disconnected and $n_{\text{reach}} = j^*$. Conversely, if j^* does not exist, then the network is topologically connected and $n_{\text{reach}} = N$. Obviously, the average value of the ratio n_{reach}/N is a meaningful metric to evaluate the connectivity level of the network.

In Figure 3.2, $\mathbb{E}[n_{\text{reach}}/N]$ is shown as a function of the product $\rho_s z$, considering both simulation and analytical results. More precisely, the simulation results are obtained by averaging, for each value of $\rho_s z$, the values of the ratio n_{reach}/N obtained over 1000 network topologies generated according to the previous assumptions.[2] Recalling that $N' = N-1$ is approximately Poisson$(\rho_s L - 1)$, the average value $\mathbb{E}[n_{\text{reach}}/N]$ can be analytically approximated as follows:

$$\begin{aligned}\mathbb{E}\left[\frac{n_{\text{reach}}}{1+N'}\right] &= \sum_{j=0}^{\infty} \mathbb{E}\left[\frac{n_{\text{reach}}}{1+N'}\middle|N'=j\right] P\{N'=j\} \\ &\simeq \sum_{j=0}^{\infty} \frac{1}{1+j}\mathbb{E}\left[n_{\text{reach}}\middle|N'=j\right] \frac{(\rho_s L-1)^j e^{-(\rho_s L-1)}}{j!}. \end{aligned} \tag{3.1}$$

Given that $N'=j$, n_{reach} can assume values between 1 (if only the first node is con-

$f_{d_{0,1}}(\tau) = \frac{\rho_s e^{-\rho_s \tau}}{1-e^{-\rho_s z}}[U(\tau)-U(\tau-z)]$, where $U(\cdot)$ is the unit step function. It can be shown that $\mathbb{E}[d_{0,1}] = 1/\rho_s - z e^{-\rho_s z}/(1-e^{-\rho_s z})$ is well approximated by $1/\rho_s$, i.e., by the average value of a (non-truncated) exponential distribution.

[2] Note that the assumption that $d_{0,1} < z$, i.e., $N \geq 1$, makes the chosen metric meaningful.

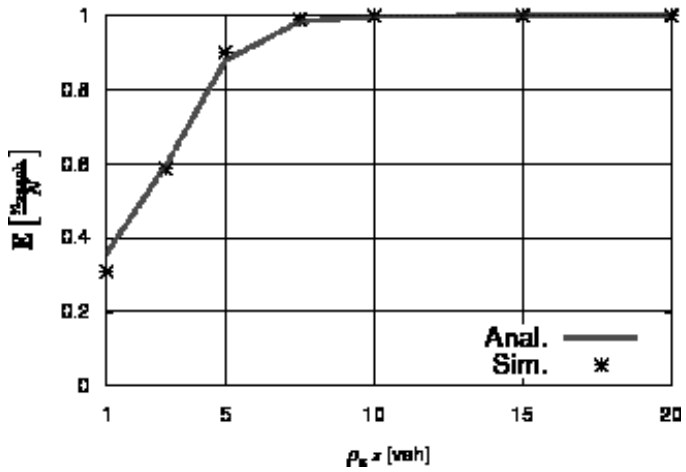

Figure 3.2: The average ratio $\mathbb{E}[n_{\text{reach}}/N]$ as a function of $\rho_s z$.

nected) and $j+1$ (if all nodes are connected). More precisely

$$P\{n_{\text{reach}} = \ell | N' = j\} \simeq \begin{cases} (1-P_{\text{D}})^{\ell} P_{\text{D}} & 1 \leq \ell \leq j-1 \\ (1-P_{\text{D}})^{j} & \ell = j \end{cases}$$

where $P_{\text{D}} = e^{-\rho_s z}$ is the probability that two consecutive nodes are disconnected, i.e., that the distance between them is longer than z. Therefore,

$$\mathbb{E}\left[n_{\text{reach}} \middle| N' = j\right] \simeq \sum_{\ell=1}^{j-1} \ell (1-P_{\text{D}})^{\ell} P_{\text{D}} + j(1-P_{\text{D}})^{j} \tag{3.2}$$

and, inserting (3.2) into (3.1), the desired average value can be approximated. As one can see from the results in Figure 3.2, the proposed analytical approximation is very accurate. It can be observed that $\mathbb{E}[n_{\text{reach}}/N]$ is an increasing function of $\rho_s z$ that approaches 1 for $\rho_s z \geq 12$ veh. In other words, for $\rho_s z \geq 12$ veh the network is completely connected. This preliminary network connectivity analysis will allow to better characterize all performance results, relative to the IF protocol, which will be presented in Section 3.3.

3.3 The IF Protocol

In a self-organizing traffic information system, vehicles share and distribute the traffic information by rebroadcasting a received information packet to their neighbors. Reducing the number of redundant packets, while still ensuring good coverage and reachability, is one of the main objectives in multi-hop broadcasting. In this chapter, we propose a new probabilistic-based broadcasting scheme for multi-hop linear networks (e.g., highway vehicular networks), denoted as Irresponsible Forwarding (IF), where each vehicle rebroadcasts a received data packet on the basis of (i) its distance from the source and (ii) the spatial density of its neighbors. The key idea is that a node implicitly evaluates the probability that there is another node, in its proximity, which can rebroadcast. If this probability is sufficiently high, then the former node "irresponsibly" chooses not to rebroadcast. Unlike other existing probability assignment schemes, IF takes into account the statistical distribution of the vehicles on the road. Moreover, for sufficiently large values of the node spatial density the average number of rebroadcast packets can be regulated by properly tuning a single parameter.

Let us consider a vehicle, at a generic distance d from the source node (positioned at the origin of the horizontal axis), within the transmission range of the source. In Figure 3.1, N_z denotes the number of nodes within the transmission range of the source, i.e., $d \in \{d_1, d_2, \ldots, d_z\}$. According to the idea of the IF protocol, the vehicle should rebroadcast the packet only if the probability of finding another vehicle in the consecutive interval of length $z-d$ is low; otherwise, it should not. More specifically, when a vehicle receives a packet, it compares its position with that of the transmitter and computes its rebroadcast probability as follows:

$$p \quad = \quad \exp\left\{-\frac{\rho_s^v(z-d)}{c}\right\} \tag{3.3}$$

where $c \geq 1$ is a tunable parameter which can be selected to "shape" the probability of rebroadcasting (as a function of d)—the higher the value of c, the higher the probability of rebroadcasting at any position d—and ρ_s^v is the *local* vehicle spatial density, evaluated by each vehicle, independently from the other vehicles, at time t. The local spatial density $\rho_s^v(t)$ can be significantly different from the average vehicular density.

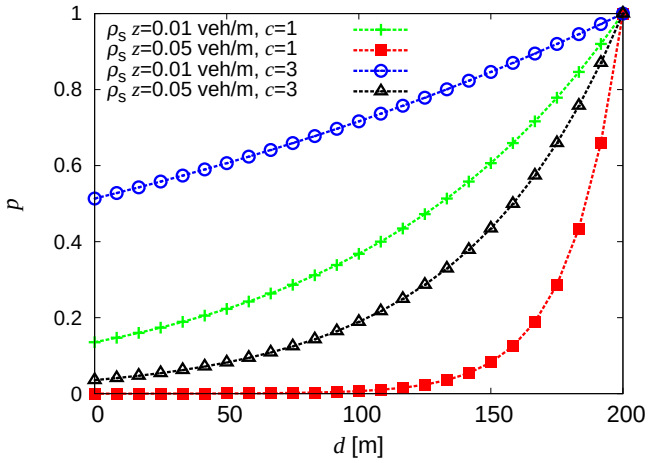

Figure 3.3: Rebroadcast probability, as a function of the distance, with $z = 200$ m, $c \in \{1,3\}$, and $\rho_s \in \{0.01, 0.05\}$ veh/m.

In static scenario as the ones considered in this chapter, the time-dependence has no effect and therefore $\rho_s^v(t) \equiv \rho_s^v$. We remark that the IF protocol acts on a per-packet basis and does not keep memory of past forwarding decisions.

According to the considerations expressed in Section 1.5, this approach can be also interpreted by means the minimum connected set theory [57, 59], according with, ideally one always want to select the node with the maximum extended coverage. In a one-dimensional scenario this coincides with selecting the furthest node from the transmitter, thus motivating the retransmission probability expression of equation (3.3).

In Figure 3.3, the rebroadcast probability is shown, as a function of the distance between the receiver and the transmitter, for various values of c and $\rho_s z$. This figure can be interpreted as follows. When d is small, the value of p is also small because the receiving vehicle is very close to the transmitter and, therefore, it should let the other node take the responsibility of rebroadcasting. When d becomes larger, the value of p becomes larger and approaches 1 when the node is at the edge of the transmission range. Note that with the probability assignment in (3.3), the node

spatial density is also taken into account. When the network is sparse, the overall rebroadcast probability should be high (e.g., even if the receiving node is relatively close to the transmitter) in order to ensure complete reachability. As observed in Figure 3.3, when $\rho_s z$ decreases from 0.05 veh/m to 0.01 veh/m, the overall forwarding probability also increases. In addition, the coefficient c is also effective at shaping the rebroadcast probability, as the overall rebroadcast probability can be increased by increasing the value of c.

3.4 Performance Analysis of IF in Ideal Networks

In this section, we investigate the performance of the IF protocol in "ideal" (collision free) networks. As a meaningful performance metric, we consider the average number of redundant packets, rebroadcast by the nodes in the network, upon transmission of a single packet by the source. This metric is illustrative of the energy consumption incurred by the network in broadcasting a single information packet generated by the source. Obviously, the average number of rebroadcast packets should be kept as small as possible, yet guaranteeing complete network reachability. The broadcast process, upon transmission of a data packet from the source (placed at the origin of the axis), evolves according to the following consecutive rebroadcast rounds:

- in the first round, some of the nodes in $(0, z)$ will rebroadcast the received packet;
- in the second round, some of the nodes receiving the rebroadcast packets, will rebroadcast them on their own;[3]
- the process continues in the following rounds until no node forwards the packet further.

Consider the first rebroadcast round. The average number of redundant packets coincides with the average number of vehicles that rebroadcast the packet transmitted

[3]Obviously, we are implicitly assuming that once a node has received a packet, regardless of the fact that it rebroadcasts the packet or not, it will rebroadcast no more copies of the same packet.

by the source. Suppose that we indicate the vehicles in $(0,z)$ from 1 to N_z in an increasing order of distance from the origin, as shown in Figure 3.1. According to the considered Poisson point distribution, it is immediate to conclude that N_z has a Poisson distribution with parameter $\rho_s z$. Let V_i, $i \in \{1,\ldots,N_z\}$, be the following Bernoulli random variable:

$$V_i = \begin{cases} 1 & \text{if vehicle } i \text{ rebroadcasts} \\ 0 & \text{otherwise.} \end{cases}$$

Let M_1 be the random variable denoting the number of vehicles that rebroadcast in the first round. The average number of vehicles in $(0,z)$ which rebroadcast the packet can then be written as:

$$\mathbb{E}[M_1] = \sum_{i=1}^{N_z} V_i. \tag{3.4}$$

In the Section A of the Appendix, it is shown that (3.4) can be expressed, assuming that ρ_s is known, as follows:

$$\mathbb{E}[M_1] = \begin{cases} \sum_{n=1}^{\infty} \frac{(\rho_s z)^n e^{-\rho_s z}}{n!} \sum_{i=1}^{n} \frac{(\rho_s z)^i e^{-\rho_s z}}{i!} \cdot \frac{1}{1-e^{-\rho_s z}\sum_{j=0}^{i-1}\frac{(\rho_s z)^j}{j!}} & \text{if } c = 1 \\ \sum_{n=1}^{\infty} \frac{(\rho_s z)^n e^{-\rho_s z}}{n!} \sum_{i=1}^{n} \left(\frac{c}{c-1}\right)^i e^{-\frac{\rho_s z}{c}} \cdot \frac{1-e^{-\rho'_s z}\sum_{j=0}^{i-1}\frac{(\rho'_s z)^j}{j!}}{1-e^{-\rho_s z}\sum_{j=0}^{i-1}\frac{(\rho_s z)^j}{j!}} & \text{if } c > 1 \end{cases} \tag{3.5}$$

where $\rho'_s \triangleq \rho_s(1-1/c)$. The final expression (3.5) for $\mathbb{E}[M_1]$ can be evaluated numerically. In particular, this expression is a function of c and $\rho_s z$. As will be shown at the end of this section and the next, by properly selecting the value of c it is possible to asymptotically (for large values of $\rho_s z$) "tune" the number of rebroadcasts. If $c \gg 1$, it can be shown that (see Section A of the Appendix)

$$\mathbb{E}[M_1] \simeq \rho_s z e^{-\frac{\rho_s z}{c}}. \tag{3.6}$$

Computing the average number of packets transmitted in the second rebroadcast round is much more complicated, since it depends *not only* on the average number of vehicles which rebroadcast in the first round, *but also* on their specific positions. Moreover, there might be a vehicle outside $(0,z)$ which receives two rebroadcast copies by two different vehicles in $(0,z)$. In general, denoting by M_j the number of vehicles which rebroadcast at the j-th rebroadcasting round, with $j = 2,3,\ldots$, evaluating $\mathbb{E}[M_j]$ analytically is a challenging and open problem. However, it is possible to analyze the redundancy rate by resorting to simple simulations, as discussed in the remainder of this subsection.

We have implemented a Matlab-based simulator for evaluating the average number of packets collectively rebroadcast by vehicles in the network. In each simulation trial, vehicles are placed on a straight line of length $L = 10$ km according to a Poisson point process with density ρ_s. In all simulation scenarios, we consider a fixed transmission range of $z = 100$ m. The first vehicle is designated as the source and transmits one information packet. The initial transmission of a new packet from the source is denoted as the 0-th hop transmission, while the source itself identifies the so-called 0-th *transmission domain*. After the source transmission, the packet is then received by a subset of the source's neighbors, that are the potential rebroadcasting nodes for the 1-st hop. Hence, their union constitutes the 1-st transmission domain.

Each vehicle in the 1-st transmission domain decides to forward the packet with a probability given in (3.3), where the value of ρ_s corresponds exactly to the density of the Poisson point process (assumed to be known by all nodes).

It is possible that more than one vehicle, in the first rebroadcast round, decide to rebroadcast the packet. As a result, a vehicle in the second rebroadcast round may receive more than one copy of the information packet. In this case, a vehicle will make the rebroadcast decision upon the reception of the first copy of the packet only and other copies of the packet will be ignored. This rebroadcasting process continues until either the packet dies (i.e., no vehicle rebroadcasts the packet further) or the packet reaches the last vehicle in the network. The number of packets transmitted in each rebroadcast round is recorded and collected at the end of the simulation trial. The simulation is repeated for 100,000 trials and the *average* number of packets

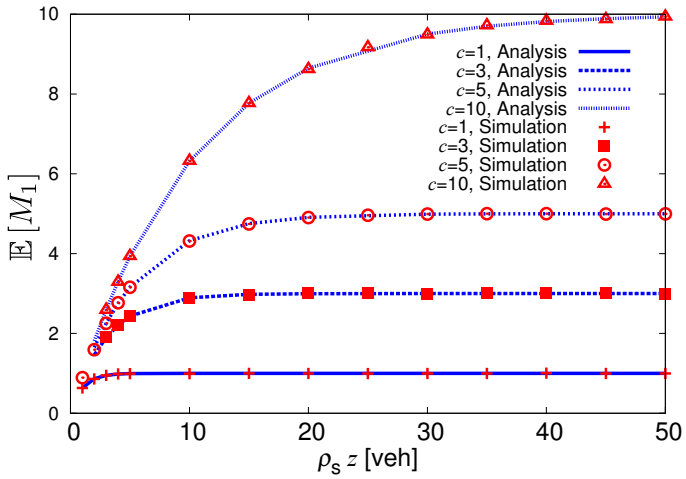

Figure 3.4: Average number of packets rebroadcast in the first rebroadcast round as a function of $\rho_s z$. Various values of $c = 1, 3, 5, 10$ are considered. Analytical (lines) and simulation (symbols) results are compared.

collectively rebroadcasted in each round is computed.

First, we validate the analytical results, relative to the first broadcast round, with simulations. In particular, we compare the average number of rebroadcasts, given by (3.5), with the simulation-based estimated value.[4] In Figure 3.4, $\mathbb{E}[M_1]$ is shown, as a function of $\rho_s z$, considering various values of c and $i = 1$. It can be observed that analytical and simulation results are in perfect agreement. This verifies the validity of the analytical expressions in (3.5) for computing the average number of packets rebroadcast by the vehicles in the first round. Moreover, from the results in Figure 3.4, one can also conclude that:

$$\lim_{\rho_s z \to \infty} \mathbb{E}[M_1] = c. \tag{3.7}$$

In other words, when the average number of vehicles, within a transmission range, becomes sufficiently large, the average number of vehicles which rebroadcast is equal

[4]Equation (3.5) indicates that $\mathbb{E}[M_i]$ is a function of the product $\rho_s z$ and of the shaping parameter c however, with the aim of simplifying the notation, we omit this explicit relationship throughout the whole text.

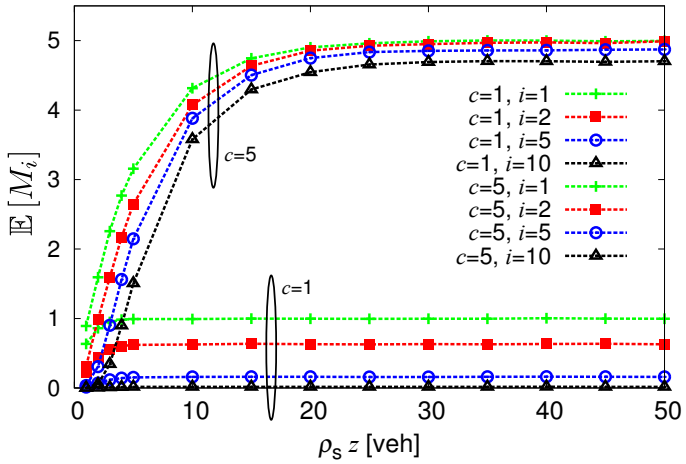

Figure 3.5: Average numbers of rebroadcast packets in the first, second, fifth, and tenth rebroadcast rounds (i) as functions of $\rho_s z$. The value of c is set to 1 (bottom curves) and 5 (upper curves). All results are simulation-based.

to the parameter c, which can be *a priori* set by the network designer. An analytical proof of (3.7) is an open problem.

Next, we investigate the characteristics of the average numbers of rebroadcasts in the next rebroadcast rounds. In Figure 3.5, the average numbers of packets rebroadcast in the first, second, fifth, and tenth rounds are shown as functions of the product $\rho_s z$. The shaping parameter c assumes two different values: 1 and 5. Regardless of the value of c, it can be observed that the average number of rebroadcast packets decreases as the packet gets farther away from the source vehicle, i.e., for increasing value of i. This is intuitively expected, due to the probabilistic broadcasting nature of IF. In the case with $c = 1$, the average number of rebroadcasts is smaller than one for $i > 1$. This implies that the packet will rarely get forwarded beyond the first round. Moreover, this indicates that the rebroadcast probability in this scenario (with $c = 1$) is too small. On the opposite, with a higher value of the shaping coefficient ($c = 5$), the average number of rebroadcast packets at the 10-th rebroadcast round is still much larger than 1. This implies that the source information packet has a high chance to make more than 10 hops. In practice, one can choose a sufficiently large value of c in

order for the packet to make a desired number of hops.

From Figure 3.5, one can conclude that when the product $\rho_s z$ is large enough, at any rebroadcast round the corresponding average number of rebroadcast packets converges to a fixed value—as already observed in Figure 3.4 for the first rebroadcast round. This is a desirable characteristic, which is unique to our forwarding scheme. In other words, the IF scheme can, through proper selection of the value of the shaping parameter c, limit the number of redundant forwarded packets even if the network becomes very dense. The behavior of IF is in sharp contrast with that of simpler forwarding techniques, such as flooding, which become completely inefficient for high node spatial density. This will be discussed in more detail in Section 3.5 with a consideration on realistic IEEE 802.11 networks.

3.5 IF in IEEE 802.11b Networks

While in Section 3.4 we have considered an ideal scenario (without interference, collisions, and channel access delay), we now investigate the performance of the IF protocol when embedded in a realistic wireless communication protocol stack, namely that of an *ad-hoc* IEEE 802.11 network. The performance will be analyzed through simulations, which will be properly described before presenting the obtained results. We remark that while the traffic load is ineffective in the ideal configuration considered in the previous section, in an IEEE 802.11 network scenario it will have a relevant impact.

3.5.1 Performance Metrics

We consider two classes of performance metrics: *per-hop*, relative to the behavior shown in a single transmission domain; and *global*, for a more general characterization of the network-wide performance and independent of the specific transmission domain. For all considered metrics we only evaluate the first-order statistics (i.e., the average values), with the exception of the delay. For all the performance metrics defined in this subsection, we omit the explicit dependence from z and from the product $\rho_s z$.

The following two per-hop performance metrics are considered: (i) the average number of retransmissions at the i-th rebroadcast round, introduced in Section 3.4 and denoted as $\mathbb{E}[M_i]$, and (ii) the average domain size at the i-hop, denoted as DS_i. The domain size $DS(i,j)$ is defined as the number of nodes contained in the i-th transmission domain of the j-th packet. The average domain size DS_i can then be obtained from the arithmetic average of the domain sizes $\{DS(i,j)\}$ as follows

$$DS_i \triangleq \frac{1}{N_\mathrm{p}} \sum_{j=1}^{N_\mathrm{p}} DS(i,j).$$

The average number of rebroadcasts per-hop and the average domain size are related metrics and shed light on the ability of the IF protocol to self-sustain.

The performance of IF broadcasting schemes is analyzed considering various performance metrics, including: (i) the end-to-end delay (D) , (ii) the reachability (RE), and (iii) the transmission efficiency (TE). The first metric is the duration of the packet trip between the source and the last reachable node.[5]

The RE, originally introduced in [56], is the fraction of nodes that receive the source packet among the set of all reachable nodes. Intuitively, the RE is inversely proportional to the normalized distance between the source and the last reachable node, given by $d_{0,n_\mathrm{reach}}/z < \ell_\mathrm{norm}$. Since the RE is limited to the connected portion of the network, less connected networks (with $d_{0,n_\mathrm{reach}}/z \ll \ell_\mathrm{norm}$) generally have a higher RE than highly connected networks (with $d_{0,n_\mathrm{reach}}/z \approx \ell_\mathrm{norm}$).

The TE is a novel metric, introduced here for the first time. More precisely, for a given packet, we define the TE as the ratio between its RE and the overall number of rebroadcasts that is experienced during its transmission to the last reachable node. For instance, given a network with $n_\mathrm{reach} = 100$, a packet that reaches 80 nodes, through an overall number of retransmissions equal to 20, corresponds to a value of RE equal to $80/100 = 0.8$ and a value of TE equal to $0.8/20 = 0.04$. Obviously, one would like to have the highest possible value of TE. Generally, a high value of TE indicates that a broadcasting protocol can minimize the latency while still being able to guarantee the high value of RE. In fact, the TE is an indicator of the ability of the protocol to

[5] We remark that only the packets received correctly at the n_reach are considered for evaluation of D.

select the "optimal" forwarding node.

3.5.2 Simulation Setup

In each simulation trial, ℓ_{norm} is set to be 8. In each topology the source generated a finite number (burst) of $N_{\text{p}} = 1000$ packets according to a Poisson process with parameter λ (dimension: [pck/s]). [6] Each packet a fixed small size PS $= 100$ bytes, since alert messages typically carries a small amount of information. The data rate is set to 1 Mbit/s. Two values of λ are considered. The first, $\lambda = 0.1$ pck/s, leads to a very small traffic load of only 0.08 Kbits/s, while the second value, $\lambda = 100$ pck/s determines a high traffic load of 80 Kbits/s, roughly one tenth of the theoretical available data-rate of 1 Mbit/s. Two values of the parameter c, namely 1 and 5, are chosen as representative of mild and aggressive rebroadcasting policies, respectively. The results are obtained for a fixed node spatial density $\rho_{\text{s}} = 0.01$ veh/m, while the possible values of the transmission range z are listed in Table 3.1. In particular, the values of z are selected so that the corresponding values of $\rho_{\text{s}} z$ are between 1 veh and 20 veh. This choice is motivated by the results of Figure 3.4 and Figure 3.5, which clearly show that, for values of $\rho_{\text{s}} z$ larger than 20 veh, the behavior of IF remains the same (in fact, the network is fully connected as shown in Figures 3.3). In order to have a more realistic simulation setup, we assume that every node uses, as the value for $\rho_{\text{s}}^{\text{v}}$ in the probability assignment function (3.3), its *local* node spatial density, denoted as $\rho_{\text{s}}^{\text{i}}$, computed as the ratio between the number of single-hop neighbors and $2z$. However, as we will see in Subsection 3.5.4, the assumption of local node spatial density estimation has a negligible impact on the IF protocol performance, with respect to a scenario where all nodes use the same overall average value ρ_{s} of the nodes' Poisson distribution.

The IF protocol is "inserted" on top of the IEEE 802.11b model in ns-2.34 [48], described in Section 2.4, and adopting the Friis free-space propagation model introduced in Section 2.3. The relevant parameters of the IEEE 802.11b network and of the IF protocol are listed in Table 3.1. Finally, in order to have a performance bench-

[6] All the results presented are accurate within $\pm 5\%$ of the values shown with 95% confidence.

Table 3.1: Main IEEE 802.11b network simulation parameters for IF.

c	$\{1,5\}$
λ	$\{0.1,100\}$ pck/s
ρ_s	0.01 veh/m
z	$\{100,300,500,750,1000,1500,2000\}$ m
ℓ_{norm}	8
Packet Size	100 bytes
Carrier Freq.	2.4 GHz
Data rate	1 Mbps
CW_{min}	31

mark, we have also carried out simulations of the naive flooding protocol (denoted as "flood" in the following figures), whose forwarding policy is trivial: every node rebroadcasts any fresh packet with probability equal to 1 (i.e., always).

3.5.3 Performance Analysis

We investigate the behavior of the IF protocol analyzing the two per-hop metrics DS_i and $\mathbb{E}[M_i]$. The average domain size is evaluated, as a function of the hop index i, in Figure 3.6, using $\rho_s z = 20$ veh (as shown in Figure 3.3 this guarantees full network connectivity with a high probability). From the results in Figure 3.6, one can observe that if the packet interference is limited—this happens if the traffic load is low (λ=0.1 pck/s) or the rebroadcast policy is non-aggressive ($c = 1$)—the initial value of DS_i (e.g., DS_1) is equal to $\rho_s z$, which is the average number of nodes in the region $(0,z)$ (see Section A of the Appendix). This means that all the nodes within the transmission range of the source correctly receive the packets. Conversely, when there is a significant level of interference, DS_1 is much smaller than $\rho_s z$, since the packet loss naturally leads to a reduction of the number of receiving nodes. From the results in Figure 3.6, it can be concluded that $DS_i \leq DS_1$, for all values of i. After the 9-th hop, DS_i tends to zero, regardless of the broadcast scheme, since all network

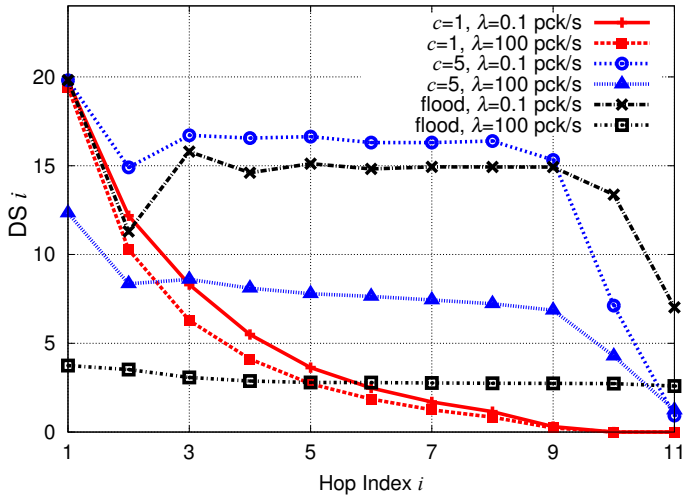

Figure 3.6: Average per-hop domain size as a function of the hop index, for $\rho_{sz} = 20$ veh. Various values of c (1 and 5) and λ (100 pck/s and 0.1 pck/s) are considered.

nodes have been covered (being completely connected).

One can observe that the domain size remains practically constant for both flooding and IF with $c = 5$ (regardless of the value of λ). At the opposite, for the IF protocol with $c = 1$, it quickly drops to zero (regardless of the value of λ) for increasing values of i. In other words, when $c = 1$ the IF protocol is not able to facilitate the propagation of the packets in a large network, even in the presence of a high node spatial density. Conversely, a value of $c = 5$ is sufficiently high to keep the forwarding process alive. Indirectly, from the scenario with $c = 5$ one can conclude that the self-interference introduced by the IF protocol is not critical, at least with the considered traffic loads, since the domain sizes experience an approximately constant decrease. In fact, if this were not the case, there would have been a sudden drop in the domain sizes. Finally, we observe that a high traffic load (λ = 100 pck/s) does not change the general behavior of the protocol, but for a strong reduction of DS_1.

In Figure 3.5.3, $\mathbb{E}[M_i]$ is shown at the first ($i = 1$) and fourth ($i = 4$) transmission domains as a function of the product $\rho_s z$, with $\lambda = 0.1$ pck/s. The IF protocol is used with two different settings of the shaping coefficient c (1 and 5). The results

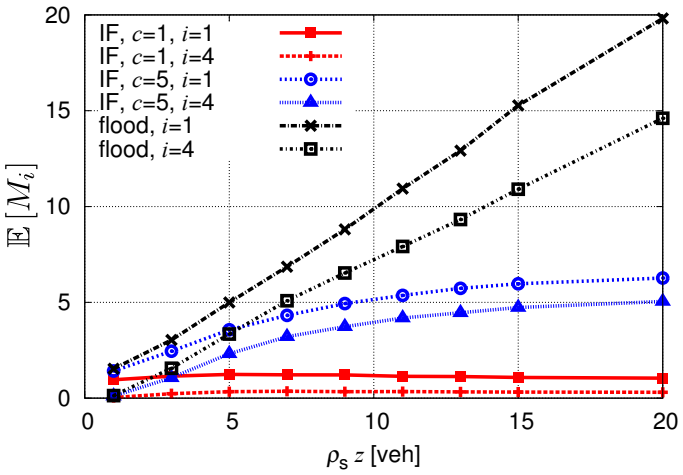

(a) $\lambda = 0.1$ pck/s

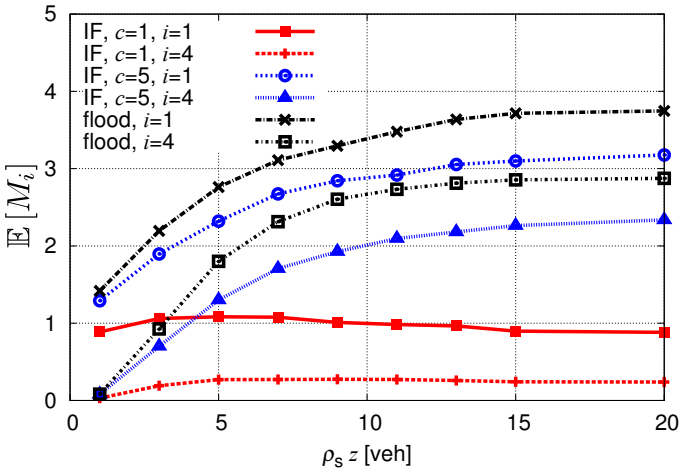

(b) $\lambda = 100$ pck/s

Figure 3.7: Average number of rebroadcast packets, as a function of $\rho_s z$. Various values of c and i are considered. The performance with the flooding protocol are also shown.

in Figure 3.5.3 are obtained with the same conditions of Figure 3.5.3, but for the value of λ which is instead fixed to 100 pck/s (high traffic region). In both figures,

the performance of flooding is also shown for comparison. From the results shown in Figure 3.7, the IF protocol shows two clearly distinguishable trends, regardless of the values of i, c, and λ: (i) $\forall i, \mathbb{E}[M_i]$ is a decreasing function of the hop index; (ii) $\forall i, \mathbb{E}[M_i]$ is an increasing function of $\rho_s z$ and converges to a saturation value which depends on the shaping parameter c. It is straightforward to verify that these general trends are coherent with those emerged by the analysis performed in Section 3.5 for ideal networks.

By comparing the performance of flooding with that of the IF protocol, it is possible to observe the consistent gain, in terms of number of rebroadcasts, guaranteed by the IF protocol in all considered scenarios. Moreover, from Figure 3.7, a significant difference between the two protocols emerges. In particular, with the IF protocol, $\mathbb{E}[M_i]$ saturates when the product $\rho_s z$ is high. In addition, the saturation value depends on the value of c but not on the value of i. In contrast, with the flooding protocol $\mathbb{E}[M_i]$ is an approximately linear function of the product $\rho_s z$. Specifically, in Figure 3.5.3 we observe that for a limited traffic intensity, the slope of the $\mathbb{E}[M_1]$ curve is equal to 1, in other words, it exactly coincides with the domain size at the same hop (DS_1) (e.g., all the nodes receive and rebroadcast the packet). After having exhaustively investigated the local mechanisms of the IF protocol through per-hop metrics, we now turn our attention to the global metrics, of particular interest from an application perspective.

We now analyze the results in terms of RE shown in Figure 3.5.3. First, we concentrate on the flooding protocol, whose behavior heavily depends on the traffic load. In fact, it is increasing when the traffic load is small, and it shows an opposite decreasing trend when the traffic load is high. When $\lambda = 0.1$ pck/s, the flooding protocol always outperforms the IF protocol, clearly at the cost of a larger number of rebroadcasts (as previously shown). Conversely, flooding suffers a performance loss when $\lambda = 100$ pck/s and the node spatial density is high ($\rho_s z \geq 10$ veh). With the exception of the case with $c = 5$ and $\lambda = 0.1$ pck/s, which will be discussed later, all the RE curves of the IF schemes exhibit the same monotonically decreasing trend, converging to a (small) saturation value. There is a region, for $\rho_s z < 5$ veh, with a very fast decrease, while for $\rho_s z \geq 10$ veh the curves are relatively constant. Taking into account the results shown in Figure 3.3, it can be observed that the decreasing

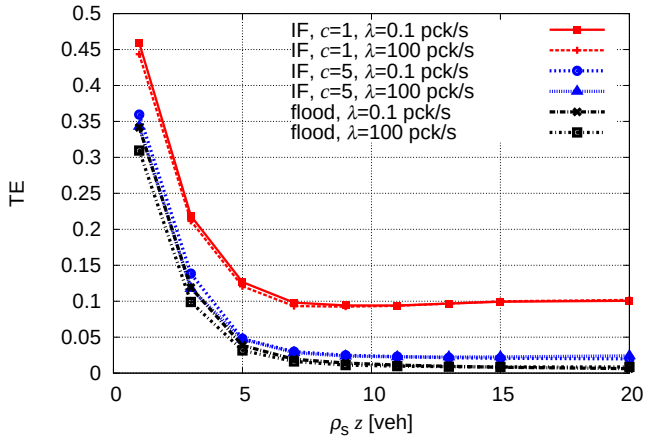

(a) TE

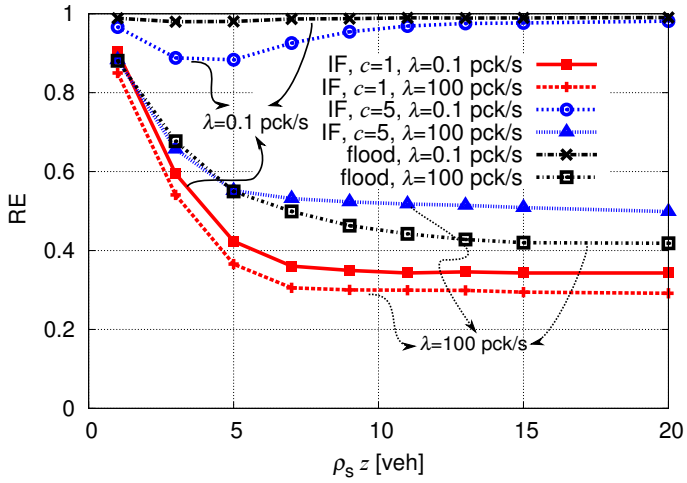

(b) RE

Figure 3.8: (a) TE and (b) RE as functions of $\rho_s z$, considering flooding (black) and the IF protocol with $c = 1$ (red) and $c = 5$ (blue). Two values of the traffic load are used, respectively, $\lambda = 100$ pck/s (dashed lines) and $\lambda = 0.1$ pck/s (solid lines).

trend appears when the ratio n_{reach}/N is small, while it disappears as the ratio n_{reach}/N

converges to 1.

The behavior of the IF protocol with $c = 5$ and $\lambda = 0.1$ pck/s is radically different from that of the others schemes. In this case, the RE is monotonically increasing, with the exception of a limited region below $\rho_s z = 5$ veh. Moreover, when the network is connected, the RE slowly continues to grow (with a small slope), until it reaches a value around 0.9. This (undesired) decreasing trend for $\rho_s z = 5$ veh can be explained as follows. When $c = 1$, the domain sizes drastically reduce (as shown in Figure 3.6). The IF protocol cannot thus exploit the node spatial density. In this situation, the maximum RE is obtained for $n_{\text{reach}}/N \ll 1$, i.e., when the network is not operational, being poorly connected. A value of $c = 5$, on the other hand, seems to be sufficiently high to exploit the node spatial density, since the domain sizes tend to remain almost constant (as shown in Figure 3.6). Even in this case, though, an excessive traffic load (e.g., $\lambda = 100$ pck/s), generates an increased amount of channel contentions (especially in the first hops), thus eliminating the advantage of the larger value of c and leading to a small RE. Therefore, one can predict the existence of an optimal value of c for given values of the average traffic load λ and of the product $\rho_s z$.

Finally, in Figure 3.9 D is shown as a function of $\rho_s z$. One can observe that in the saturation region (high values of $\rho_s z$) the flooding protocol is very sensitive to the traffic load, as shown by the "explosion" of the delay in the case with $\lambda = 100$ pck/s. Conversely, all the IF curves exhibit an "attractive" behavior, since they are slightly increasing in the region with low network connectivity (small values $\rho_s z$), while they become approximately constant in scenario with high connectivity ($\rho_s z \approx 20$). We stress the fact that all IF schemes (with $c = 1$ and $c = 5$) have approximately the same delay, in the saturation region whereas there is a gap for small values of $\rho_s z$. This behavior is mostly due to the CSMA/CA mechanism. In fact, in the poorly connected region, on average, the packets experience a small number of hops. In addition the CSMA/CA manifests its effect mostly in the very first hops experienced by the packet when the traffic load is more intense due to the proximity to the source.

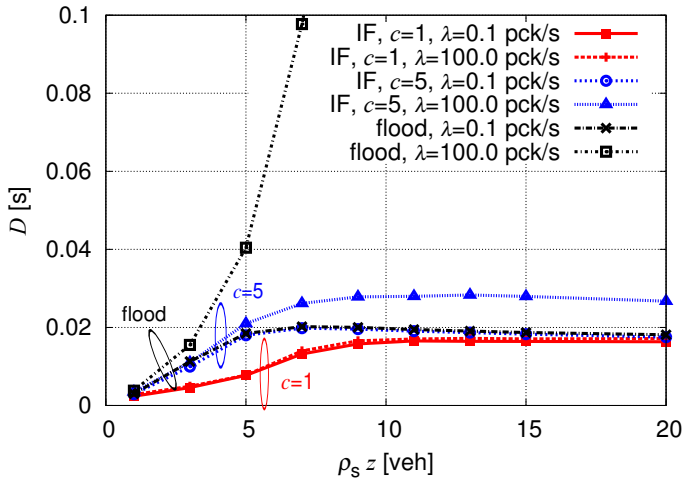

Figure 3.9: D as a function of $\rho_s z$, obtained for $\lambda = 100$ pck/s and $\lambda = 0.1$ pck/s. The curves are obtained for the IF protocol with $c = 1$, $c = 5$ and for the flooding protocol (flood).

3.5.4 On the Impact of Local Node Spatial Density Estimation

As anticipated in Subsection 4.4.1, the simulation-based performance analysis in IEEE 802.11b networks has been carried out considering local node spatial density estimation. As intuitively expected, this should lead each node to a more accurate selection of the probability of retransmission, thus optimizing the performance of the IF protocol. However, in order to further simplify the practical communication protocol to be used (more precisely, to eliminate the need for exchanging hello messages between neighbors), it is of interest to investigate the impact of the use of the estimated global node spatial density at each node. This is coherent with the theoretical analysis carried out in Section 3.5 and is meaningful for highway scenarios where a vehicle could adaptively select the value of the node spatial density depending on the period of the day (e.g., high node spatial density value during the rush hours and low node spatial density value during the night).

In Figure 3.10, we directly compare the performance of the IF protocol with $c = 5$ in scenarios with local node spatial density estimation (the simulation set-

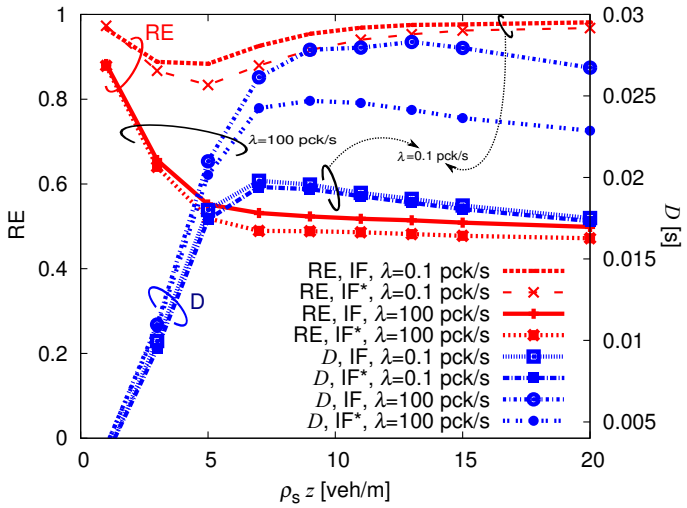

Figure 3.10: D (blue curves) and RE (red curves) as a function of $\rho_s z$, obtained for $c = 5$ and $\lambda = 100$ pck/s, $\lambda = 0.1$ pck/s. Nodes use a global value of ρ_s (IF* curves) or a local value (IF curves).

up considered in the previous subsections) and global node spatial density (denoted as IF* in the figure). In particular, our comparison is carried out, in terms of RE and delay, considering two possible values of λ (representative of high and low data traffic, respectively). As one can see, the differences, in terms of RE, are negligible for all considered data traffic levels. Considering the delay, it can be observed that, in the presence of high data traffic, the use of a global node spatial density slightly reduces the delay.

3.6 Concluding Remarks

In this chapter, we have proposed a probabilistic-based rebroadcast scheme, denoted as IF, for linear networks (e.g., highway-like vehicular ad-hoc networks). Unlike other existing approaches, the IF protocol take into account the node spatial distribution. The proposed scheme is inherently distributed. In fact, each vehicle can compute its own rebroadcast probability without relying on any central authority. On the other

hand, provided that the network is sufficiently dense, the IF protocol can automatically control the average number of rebroadcast packets at each hop by properly setting a single shaping parameter.

Chapter 4

The Impact of Mobility on Broadcast Data Dissemination

Never underestimate the bandwidth of a station wagon full of tapes hurtling down the highway.

– Andrew S. Tanenbaum

4.1 Introduction

In this chapter, we examine the problem of disseminating data in I2V IEEE 802.11 networks. Our investigation is carried out by comparing, through simulations, the performance of IF in many radically different mobility conditions: a static highway VANET (e.g., a scenario where all cars move at the same speed); a mobile highway VANET in stationary conditions; several mobile urban VANET scenarios, with junctions controlled by Traffic Lights (TLs) and Roundabouts (R)s. The performance analysis is carried out, first, from a single packet prospective (meaningful for safety-related applications) and, then from an information flow prospective. In this latter case, we evaluate the maximum amount of transferable data, in terms of throughput, from the RSU to the vehicles lying in a Region Of Interest (ROI) around a fixed Road

Side Unit (RSU). The structure of this chapter is the following. In Section 4.2, we introduce the VANET scenarios considered in our simulation analysis. Section 4.3 is dedicated to the characterization of the used mobility models. In Section 4.4, we describe the IF protocol, the considered performance metrics, and the simulation setup. In Section 4.5 and Section 4.6, we evaluate the per-packet and the per-flow system performance, respectively. Finally, conclusions are drawn in Section 4.7.

4.2 Reference Scenarios

In [104], we have originally studied the performance of IF in a multiple-lane bidirectional highway. In this work we have extend the analysis to encompass also several mobile urban scenarios constituted by a few consecutive road intersections and, therefore, characterized by a non-homogeneous vehicle distribution. The highway scenarios are described in Subsection 4.2.1 (mobile) and Subsection 4.2.2 (static), whereas the urban scenarios are described in Subsection 4.2.3. Despite their differences, the considered scenarios have the following common features.

- Each vehicle is equipped with an omni-directional antenna and is characterized by a fixed transmission range, denoted as z (dimension: [m]).
- Each vehicle is equipped with a Global Positioning System (GPS) receiver. Therefore, we assume that each vehicle knows its own position at any given time.
- Each vehicle has the same length $L_{\mathrm{v}} = 5$ m.

4.2.1 Mobile Highway Scenario

The reference mobile highway scenario is shown in Figure 4.1 and will be denoted, in the following, as $\mathrm{H}_{\mathrm{mob}}$. The road is composed by $N_{\mathrm{lane}} = 6$ adjacent lanes (3 per direction of movement), each with width equal to $w_{\mathrm{lane}} = 4$ m. As indicated in Figure 4.1, we consider a portion of a highway whose length L is set proportionally to the nodes' transmission range as follows: $L \triangleq \ell_{\mathrm{norm}} z$, where ℓ_{norm} is the adimensional

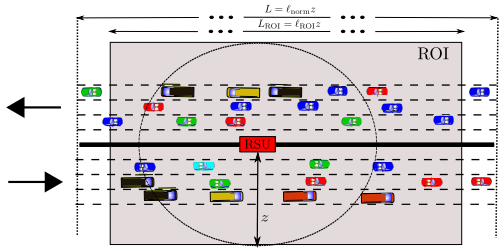

Figure 4.1: The mobile linear network topology in an highway scenario.

factor already defined in Section 3.2. The vehicles in the three lanes at the bottom are directed towards right (eastbound), whereas the vehicles in the upper three lanes are directed towards left (westbound).

The ROI is defined as the region centered around the RSU and with length $L_{\text{ROI}} = \ell_{\text{ROI}} z$, where $\ell_{\text{ROI}} < \ell_{\text{norm}}$. All the nodes lying in the ROI are implicitly interested in the reception of the packets generated by the RSU. We assume that the highway operates under stationary and stability conditions. In other words, the entering flux of vehicles in the ROI is the same of the exiting flux of vehicles: more precisely, when a node exits from the network area, it is assumed to re-enter instantaneously. The number of vehicles in the ROI is the random process $N_{\text{ROI}}(t)$.

Under the above assumptions, it is possible to define the instantaneous linear vehicle spatial density within the ROI as $\rho_{\text{s}}^{\text{R}}(t) \triangleq N_{\text{ROI}}(t)/L_{\text{ROI}}$ (dimension: [veh/m]). Conversely, the time-independent linear vehicle spatial density (dimension: [veh/m]) within the whole highway section is

$$\rho_{\text{s}} \triangleq \frac{N}{L}. \tag{4.1}$$

We stress the fact that the highway portion depicted in Figure 4.1 will be considered as a quasi-monodimensional network,[1] since the width of the road is much shorter than its length ($\ell_{\text{norm}} z \gg N_{\text{lane}} \cdot w_{\text{lane}}$) and of the node transmission range that is in the order of the hundreds of meter as shown in Section 2.3.

[1] In Figure 4.1, for illustration purposes the scale is not realistic.

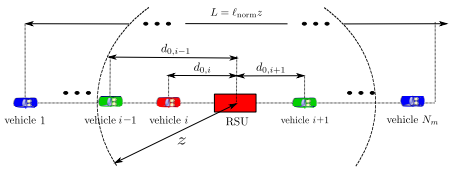

Figure 4.2: The linear network topology in a single lane of a highway scenario.

4.2.2 Static Highway Scenario

A static highway scenario can be obtained by taking a snapshot of the mobile scenario or, equivalently, on the basis of the single-lane static model introduced in Section 3.2. An N_{lane} static scenario could be obtained by simply replicating N_{lane} times a single lane, and by moving the source in the middle of the network. This scenario is denoted as H_{sta}. A representative realization of the topology of any lane of the highway is shown in Figure 4.2. In this case, since border effects can be neglected, the length of the highway section is $L = \ell_{\text{norm}} z = \ell_{\text{ROI}} z$. There is a single source RSU, placed in the center of the network and identified by the index 0. The m-th lane ($m \in \{1,2,\ldots,N_{\text{lane}}\}$) contains N_m nodes (each node is uniquely identified by an index $j \in \{1,2,\ldots,N_m\}$), where N_m is a random variable. As usual, the positions of the N_{m} nodes are determined by a monodimensional Poisson point process with parameter $\rho_{\text{s}}/N_{\text{lane}}$ (dimension: [veh/m]), where ρ_{s} is the vehicle linear spatial density defined in Subsection 4.2.1. By replicating this process N_{lane} times, we deploy in the highway a random number of vehicles, given by the superposition of N_{lane} Poisson point processes. By the property of the superposition of Poisson processes, the overall random process (in the horizontal axis) is still a Poisson process of parameter ρ_s. For comparison purposes, we assume that overall number of vehicles in the N_{lane} lanes is given by the random variable N, as in the mobile case. In other words, we assume that

$$N = \sum_{n=1}^{N_{\text{lane}}} N_m.$$

4.2.3 Mobile Urban Scenarios

While a highway can easily be represented by a multi-lane straight road, a meaningful representation of an urban scenario is more difficult. For this reason, we consider a few urban scenarios, obtained by simple variations of a starting reference scenario. In particular, we have taken into account a general scenario, constituted by a single horizontal (east-west) road and several intersecting vertical (south-north) roads, whose number is denoted as $N^{\mathrm{v}}_{\mathrm{road}}$. In all considered scenarios, $N^{\mathrm{v}}_{\mathrm{road}} \in \{0,1,2\}$. When $N^{\mathrm{v}}_{\mathrm{road}} = 0$ the vehicles can only proceed east or west, as there is no route towards north and south. On the contrary, when $N^{\mathrm{v}}_{\mathrm{road}} > 0$ at each junction the vehicles can move towards all four cardinal directions.

Each road has a length equal to $L_{\mathrm{road}} = \ell_{\mathrm{norm}} z$ and is composed by N_{lane} adjacent lanes: $N_{\mathrm{lane}} - 1$ are reserved for the vehicles entering the network (inbound) and the remaining one is reserved for the vehicles exiting the network (outbound). We foresee two types of junctions: (i) the first one is regulated by a roundabout (R) with radius 10 m, whereas (ii) the second one is regulated by traffic lights (TLs), whose number is equal to the number of available directions. During its duty cycle, a TL stays green for $T_{\mathrm{green}} = 55$ s, red for $T_{\mathrm{red}} = 60$ s, and amber for $T_{\mathrm{amber}} = 5$ s. Obviously, the TLs lying in orthogonal roads have an orthogonal duty cycle with respect to those in the horizontal road, under the assumption that the amber and green colors are orthogonal with respect to the red color. Moreover, in the presence of multiple intersections we assume that all TLs in the horizontal road are synchronized. The number of junctions will be denoted as N_{jun}.

The vehicles enter the considered spatial region according to a *global* (i.e., over all inbound lanes of the scenario at hand) time-domain Poisson process of parameter γ (dimension: [veh/s]). Once generated, each vehicle appears, according to a uniform selection, in one of the available inbound lanes. Once a vehicle enters the network, it follows a random itinerary along the available roads, randomly determining its direction in correspondence to each junction. The vehicle generation process stops as soon the number of generated vehicles reaches a pre-fixed value denoted as N (as in

the highway scenario).[2]

By construction, the urban scenario is square-shaped with edges of fixed length $L = L_{\text{road}}$. The RSU is always placed at the center of the square region and we define the ROI as the square region centered around the RSU with edges of fixed length $L_{\text{ROI}} = \ell_{\text{ROI}} z$. Despite its square shape, urban scenario cannot be considered as a purely bi-dimensional scenario, since the positions of the vehicles are still constrained by the road infrastructure, which encompasses only the presence of horizontal and vertical roads. Conversely, if we ignore the relatively small area of the junctions, the horizontal and vertical roads can be considered as quasi-monodimensional spaces. This assumption allows one to define the following approximate *per-road* vehicle linear spatial density:

$$\rho_{\text{s}} \simeq \frac{N}{\left(1 + N^{\text{v}}_{\text{road}}\right) L_{\text{road}}} \tag{4.2}$$

where 1 horizontal road and $N^{\text{v}}_{\text{road}}$ vertical roads are considered. The symbol used to denote the per-road vehicle spatial density is the same used in the highway scenario. However, while in the highway scenario the definition of ρ_{s} given in (4.1) is exact, in the current case the per-road linear spatial density given by (4.2) is an approximation. In the special case with $N^{\text{v}}_{\text{road}} = 0$, the linear vehicular density on the right-hand side of (4.2) becomes exact. Similarly to the highway scenarios, in the urban scenarios $\rho^{\text{R}}_{\text{s}}(t)$ denotes the instantaneous average per-road (linear) vehicle spatial density in the ROI, where the average is carried out over all roads—in fact, different roads in the ROI are likely to have, at the same instant, different instantaneous vehicle spatial densities. In other words, $\rho^{\text{R}}_{\text{s}}(t)$ is obtained from (4.2) by replacing N with $N_{\text{ROI}}(\text{t})$.

We consider eight instances of the above common urban topology reference scenario, by varying the junction type and the values of $N^{\text{v}}_{\text{road}}$ and N_{jun}. A generic urban scenario instance will be denoted as $\text{X}^{\text{Z}}_{\text{Y}}$, where X indicates the junction type (R or TL), Y indicates the number of junctions ($N_{\text{jun}} \in \{1,2\}$), and Z denotes the presence of vertical roads—in particular, "Z=hv" when $N^{\text{v}}_{\text{road}} > 0$, and "Z=h" when $N^{\text{v}}_{\text{road}} = 0$. The eight considered urban scenario and their main parameters are summarized in

[2] We remark that, as in the highway scenario, once N cars are generated, they will remain in the scenario till the end of the simulations. In fact once a car exits from an outbound lane it re-enters immediately from an in-bound lane.

Table 4.1: Parameters of the considered mobile urban scenarios.

Scen.	$N^{\mathrm{v}}_{\mathrm{road}}$	N_{jun}	Jun. Type	N_{lane}
$\mathrm{TL}^{\mathrm{h}}_1$	0	1	TL	3
$\mathrm{TL}^{\mathrm{h}}_2$	0	2	TL	3
$\mathrm{R}^{\mathrm{h}}_1$	0	2	R	2
$\mathrm{R}^{\mathrm{h}}_2$	0	2	R	2
$\mathrm{TL}^{\mathrm{hv}}_1$	1	1	TL	3
$\mathrm{TL}^{\mathrm{hv}}_2$	2	2	TL	3
$\mathrm{R}^{\mathrm{hv}}_1$	1	1	R	2
$\mathrm{R}^{\mathrm{hv}}_2$	2	2	R	2

Table 4.1. The urban topologies with $N^{\mathrm{v}}_{\mathrm{road}} = N_{\mathrm{jun}} > 0$, (namely, $\mathrm{TL}^{\mathrm{hv}}_1$, $\mathrm{TL}^{\mathrm{hv}}_2$, $\mathrm{R}^{\mathrm{hv}}_1$, and $\mathrm{R}^{\mathrm{hv}}_2$) are shown in Figure 4.3 and Figure 4.4. The scenarios with $N^{\mathrm{v}}_{\mathrm{road}} = 0$ can be obtained by simply removing the vertical roads from the topologies shown in Figure 4.3 and 4.4, still leaving the junctions. Although this may not be realistic from a practical viewpoint (there is no point in using a R or TL if there is no crossing road), it is meaningful from an information dissemination viewpoint (the propagation of information along a single direction may be meaningful).

The approximate definition of *per-road* vehicular linear spatial density given in (4.2) is valid regardless of the urban topology at hand, i.e., the type of the horizontal road (with single or double TL or R). However, the dynamic behavior of $\rho^{\mathrm{R}}_{\mathrm{s}}(t)$ can vary significantly in the various cases.

4.3 Mobility Models

In this section, we characterize the mobile highway and urban scenarios introduced in Section 4.2, emphasizing the different mobility characteristics of these topologies. The mobile highway scenario will be generated using VanetMobiSim, while the mobile urban scenarios will be generated using SUMO, two mobility simulator already

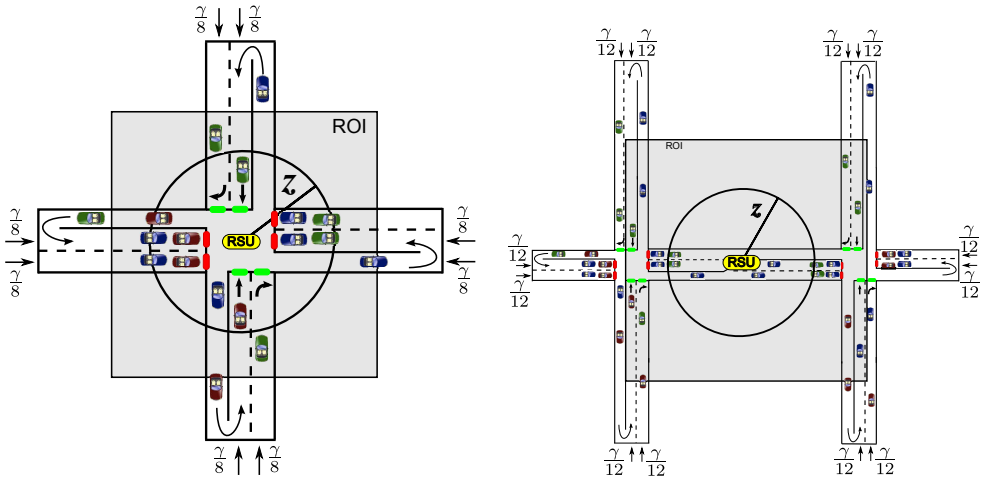

(a) (b)

Figure 4.3: (a) $\mathrm{TL}_1^{\mathrm{hv}}$, and (b) $\mathrm{TL}_2^{\mathrm{hv}}$ urban topologies, with $N_{\mathrm{road}}^{\mathrm{v}} > 0$, and the main parameters set as in Table 4.1.

introduced in Section 2.2. As a by-product of this choice, the comparative results presented here can also be used to reciprocally validate these software. In all the scenarios considered in this section, $\ell_{\mathrm{ROI}} = 8$ and $\ell_{\mathrm{norm}} = 10$, with the only exception of the $\mathrm{H}_{\mathrm{sta}}$ scenario, where $\ell_{\mathrm{norm}} = 8$.

4.3.1 Highway Scenarios

While in the static highway scenario (introduced in Subsection 4.2.2) all vehicles have zero relative speed differences (equivalently, do not move), in the mobile highway scenario (introduced in Subsection 4.2.1), the IDM-LC mobility model defined in Subsection 2.2.1 is used to characterize the mobility of vehicles—please recall that the RSU is static. Table 4.2 summarizes the significant parameters of the IDM-LC model, tuned according to the empirical data presented in [116].

In order to validate the highway model, in Figure 4.5 we show the time evolution of $\rho_{\mathrm{s}}^{\mathrm{R}}(t)$, for $v^{\min} = 20$ m/s and $v^{\max} = 50$ m/s. Three values of ρ_{s} (namely, 0.2 veh/m, 0.3 veh/m, and 0.5 veh/m) are considered. The results in Figure 4.5 show that, regard-

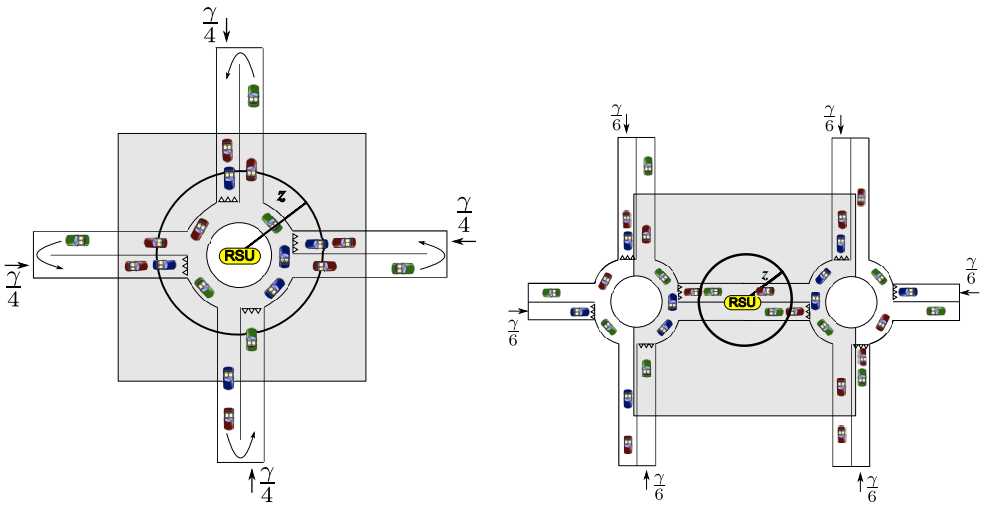

(a) (b)

Figure 4.4: (a) R_1^{hv}, and (b) R_2^{hv} urban topologies, with $N_{road}^{v} > 0$, and the main parameters set as in Table 4.1.

less of the value of ρ_s, after an initial transient period, $\rho_s^R(t)$ finally converges to a stationary value. This guarantees that the considered mobile scenario can effectively model a stationary highway.

4.3.2 Urban Scenarios

The mobility of the vehicles in urban scenarios was modeled using the KWG model introduced in Subsection 2.2.2. The values of the relevant parameters of the KWG mobility model are summarized in Table 4.3. We remark that with respect to the IDM-LC model adopted in the H_{mob} scenario (Table 4.2), the value of v^{max} is significantly smaller.

In Figure 4.6, the time evolution of the instantaneous average per-road (linear) vehicle spatial density (in the ROI) is analyzed in the two urban scenarios (with vertical crossing roads and TLs) considered in Figure 4.3: (a) TL_1^{hv}, and (b) TL_2^{hv}. In Figure 4.7 the same results are shown with respect to the Rs scenarios, namely, (a)

Table 4.2: Main parameters of the IDM-LC and MOBIL models and their (empirical) values.

Parameter (i)	Value
$v^{\min}$	30 m/s
$v^{\max}$	40 m/s
T	2 s
a	0.6 $\mathrm{m/s^2}$
b	0.9 $\mathrm{m/s^2}$
P	0.5
b_{safe}	4 $\mathrm{m/s^2}$
a_{thr}	0.2 $\mathrm{m/s^2}$
$\mathrm{L_v}$	5 m

$\mathrm{R}_1^{\mathrm{hv}}$, and (b) $\mathrm{R}_2^{\mathrm{hv}}$. In each case, various values of the average per-road vehicle spatial density ρ_{s} (namely, 0.05 veh/m, 0.1 veh/m, 0.15 veh/m, and 0.2 veh/m) are considered. By observing the results in Figure 4.6 and 4.7s, the following comments can be carried out.

- According to the results in Figure 4.6 (a) and Figure 4.6 (b), in the scenarios with *TLs* $\rho_{\mathrm{s}}^{\mathrm{R}}(t)$, after an initial transient, exhibits a cycle-stationary behavior, with period roughly equal to $T_{\text{green}} + T_{\text{red}} + T_{\text{amber}} = 120$ s. The cycle-stationary nature of $\rho_{\mathrm{s}}^{\mathrm{R}}(t)$ is especially evident in $\mathrm{TL}_1^{\mathrm{hv}}$ scenario (case (a)). Note that the average (over time) value of $\rho_{\mathrm{s}}^{\mathrm{R}}(t)$ in the $\mathrm{TL}_2^{\mathrm{hv}}$ scenario (case (b)) is slightly smaller than the "target value" ρ_{s} in the case with $\rho_{\mathrm{s}} = 0.2$ veh/m. This is mostly due to the fact that the ROI is placed between the two traffic junctions, as shown in Figure 4.3 (b).

- In the scenarios with Rs, from the results in Figure 4.7 (a) and Figure 4.7 (b) one can conclude that $\rho_{\mathrm{s}}^{\mathrm{R}}(t)$, after the initial transient, tends to a stationary condition. At regime, there are still minor oscillations, which do not seem periodic. Unlike the scenarios with TLs, in both scenarios $\mathrm{R}_1^{\mathrm{hv}}$ and $\mathrm{R}_2^{\mathrm{hv}}$, the steady-state

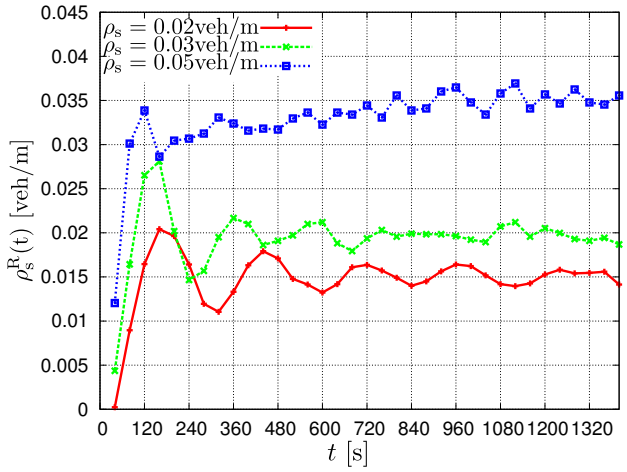

Figure 4.5: The time evolution of $\rho_s^R(t)$ within the ROI in the H_{mob} scenario. Three possible values for ρ_s are considered: 0.02 veh/m, 0.03 veh/m, and 0.05 veh/m. In all cases, $v^{min} = 20$ m/s and $v^{max} = 40$ m/s.

average (over time) value of $\rho_s^R(t)$ tends to be greater than the "target" value ρ_s, especially for high values of ρ_s. This happens because a R junction has a smaller vehicle capacity of a TL junctions.

4.3.3 Comparison Between Highway and Urban Scenarios

First of all, by comparing Figure 4.5 with respect to Figure 4.6, and Figure 4.7, one can observe that with both SUMO and VanetMobiSim it is not straightforward to obtain a "target" value of ρ_s. However, SUMO seems to guarantee a more refined control on the vehicle spatial density than VanetMobiSim. A better control could be obtained by considering wider areas and a larger number of vehicles, but this would lead to an explosion of the simulation time.

Secondly, due to the significant differences between urban and highway scenarios, we have chosen different values of speeds and vehicle spatial densities. In order to emphasize this difference, in Figure 4.8 (a) we show the dispersion diagrams of the instantaneous per-road vehicle spatial density $\rho_s^R(t)$ with respect to the node

Table 4.3: Values of the parameters used by SUMO for the generation of mobile urban scenarios.

Parameter (i)	Value
$v^{\max}$	20 m/s
a	0.8 m/s^2
b	4.5 m/s^2
σ	0.5
τ	1 s
L_v	5 m

speed $v(t)$, in the H_{mob} and TL_1^{hv} scenarios. In the H_{mob} scenarios, three values of ρ_s (0.02 veh/m, 0.03 veh/m, and 0.05 veh/m) are considered, whereas in TL_1^{hv} scenario four values of ρ_s (0.05 veh/m, 0.1 veh/m, 0.15 veh/m, and 0.2 veh/m) are considered. In Figure 4.8 (b), an enlarged version of the dispersion diagrams of the H_{mob} scenarios of Figure 4.8 (a) are shown. For each specific dispersion diagram, each point, the pair $(\rho_s^R(t), v(t))$ corresponds to a specific time instant of the simulation. From the results in Figure 4.8, one can observe that in the TL_1^{hv} scenarios the dispersion diagrams tend to aggregate around the average density-speed pair. Furthermore—as expected—in all cases the average speed is a decreasing function of the average vehicle spatial density. However, one can observe that the average vehicle speeds are generally lower than the maximum speeds set in Table 4.2 and Table 4.3. In the TL_1^{hv} scenario, this behavior can be easily justified by the presence of the junctions. On the other hand, in the H_{mob} scenario this can be motivated by the fact that the vehicles do not encounter a sufficiently long free space to reach their target speed. Nonetheless, the maximum speed value (around 30 m/s) observed in H_{mob} scenario with $\rho_s = 0.02$ veh/m is realistic for a stationary highway in most of the western countries.

Finally, in Figure 4.9 we show the dispersion diagrams $(\rho_s^R(t), v(t))$ relative to the horizontal road of the TL_2^{hv} scenario, considering the four values of ρ_s already considered in Figure 4.8 (a) for the TL_1^{hv} scenario. In this case, the ROI, placed bet-

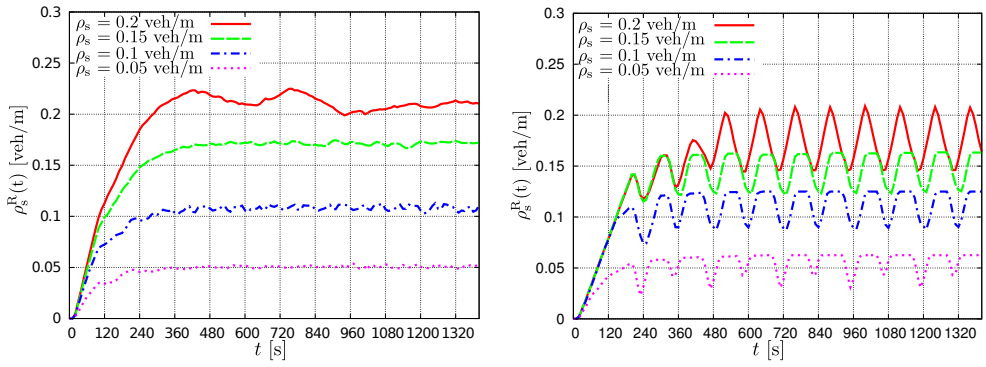

(a) (b)

Figure 4.6: Average instantaneous per-road (linear) vehicle spatial density (in the ROI) in the two urban scenarios considered in Figure 4.3: (a) TL_1^{hv}, and (b) TL_2^{hv}. In each case, various values of ρ_s are considered.

ween two junctions, surrounds both intersections (with TLs) and the horizontal road between them. Therefore, the mobility in the horizontal road between the traffic junctions is influenced by both TL plants, thus yielding to a much higher speed variance with respect to the average (with respect to all roads in the ROI) behavior shown in Figure 4.8 (a).

4.4 Irresponsible Forwarding in Mobile Scenarios

The performance analysis of the IF protocol (introduced in Section 3.3) will be carried out considering both per-packet and per-flow metrics. The former type of metrics is suitable to validate the performance of applications, such as safety-related applications, where a single broadcast packet needs to be disseminated. The latter type of metrics, instead, is suitable to evaluate the performance of applications, such the content distribution applications, where a significant amount of information needs to be distributed using a flow of hundreds of broadcast packets. In all cases, these metrics will be evaluated through simulations.

Two per-packet performance metrics are considered: (i) the Reachability (RE),

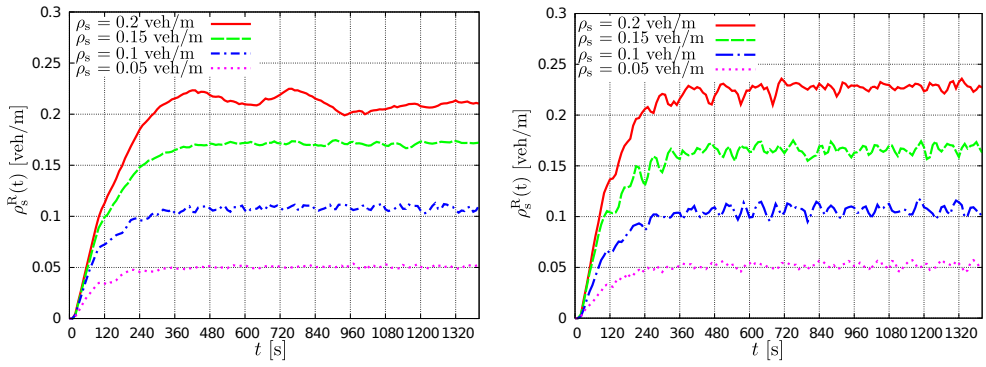

(a) (b)

Figure 4.7: Average instantaneous per-road (linear) vehicle spatial density (in the ROI) in the two urban scenarios considered in Figure 4.4: (a) R_1^{hv}, and (b) R_2^{hv}. In each case, various values of ρ_s are considered.

as defined in Section 3.5.1; (ii) the average end-to-end delay at the i-th hop, denoted as D_i (dimension: [s]) and computed as follows. In each simulation run, we average over the delays experienced by all vehicles which receive the packet at the i-th hop in order to derive the average end-to-end delay at the i-th hop. The average end-to-end delay at the i-th hop is evaluated as:

$$D_i = \sum_{j=1}^{i} D_{\text{hop}-j} \tag{4.3}$$

where $D_{\text{hop}-j}$ is the delay of the j-th hop along the multi-hop path.

A single per-flow performance metric is considered, namely the instantaneous throughput. This metric, associated to a specific vehicle, is defined as

$$S^{(i)}(t) \triangleq \frac{N_{\text{p-rx}}^{(i)}(t)}{N_{\text{p}}}$$

where $N_{\text{p-rx}}^{(i)}(t)$ is the number of received packets till time t by the considered i-th vehicle—assuming that the simulation run starts at time 0—and N_{p} is the number of packets of the flow.

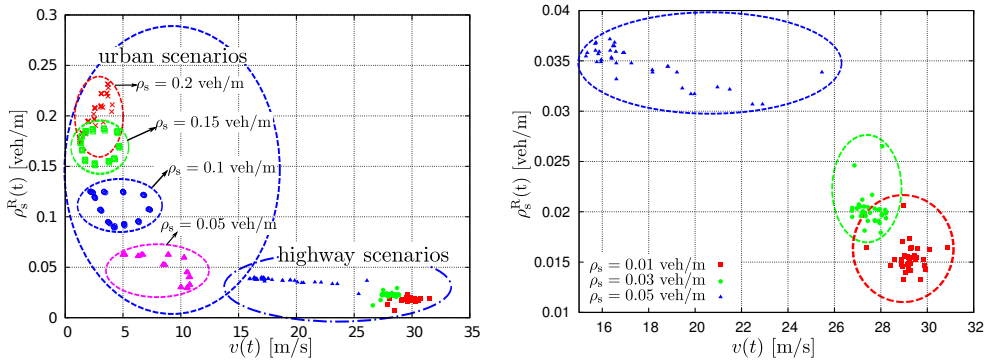

(a) (b)

Figure 4.8: Average instantaneous per-road (linear) vehicle spatial density (in the ROI) ($\rho_s^R(t)$) as a function of the average speed ($v(t)$), parametrized with respect to the time t, considering various values of ρ_s. In (a) there is a comparison between H_{mob} and TL_1^{hv} scenarios, while in (b) there is an enlargement of the H_{mob} scenario of (a).

We finally observe that, differently from static scenarios the local spatial density $\rho_s^v(t)$, used in equation (3.3), can be significantly different from the per-road vehicle spatial $\rho_s^R(t)$, because the mobility of the vehicles determines consistent variations, especially in urban scenarios.

4.4.1 Simulation Setup

In this analysis we are interesting in validating the idea of disseminating data from a RSU, using a multihop broadcast protocol, instead of limiting to single-hop transmission as commonly done in practice. We have implemented IF on top of the IEEE 802.11b model present in ns-2.34 [48], after fixing some bugs present in this release, as described in Section 2.4, and we have adopted the deterministic Friis free-space propagation model, as defined in Section 2.3. The transmission range varies according to the desired value of the product $\rho_s z$. We use the standard value of the contention window, ($CW_{min} = 31$) and the lowest data rate (1 Mbit/s). As usual, the RSU generates packets according to a Poisson transmission distribution with parameter λ

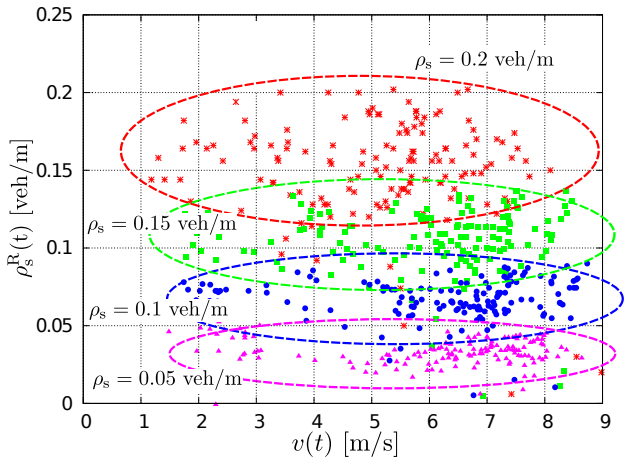

Figure 4.9: Average instantaneous vehicle spatial density (in the horizontal road of the ROI) ($\rho_s^R(t)$) as a function of the average speed ($v(t)$), parametrized with respect to the time t, considering various values of ρ_s.

(dimension: [pck/s]). . In other words, our analysis of urban scenarios aims at investigating the impact of traffic control (through TLs or Rs). The extension of our analysis to urban scenarios with tall buildings around the streets (e.g., in Manhattan, New York), which create wireless “waveguides," would require careful modeling of the propagation conditions.

In the case of *per-packet* (Section 4.5) and *per-flow* (Section 4.6) performance analysis, the packet size (PS) will be fixed to either 100 bytes or 1000 bytes. The considered performance metrics will be evaluated by averaging over 100 simulation runs.

- In the *per-packet* analysis, a single simulation run corresponds to a randomly generated VANET scenario (nodes' generation and associated mobility patterns) and to the transmission of $N_p = 1000$ packets by the RSU. At the end of each simulation run, the delay and reachability are obtained by averaging over the delays and reachabilities of all vehicles. The final results of the simulation are then obtained by averaging over the results of all simulation runs.

- In the *per-flow* analysis, in each simulation run we consider the same randomly generated VANET scenario (nodes' generation and mobility pattern)—in other words, the scenario generated at the first run is kept unchanged in the following 99 runs. However, run by run the transmission scheduling of the $N_{\mathrm{p}} = 1000$ packets by the RSU varies, according to their generations. At the end of each simulation run, we evaluate the throughput experienced by all vehicles within the ROI. Finally, after all simulation runs, we evaluate the average throughput experienced by each vehicle. Note that the fact of keeping the VANET scenario fixed allows to reevaluate the throughput of each vehicle, thus emphasizing the role of the specific path followed by each vehicle.

In both per-packet and per-flow performance analysis, simulations will be carried out considering the (highway and urban) scenarios described in Section 4.2, using the mobility models introduced and characterized in Section 4.3. Therefore, the only information source in the network is the RSU, always placed at the center of the ROI.

As considered in Section 4.2 for the characterization of the mobility models, in Section 4.5 and Section 4.6 the performance analysis of the IF protocol will be carried out considering $\ell_{\mathrm{ROI}} = 8$ and $\ell_{\mathrm{norm}} = 10$ in all scenarios but the $\mathrm{H}_{\mathrm{sta}}$ scenario, where $\ell_{\mathrm{norm}} = 8$. In all cases, the shaping factor c of the IF protocol in equation (3.3) will be set to 5.

In order to obtain fair results, in all the comparisons carried out in Section 4.5 and Section 4.6, we fix the same we fix a target per-road density ρ_{s} in every scenario. As a consequence of that, the number of nodes N varies from scenario to scenario. In particular, if we fix a target per-road density ρ_{s}, from the equation (4.2) we obtain that the overall number of nodes is given by:

$$N = \rho_{\mathrm{s}} L_{\mathrm{road}} \left(1 + N_{\mathrm{road}}^{\mathrm{v}}\right),$$

where $\rho_{\mathrm{s}} L_{\mathrm{road}}$ is the number of per-road nodes.

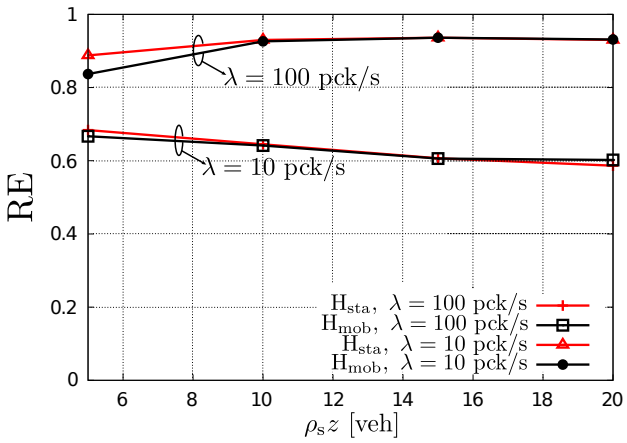

Figure 4.10: RE, as a function of $\rho_s z$, in the H_{sta} and the H_{mob} scenarios. Two values of λ are considered, namely, 10 and 100 pck/s.

4.5 Per-packet Performance of IF

4.5.1 Highway Scenarios

Although the static (H_{sta}) and mobile (H_{mob}) highway scenarios have the same road topology, they are characterized by very different dynamic conditions. A direct comparison of the performance of the IF protocol in these two cases allows to clearly understand the impact of dynamic conditions in a highway scenario. In Figure 4.10, the RE is shown as function of $\rho_s z$, considering two values of λ (10 pck/s and 100 pck/s). From the results in Figure 4.10, it emerges clearly that in a stationary highway scenario the behavior of a broadcast protocol such as IF is not significantly affected by the dynamic state of the vehicle. In fact, for a given value of λ, the performance experienced in a mobile scenario is basically identical (but for minor differences at low values of $\rho_s z$) to that in a static scenario, because the mobility has no effect on the performance of IF, due to the stateless nature of the broadcast protocol.

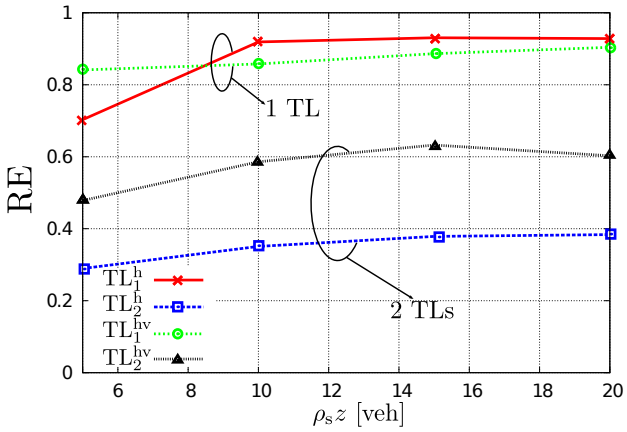

Figure 4.11: RE as a function of $\rho_s z$, in the TL_1^{hv}, TL_2^{hv}, TL_1^h, and TL_2^h urban scenarios. In all cases $\lambda = 10$ pck/s.

4.5.2 Urban Scenarios

In Figure 4.11, the RE obtained in urban scenarios with TLs is shown as a function of $\rho_s z$. All four urban scenarios with TLs shown in Table 4.1 are considered. In all cases, $\lambda = 10$ pck/s. From the results in Figure 4.11, it can be concluded that the number of TLs has a strong impact on the RE. In fact, the performance with one TL is better, regardless of the presence of an intersecting vertical road, than the performance with two TLs. Depending on the number of TLs, the following comments can be carried out.

In the presence of one *TL*, it can be observed that in the TL_1^{hv} scenario (there is an intersecting vertical road) the RE has roughly the same behavior (slightly increasing with respect to $\rho_s z$) of that in the highway scenarios. This can be easily justified. In fact, when the TL in one of the two intersecting roads is green, the vehicle configuration along this road is quite similar to the highway scenario, with the exception of a lower average speed and a smaller number of lanes: therefore, the behavior is similar. Conversely, when the TLs of this road become red (the other road has green TLs, i.e., it behaves as described before), there are two local clusters of highly connected static vehicles, thus leading to a higher probability of successful packet forwarding.

In the TL_1^h scenario (there is no intersecting vertical road), the RE is lower than that of the TL_1^{hv} scenario for small values of $\rho_s z$ and then becomes higher for increasing values of $\rho_s z$. Since there is no intersecting vertical road, connectivity is completely "delegated" to the horizontal road. When the TLs are green, if $\rho_s z$ is too small the VANET becomes sparse, connectivity is lost, and the RE is low. For sufficiently large values of $\rho_s z$, even when the TLs are green, the moving cars are sufficiently dense and packet forwarding is guaranteed. In particular, the RE becomes slightly higher than in the TL_1^{hv} scenario, as there is a reduced number of forwarding collisions around the junction—recall that in the TL_1^{hv} case, when the TLs along the horizontal road are green there are clusters of stopped vehicles in the vertical road.

In presence of two *TLs*, the RE exhibits a radically different behavior with respect to the previous case and significantly lower values. Recalling the structure of the ROI shown in Figure 4.3 (b), the results in Figure 4.11 can be interpreted as follows. In the TL_2^h scenario (there are no intersecting vertical roads), when both TLs (along the horizontal road) are red, there are two separated clusters of connected static vehicles, relatively distant from the RSU. Therefore if a packet cannot reach one of these clusters, say the leftmost one, all the vehicles at the left side of the network will not receive the packets transmitted by the RSU.

Unlike the case with one TL, in the scenarios with two TLs the presence of intersecting vertical roads has a very beneficial impact: in Figure 4.11, the RE in the TL_2^{hv} scenario is significantly higher, regardless of the value of $\rho_s z$, than in the TL_2^h scenario. In fact, the presence of vertical intersecting roads guarantees that even if the TLs along the horizontal road are red, there will be some vehicles, coming from the vertical roads, which turn towards the RSU, thus guaranteeing connectivity in the street segment, between the two junctions, in the middle of which the RSU is placed.

In Figure 4.12, the RE obtained in urban scenarios with Rs is shown as a function of $\rho_s z$—this figure is the equivalent of Figure 4.11, with the same settings, but for the replacement of TLs with Rs. A very different behavior, with respect to the urban scenarios with TLs can be observed.

- In the scenarios *without vertical crossing roads* (R_1^h and R_2^h), the RE is very high, regardless of the number of Rs. In other words, the number of round-

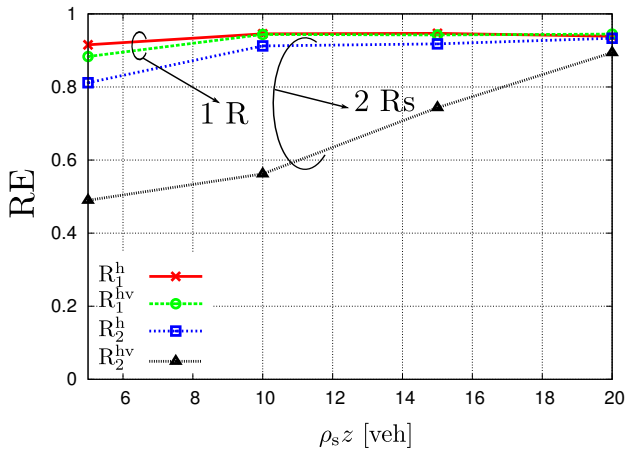

Figure 4.12: RE, as a function of $\rho_s z$, in the R_1^{hv}, R_2^{hv}, R_1^h, and R_2^h urban scenarios. In all cases $\lambda = 10$ pck/s.

abouts has no impact. In fact, even in very dense scenarios (large values of $\rho_s z$), the roundabouts make the traffic along the horizontal road very fluid, so that the VANETs are almost always connected and packet forwarding is effective.

- In the scenarios *with vertical crossing roads* (R_1^{hv} and R_2^{hv}), the RE is high only in the presence of a single R (R_1^{hv})—for $\rho_s z \geq 10$, the RE is almost the same of that in the scenarios with no crossing roads. Unlike the TL_2^{hv} scenario, in the R_2^{hv} (two vertical crossing roads), the RE is low for small values of $\rho_s z$, and reaches a high value (around 0.8) only for very large values of $\rho_s z$. In other words, it turns out that in the case with two consecutive Rs and low vehicle spatial density, the Rs tend to reduce the vehicle flow along the horizontal road (this does not happen in the TL_2^h scenario), making the VANET around the RSU disconnected.

In Figure 4.13, we analyze the delay, as a function of the hop number, in the scenarios (a) with TLs and (b) Rs. The obtained results (with the slight exception of TL_2^{hv} in Figure 4.13 (a)) show that in all scenarios the delay is basically the same till

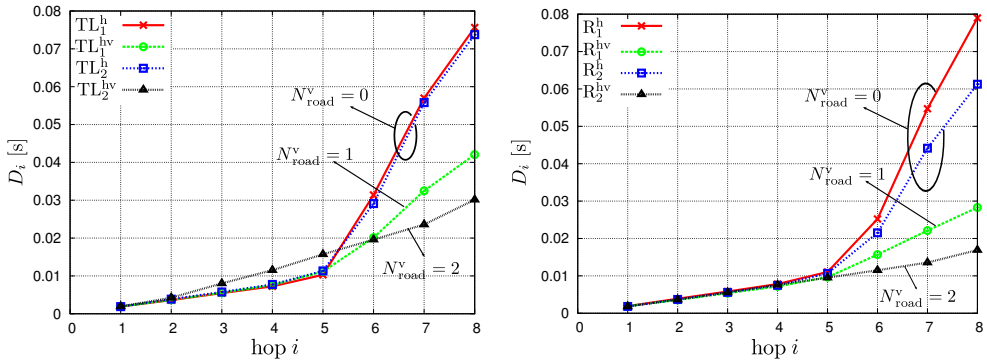

(a) (b)

Figure 4.13: Delay, as a function of the hop index, in scenarios (a) with TLs and (b) with Rs. In all cases, $\lambda = 10$ pck/s, and $\rho_s z = 20$ veh.

the 5-th hop. Since $\ell_{ROI} = 8$ (as stated at the end of Subsection 4.4.1) and $z = 100$ m, the side of the square ROI is $\ell_{ROI} z = 800$ m. Being the RSU placed at the center of the ROI, if the VANET is completely connected, then the transmitted packet reaches all vehicles in at most 5 hops in all scenarios. This is confirmed by the results shown in Figure 4.14, discussed in the following. After the 5-th hop, the presence of vertical crossing roads has a relevant impact.

- In the *absence* of vertical crossing roads (TL_1^h, TL_2^h, R_2^h, R_2^h), the delay increases steeply. This is due to the fact that most of the vehicles in the ROI have already received the packet and, therefore, drop newly received versions of the same packet. If a vehicle has not received the packet yet, it will have to wait longer.

- In the *presence* of vertical crossing roads (TL_1^{hv}, TL_2^{hv}, R_2^{hv}, R_2^{hv}), the delay increases smoothly. This is due to the fact that the vehicles entering the ROI from the vertical roads may retransmit the packet and, therefore, keep the delay short. Recall, however, that in the presence of vertical crossing roads the RE is lower than in the absence of them. In other words, fewer vehicles receive the packet but, when they do, the delay is more shorter.

As anticipated above, in Figure 4.14 the reachability is shown as a function of

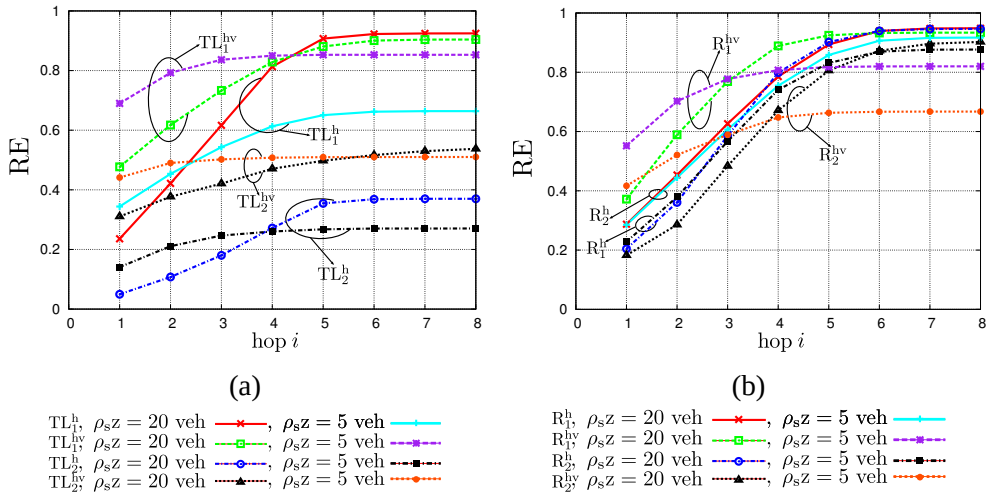

Figure 4.14: RE, as a function of the hop index, in scenarios (a) with TLs and (b) with Rs. In all cases, $\lambda = 10$ pck/s, and $\rho_s z = 20$ veh.

the hop number, considering scenarios (a) with TLs and (b) with Rs. In both cases, two representative values of $\rho_s z$, namely 5 veh (low vehicle density) and 20 veh (high vehicle density), are considered. Characteristic trends can be observed in both the cases with TLs and Rs. From Figure 4.14 (b)) we observe that in the scenarios with Rs without vertical roads (R_1^h and R_2^h) the value of $\rho_s z$ has, basically, no impact. In all the other cases, namely, scenarios with TLs (Figure 4.14 (a)) and scenarios with Rs with vertical roads, it can be observed that, for each specific scenario, at the first hops, the RE is higher for $\rho_s z = 5$ veh, whereas for larger number of hops it becomes higher for $\rho_s z = 20$ veh. This behavior can me motivated as follows. With $\rho_s z = 5$ veh the network is weakly connected and a very small number of vehicles can be physically reached by the RSU. For this reason, at the very first hops almost all the reachable nodes receive the packet. On the contrary, due to the scarce connectivity in this condition it is very difficult to reach all the reachable nodes. We finally observe that, coherently with the results of Figure 4.13, in all cases, either with TLs or Rs, the maximum reachability is approximately achieved at the 5-th hop.

4.6 Per-flow Performance of IF

In this section we try to characterize the maximum amount of transferable data from the RSU to the vehicles passing through the ROI, by measuring the throughput, as defined in Section 4.4. Our goal is to derive an optimal strategy for content distribution applications, in order to maximize the amount of transferred data, by tuning systems parameters such as λ and PS. We assume that the RSU transmits, every 100 s, a new information flux constituted by $N_{\mathrm{p}} = 1000$ equal size packets. We have considered two values of λ, respectively 10 and 100 pck/s, and two values of PS, respectively, 100 and 1000 bytes, leading to 4 different configurations. Since N_{p} is fixed, the duration of the transmission is solely determined by λ (10 or 100 s), while the PS determines the total amount of transmitted information (100 Kbytes or 1 Mbytes). We observe that the configuration ($\lambda = 100$ pck/s, PS=1000 bytes) represents a saturation condition since the RSU emits packets with a data rate of 800 Kbit/s (80% of the theoretical data rate of 1 Mbps). Conversely, the configuration ($\lambda = 10$ pck/s, PS=100 bytes) leads to an highly unsaturated condition, since the data rate is equal 8 Kbit/s (0.8% of the theoretical data rate). The remaining configurations ($\lambda = 10$ pck/s, PS=1000 bytes) and ($\lambda = 100$ pck/s, PS=100 bytes) are both characterized by a data rate of 80 Kbit/s (8% of the theoretical data rate), and they allow to evaluate the impact of the transmission duration (respectively 100 and 10 s) on the throughput.

In all scenarios taken in account we set $\rho_{\mathrm{s}} z = 20$ veh, thus yielding to a per-road density ρ_{s} equal to 0.02 veh/m. Therefore, considering that $\ell_{\mathrm{norm}} = 10$, each scenario has a number of nodes give by $N = 200\left(1 + N^{\mathrm{v}}_{\mathrm{road}}\right)$, but in H_{sta} scenario, where $N = 160$. The node indexes are assigned at the end of the simulation, after having ordered, decreasingly, the measured values. More precisely, vehicle 1 will have the highest throughput and the last vehicle will have the lowest one.

Finally, it has to be pointed out that in all the mobile scenarios there is a significant number of nodes with a zero throughput since they are lying, by construction, outside the ROI at the moment of the transmission. Moreover, the scenarios have typically a different number of vehicles N, because of the assumption of having the

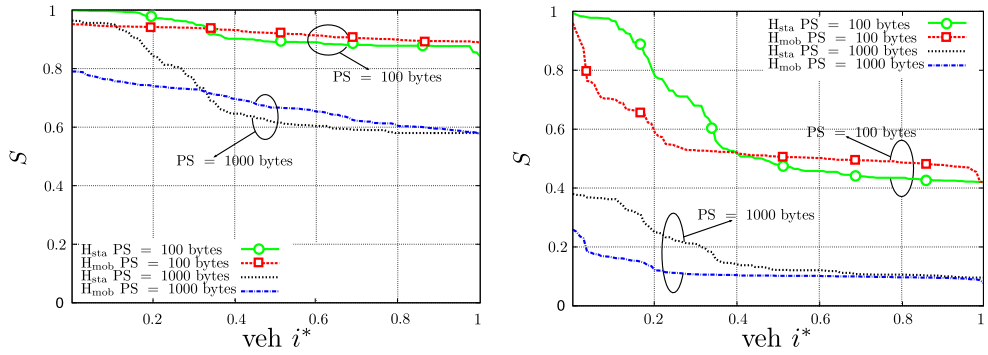

(a) (b)

Figure 4.15: Throughput, as a function of the normalized vehicle index (i^*), in H_{sta} and H_{mob} scenarios with two values of λ: (a) 10 pck/s and (b) 100 pck/s. In both cases, two values of PS are considered (100 bytes and 1000 bytes).

same average per-road vehicular density in all the horizontal and vertical roads. For these two reasons, in order to carry out a meaningful throughout comparison among scenarios with a different number of nodes, it is necessary to consider a normalized node index, defined as $i^* = \frac{i}{N}$, $i^* \in [0,1]$.

4.6.1 Highway Scenarios

In Figure 4.15, the throughput is shown, as a function of the normalized vehicle index (i^*), considering (a) $\lambda = 10$ pck/s and (b) $\lambda = 100$ pck/s. For each value of λ, we consider static (H_{sta}) and mobile (H_{mob}) scenarios, and two values of PS (100 bytes and 1000 bytes). We observe that the saturated configuration (curves with PS=1000 bytes in Figure 4.15 (b)) has unsatisfactory performance on both mobile and static scenarios. On the opposite hand, the low-traffic load configuration ($\lambda = 10$ pck/s, PS=100 bytes) shown in (Figure 4.15 (a), exhibits a throughput greater then 0.9 for all the vehicles in the ROI in both static and mobile scenarios. Therefore, we can consider the data rate of 8 Kbit/s (0.8% of the theoretical throughout) as the maximum sustainable rate.

From the results in Figure 4.15 (a) and Figure 4.15 (b), it emerges that the highest throughput (vehicle index 1) is obtained in the static (H_{sta}) scenarios. However,

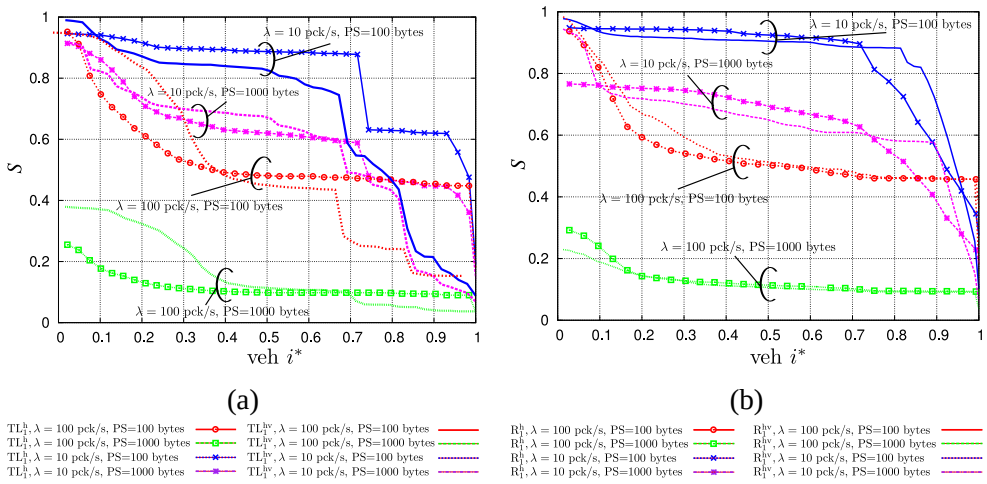

Figure 4.16: Throughput, as a function of the normalized vehicle index (i^*) (a) in the TL_1^h and TL_1^{hv} scenarios and in (b) the R_1^h and R_1^{hv} scenarios. We have considered two values of PS, respectively 100 and 1000 bytes, and two values of λ, respectively,s 10 pck/s and 100 pck/s.

while in the mobile (H_{mob}) scenarios the throughput experienced by all vehicles is similar, in the static scenarios there are relevant differences between the highest and lowest values. This is expected, as in a mobile scenario there are "less privileged" vehicles which stay longer near the RSU. However, this effect appears clearly only if the transmission duration is sufficiently long, as emerges by comparing the two configurations with a data rate equal to 80 Kbit/s. In fact, when the transmission duration is only 10 s as in the case ($\lambda = 100$ pck/s and PS=100 bytes) in Figure 4.15(b), the H_{mob} scenario exhibits an unfair trend, similarly to the H_{sta}. We finally observe that among the two 80 Kbits/s configurations does not emerge a clear winner, neither in the H_{mob} or H_{sta} scenario.

4.6.2 Urban Scenarios

In Figure 4.16 is shown the throughput as a function of the normalized node index (i^*), obtained in urban scenarios with $N_{jun} = 1$, considering both (a) TL and (b) R junctions. We have examined 4 combinations of PS and λ, by considering two values

of PS (100 bytes and 1000 bytes) and two values of λ (10 pck/s and 100 pck/s). According to Figure 4.16, the throughput in the Rs scenario has very smooth variations and it behaves similar to the highway scenarios. This happens because a roundabout allow the vehicles to passing it without stopping, thus yielding to a more fluid vehicular traffic, reducing the local spatial-temporal variation of the vehicle density. In particular, in the scenario without vertical roads, the vehicles have always the priority at the junction and they never stop. Conversely, in the TLs scenario the spatial density significantly varies both in time and space, thus motivating the more irregular throughput shape exhibited by the TLs scenarios. From Figure 4.16 we also observe that the Rs scenarios are insensitive with respect to the presence of a vertical roads, differently from the TLs scenarios are significantly affected by the presence of a vertical road. We finally remark that among the configurations with the data rate of 80 Kbit/s, in the Rs scenarios the configuration with $\lambda = 10$ pck/s exhibits a clear advantage with respect to the $\lambda = 10$ pck/s (as in the highway), while in the TLs scenarios, there is no a clear winners. Despite of these significant differences, the Rs and the Ts scenarios offer quite similar performance in terms of absolute value, especially in the scenarios without vertical roads.

4.6.3 Comparative Analysis

Finally, in Figure 4.17 we directly compare the throughput, as a function of the normalized node index, in highway and urban scenarios. In order to make a meaningful comparison, we only consider the urban scenarios without vertical crossing roads (i.e., TL_1^h, TL_2^h, R_1^h, and R_2^h). For easy of comprehension, we focus on a single configuration (PS=1000 bytes, $\lambda = 10$ pck/s) characterized by transmitting a packet flow of 1 Mbytes in 100 s, with a data rate of 80 Kbit/s. Figure 4.17 offers many insights on the characteristics of the different analyzed scenarios. First of all, both Rs scenarios exhibit a trend similar to which of the H_{mob} scenario, with slightly lower maximum values and slightly higher minimum values. This behavior is reasonable, since the Rs scenarios without vertical roads can be considered as a kind of low-speed highway, with a flux of vehicles that is regular both in space and time.

Conversely, we observe that the TL_1^h scenario behaves like the H_{sta} scenario with

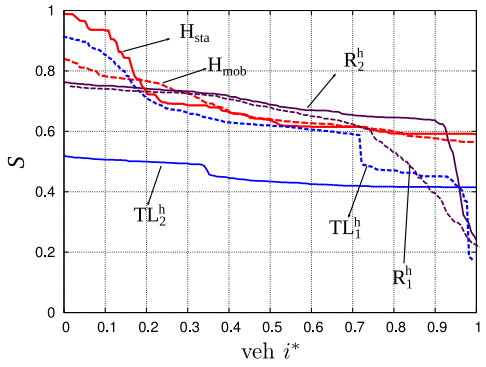

Figure 4.17: Throughput, as a function of the normalized vehicle index (i^*) in various urban and highway scenarios. We consider PS=1000 bytes and $\lambda = 10$ pck/s.

the exception of having slightly worse performance and a more irregular shape. This behavior can be easily motivated by considering that for approximately half of the transmission time the traffic lights are red, thus leading to the the formation of two clusters of static vehicles around the RSU.

Finally, we observe that TL_2^h scenario has a different behavior from the other scenarios with smaller maximum and average throughput. This performance can be motivated by considering that the position of the RSU that is in the middle between the two junctions, instead of being near the TLs as in the TL_1^h scenario. In this condition, the RSU is in spatial region where the local spatial density is smaller than the average. For this reasons the retransmissions are weak and they can be easily be interrupted for the lack of connectivity.

4.7 Concluding Remarks

In this chapter, we have analyzed the impact of the vehicular mobility on the dissemination of broadcast data in I2V networks by means of numerical simulations, supported by realistic mobility models and by considering both highway and several types of urban scenarios. In all cases, communications have relied on the use of a probabilistic forwarding protocol, namely IF. The analysis has been carried out analyzing both per-packet and per-flow system performance.

From a *single packet* perspective, the performance of a stateless broadcast protocol, such as IF, has shown to be insensitive to the vehicle mobility level, at least in highway scenarios. On the other hand, in urban scenarios the performance of the IF protocol is affected by the number and the type of functions (either TLs or Rs), since they induces significant spatial-temporal variations of the local vehicle density and of the VANET connectivity. Also, the *information flow* analysis offers several insights on the impact of vehicles' mobility on the performance of the IF protocol. Our simulations have shown that a urban road with traffic lights can be well approximated with a static highway, while a road with roundabouts have more similarities with a mobile highway scenario. This suggest that, despite of the macroscopic differences, the mobile and the static highway scenarios can be used as approximated model of complex urban topologies.

Chapter 5

Decentralized Detection in Clustered Vehicular Networks

5.1 Introduction

In this chapter, we consider a V2I scenario, where the vehicles act as a distributed wireless sensor network. In particular, we analyze the performance of vehicular decentralized detection schemes, based on the observation, by all vehicles of a VANET, of a spatially constant phenomenon of interest. Our approach consists in the creation, during a downlink phase, of a clustered VANET topology during fast broadcast data dissemination, from the Access Point (AP), through a novel clustering protocol, denoted as Cluster-Head Election IF (CHE-IF). This clustered topology is then exploited, during an uplink phase, to collect information from the vehicles and perform distributed detection. Our results highlight the existing trade-off between decision delay and energy efficiency. Unlike classical sensor networks for distributed detection, the proposed vehicular distributed detection schemes exploit the natural vehicle clustering and have to cope with their "ephemeral" nature. More precisely, vehicle mobility has a direct impact on the maximum amount of data which can be collected, thus leading to the concept of decentralized detection on the move.

The goal of this work is to analyze the performance of decentralized detection

schemes in vehicular networks, when a spatially constant phenomenon of interest (e.g., the average smog level or traffic situation on a given road) has to be detected. The CHE-IF protocol is used to determine, during the downlink phase, the "virtual" clusters and the corresponding CHs. The so-formed clustered vehicular network is then used, during the uplink phase, for data aggregation and/or fusion. In particular, local per-cluster fusion is carried out at the CHs. Various vehicular clustered topologies are analyzed, showing the trade-off between decision delay and energy efficiency. Moreover, on the basis of realistic simulation results, we estimate the average cluster lifetime, thus deriving insights on the maximum data which can be reliably collected and processed by clustered VANETs. Unlike typical sensor networks, where the clustered topology is imposed by the designer, in a VANET scenario the clustered topology naturally emerges and needs to be effectively exploited.

This chapter is structured as follows. In Section 5.2 and Section 5.3, preliminaries on the system and communication models, respectively, are provided. In Section 5.4, the performance of decentralized detection techniques in clustered vehicular networks is analyzed and discussed, considering realistic VANET clustered topologies. In Section 5.5, by characterizing the lifetime of a cluster, we derive conclusions on the amount of data which can be processed by a clustered VANET. Finally, concluding remarks are given in Section 5.6.

5.2 System Model

We consider a static one-dimensional wireless network with N (receiving) nodes. Each node is uniquely identified by the indices $i \in \{1,2,\ldots,N\}$. The source node, denoted as node 0, is placed at the left end of the network. The assumption of static nodes is not restricting and, in Section 5.5, we will provide more details on the applicability of the obtained results to mobile networks. The system model is the same used during the rest of the thesis and presented in Section 3.2. In particular, the reference scenario is represented by Figure 3.1. All vehicles observe a spatially constant phenomenon, i.e., a phenomenon whose status does not change from vehicle to vehicle along the road. For example, vehicles could monitor if the average smog (or

fog) level overcomes a critical threshold: the VANET would declare that it does if it happens for most of the road. The observed phenomenon can be generically defined as

$$H = \begin{cases} H_0 & \text{with probability } p_0 \\ H_1 & \text{with probability } 1 - p_0 \end{cases}$$

where $p_0 \triangleq \mathbb{P}\{H = H_0\}$, being $\mathbb{P}\{\mathscr{A}\}$ the probability that the event $\mathscr{A}$ happens. The value H_0 can be interpreted as the fact that the underlying physical phenomenon is, on average (along the road), below a given threshold, whereas the value H_1 can be interpreted as the fact that the underlying physical phenomenon is, on average (along the road), above a given threshold.

5.3 Clustered VANET Creation and IVCs

In this section, we derive the communication model for the vehicular distributed detection scenario. First, a downlink phase is envisioned, where the AP broadcasts a query to all vehicles in the network, in order to obtain information about the phenomenon of interest. During this phase, the CHE-IF protocol, besides guaranteeing fast information dissemination, automatically creates a clustered architecture, by opportunistically exploiting the ephemeral vehicular clusters. After a clustered network topology has been generated, during the uplink phase the decentralized detection task is performed by transferring the sensed data from the vehicles to the AP, through multi-hop communications and considering local fusion in each vehicular cluster.

5.3.1 Downlink

The philosophy of CIF protocol, proposed in [84], is to establish a weak artificial packet flow, having the task of discovering the presence of naturally formed clusters. Then, this information is exploited in order to optimize the forwarding procedure, increasing the reliability and the transmission efficiency, but without building up a true clustered infrastructure.

In this work, we propose a derivation of CIF, denoted as CHE-IF, that introduces some mechanisms expedient to make CIF a protocol capable to efficiently construct

a stable clustered infrastructure. The new CHE-IF protocol is a totally decentralized protocol, since each node designates its own CH without pursuing a common global consensus. The purpose is that of obtaining an operative clustered topology in the shortest time, in order to start the data collection process as soon as possible. This behavior fits well with the intrinsic dynamic nature of a VANET, characterized by continuous topology changes that vanish the hypothetical advantages of a centralized clusterization protocol. Moreover, a refinement of the cluster structure can be performed once the collection process is started, making small adjustment of the network topology.

The CHE-IF protocol is designated in order to choice a single CH among the retransmitting nodes of a transmission domain. This ideally yields to the creation of an unique set of connected CHs able to coverage the entire area of interest. After choosing the CHs, the cluster will naturally form. In fact, the nodes not designated as CHs become children of the nearest CH, leading to the formation of clusters of similar dimension.

The CHE-IF protocol defines 3 types of packet: (i) Cluster Initialization Packet (CIP); (ii) Probe Packet (PP); (iii) Cluster Confirmation Packet (CCP). The CHE-IF protocol is composed by three phases. In the first one, through the exchange of some dedicated packets (CIPs and PPs), every node fills a temporary routing table containing the list of the potential CHs in its transmission range. During the second phase, that starts after a time $T_{\mathrm{w}}^{\mathrm{CIP}}$ (set proportionally to the length of the network), each node elects its CH basing on the information contained in its routing table.[1] Due to the lack of global consensus, it is not guarantee that the decision of the nodes match together. For instance, some nodes could designate a CH that does not believe of being a CH. For this reason, there also a third phase, a confirmation phase, during which the AP sends a a special packet that is retransmitted only by the CHs (with probability 1). Listening to the CCP, the network nodes can become aware of the identity of the true CHs.

While the second and the third are relatively simple, the first phase is more com-

[1] A given node elects itself as a CH for the i-th transmission domain if it is the farthest retransmitter of its transmission domain.

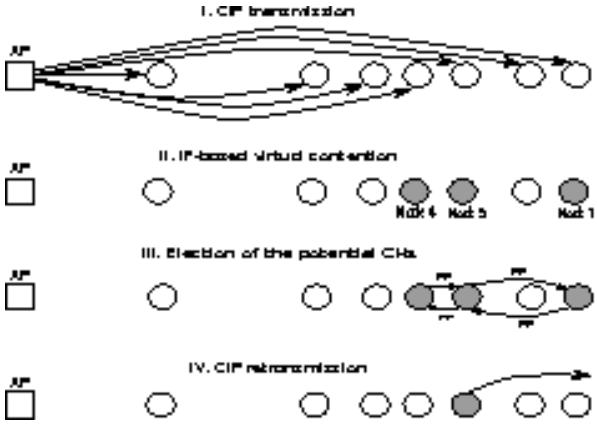

Figure 5.1: CH election of the CHE-IF protocol.

plicated, as it requires, at every hop, 4 steps that are graphically represented in Figure 5.1 and described in the following.

The first phase consists of the transmission of the CIP by a node of the $(i-1)$-th transmission domain, which leads to the identification of the *i*-th transmission domain (the AP in the case of 1-th transmission domain). The CIP is sent with a transmit power $P_{\mathrm{t}}^{\mathrm{CIP}}$ and contains an unique identification (ID) and the source address of the AP.

The second step derives directly from the IF protocol and is a sort of "virtual contention." In particular, every node in the *i*-th transmission domain decides to become or not a potential forwarder by performing the same probabilistic election mechanism of the IF protocol. The winners of this contention will begin the third step, while the others will simply discard the packet.

The third step derives from the concept of "ephemeral cluster." Once a node wins the first virtual contention, it schedules the retransmission of a very short packet, denoted as Probe Packet (PP). A PP bears just two information: (1) the unique identification (ID) of the CIP; (2) the distance from the node in the previous transmission domain from which it has received the packet. The PPs are intrinsically single hop, i.e., they are not forwarded. A PP is transmitted with a power defined as $P_{\mathrm{t}}^{\mathrm{PP}} = 0.25 P_{\mathrm{t}}^{\mathrm{CIP}}$,

in order to reduce network congestion, since a node is interested only in signaling its presence to its neighbors, and with a high priority, in order to reduce the overall latency. Moreover, a low transmission power allows to reduce channel interference. The specific power and priority setting of a PP have to be tuned according to the used MAC protocol, as shown in [84]. After winning the virtual contention, every potential forwarder sends a PP. It then waits for a short interval, denoted as $T_{\mathrm{w}}^{\mathrm{PP}} \frac{d}{z}$, where $T_{\mathrm{w}}^{\mathrm{PP}}$ is a proper constant. If, within this interval, it receives at least a PP containing a value of distance larger than its own, it stops and discards the packet (in fact, there is some other better placed forwarder); conversely, it retransmits the CIP. In the worst case, when a collision between two or more PPs happens, this selection mechanism fails and no node of the cluster is elected. In this case, the retransmitter in the previous transmission domain will retransmit the CIP for restarting the CH designation procedure at the *i*-hop. This can happen until a maximum of 3 times, otherwise the whole designation procedure is considered failed.

The fourth step corresponds to the transmission of the CIP from the designated forwarding nodes at the *i*-th transmission domain.

5.3.2 Uplink

The uplink phase exploits the clustered structure created during the downlink phase. More precisely, during the uplink phase, the data acquired by the N vehicles of the VANET are transmitted to the final AP. Note that, unlike a regular sensor network, the created VANET can be used as long as its structure does not break, due to vehicle mobility. In other words, there is a maximum amount of data which can be collected, as investigated in detail in Section 5.5.

The observed signal at the *i*-th vehicle can be expressed as

$$r_i = \begin{cases} 0 + w_i & \text{if } H = H_0 \\ s + w_i & \text{if } H = H_1 \end{cases} \qquad i = 1, \ldots, N \tag{5.1}$$

where $\{w_i\}$ are additive noise samples. Note that s is considered as a deterministic parameter. Assuming that the noise samples $\{w_i\}$ are independent random variables

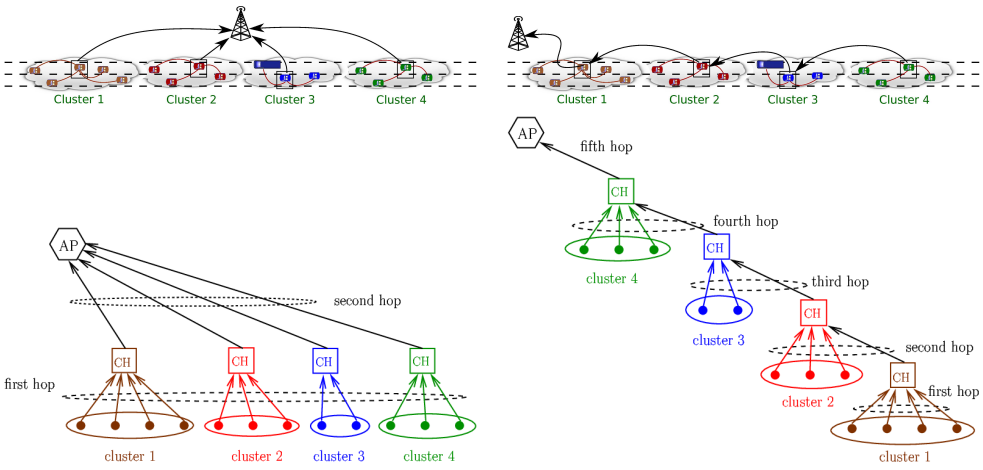

Figure 5.2: Network topologies (upper part) and their logical representations (lower part): (a) direct communications between CHs and (b) multi-hop communications between CHs and AP.

with the same Gaussian distribution $\mathcal{N}(0,\sigma^2)$, the common observation signal-to-noise ratio (SNR) at the vehicles, denoted as $\mathrm{SNR}_{\mathrm{vehicle}}$, can be defined as $\mathrm{SNR}_{\mathrm{vehicle}} \triangleq s^2/\sigma^2$ [82]. Each vehicle makes a decision comparing its observation r_i with a threshold value $\tau = s/2$ and computes a local decision $u_i = U(r_i - \tau)$, where $U(\cdot)$ is the unit step function. Note that a vehicle could transmit one single decision per packet or, by collecting consecutive phenomenon observations, it could transmit packets with more decisions. The strategy selection depends on the desired trade-off between data and overhead per transmitted packet. However, investigating this aspect goes beyond the scope of our work.

Suppose that during the downlink phase the CHE-IF protocol has lead to the creation of $n_c < N$ cluster. Each vehicle can communicate only with its local CH. Possible clustered topologies are represented in Figure 5.2, according to the particular strategy for communications towards the AP. In particular, when a sufficiently high transmit power is available, all CHs can communicate directly with the AP, as shown in Figure 5.2 (a). On the other hand, when the transmit power is not sufficiently high,

multi-hop communications are required to transfer the information from the CHs towards the AP, as shown in Figure 5.2 (b).

Once the clustered VANET topology has been determined, distributed detection has to be carried out, as described in the following section.

5.4 Decentralized Detection: Performance Analysis

According to the theoretical framework presented in [82], in the presence of a spatially constant phenomenon the key performance indicator is the probability of decision error on the final estimate at the AP and can be expressed as:

$$\begin{aligned} P_{\mathrm{e}} &= \mathbb{P}\{\widehat{H}=H_1|H_0\}\mathbb{P}\{H_0\}+\mathbb{P}\{\widehat{H}=H_0|H_1\}\mathbb{P}\{H_1\} \\ &= p_{10}p_0+p_{01}(1-p_0) \end{aligned} \tag{5.2}$$

where $\widehat{H}$ is the phenomenon estimate and the probabilities $p_{\ell m}$ ($\ell, m = 0,1$) depends on the particular network structure (number of clusters and sensors per cluster) and the considered fusion rule. The simplest fusion rule which can be considered, either at a CH or at the AP, is the following majority rule:

$$\Gamma(x_1,\ldots,x_M,k) \triangleq \begin{cases} 0 & \text{if } \sum_{m=1}^{M} x_m < k \\ 1 & \text{if } \sum_{m=1}^{M} x_m \geq k \end{cases} \tag{5.3}$$

where $x_1,\ldots,x_M$ are M binary data ($x_m \in \{0,1\}$) to be fused together and $k = \lfloor M \rfloor$+1 is the decision threshold. While a majority fusion rule guarantees a good performance in the presence of a phenomenon with equally likely states and balanced network topology, other fusion rules need will be considered in more unbalanced scenarios.

The average probability of decision error, with respect to the clustering configuration, can then be computed as follows:

$$\overline{P}_{\mathrm{e}}(\mathrm{SNR}_{\mathrm{sensor}}) = \mathbb{E}_{\mathscr{D}}\left[P_{\mathrm{e}}\left(\mathrm{SNR}_{\mathrm{sensor}}|\mathscr{D}\right)\right]. \tag{5.4}$$

where the average is performed over the probability mass function (PMF) of the number of nodes per cluster, denoted as $\mathscr{D} \triangleq (\mathscr{D}_{\mathrm{c}}^{(1)}, \mathscr{D}_{\mathrm{c}}^{(2)}, \ldots, \mathscr{D}_{\mathrm{c}}^{(n_{\mathrm{c}})})$. The first parameter

Table 5.1: Main IEEE 802.11 network simulation parameters for CHE-IF.

Packet Size	100 bytes
Carrier Freq.	2.4 GHz
Data rate	1 Mbps
$CW_{\min}$	31
$T_{\mathrm{w}}^{\mathrm{PP}}$	10 ms
$T_{\mathrm{w}}^{\mathrm{CIP}}$	200 ms

of interest for our analysis is the PMF of the number of nodes in a single cluster, which is needed to obtain the average performance with respect to the clustering configuration in (5.4). To this end, we have simulating the downlink phase by implementing CHE-IF on top of the IEEE 802.11b model present in ns-2.34 [48], after fixing some bugs present in this release, as described in Section 2.4. We have employed the deterministic Friis free-space propagation model, as defined in Section 2.3. The transmission range varies according to the desired value of the product $\rho_{\mathrm{s}}z$. The other relevant parameters are summarized in Table 5.1. We have considered a linear network with $L = 8z$ and different values of $\rho_{\mathrm{s}}z$ (e.g., 5, 8, 10, 12, 15, 20 veh), where $\rho_{\mathrm{s}} = 0.02$ veh/m. Note that values of $\rho_{\mathrm{s}}z$ smaller than 10 are representative of disconnected VANETs, whereas values larger than 10 are typical of (highly) connected networks. We also observe the values of $P_{\mathrm{t}}^{\mathrm{PP}}$ and $P_{\mathrm{t}}^{\mathrm{CIP}}$ are set in order to obtain the desired value of z. The final PMF is obtained by averaging over 500 trials, where in each simulation run a different network topology is generated.

In Figure 5.3, the PMF is shown for different values of $\rho_{\mathrm{s}}z$. As one can observe, the shape of the PMFs is the same (approximately a Poisson-like function) regardless of the value of $\rho_{\mathrm{s}}z$. The only difference is that the realizations of the cluster size increases. In fact, in this case there is a larger number of nodes in the transmission range of the nodes and, therefore, it is more likely to obtain a larger cluster for increasing values of $\rho_{\mathrm{s}}z$. Note that in (5.4) also the number of clusters n_{c} is needed. For the ease of simplicity, we set this value to the average $\overline{N}_{\mathrm{c}}$: from our simulations, we have obtained $\overline{N}_{\mathrm{c}} = 7$ for $\rho_{\mathrm{s}}z = 5$ veh and $\overline{N}_{\mathrm{c}} = 7$ for $\rho_{\mathrm{s}}z = 8, 5, 10, 12, 15, 20$ veh.

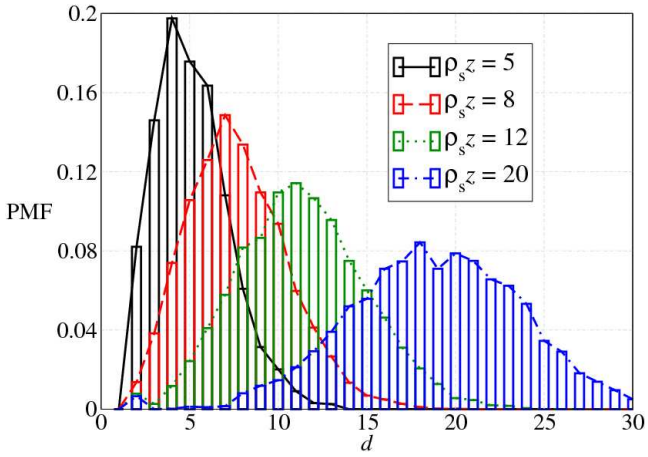

Figure 5.3: PMF of the number of nodes per cluster for different values of $\rho_s z$.

In Figure 5.4, the probability of decision error is shown, as a function of the vehicle observation SNR, in a scenario with CHs directly connected with the AP. Different values of $\rho_s z$ are considered. As one can see, the larger is the value of $\rho_s z$, the better is the performance. This has to be expected, since a larger value of $\rho_s z$ corresponds to a larger average value of sensors per cluster (as observed in Figure 5.3). In fact, it is well known that the performance of decentralized detection schemes improves by using a larger amount of sensors [82].

When the scenario depicted in Figure 5.2 (b) is considered, the same majority-like fusion rule can be considered, where, information fusion is performed over each communication between CHs and between the last CH and the AP. In this case, however, the delay is much higher, since a larger amount of time is needed before obtaining the final estimate of the phenomenon. In particular, the delay can be written as[2]

$$D = n_h T_h$$

where T_h is the time necessary to transfer 1 bit from one level to another (at each level the packet size does not increase) and n_h is the maximum number of hops between the

[2]We are implicitly assuming that the time needed by signal processing, i.e., fusion, is negligible.

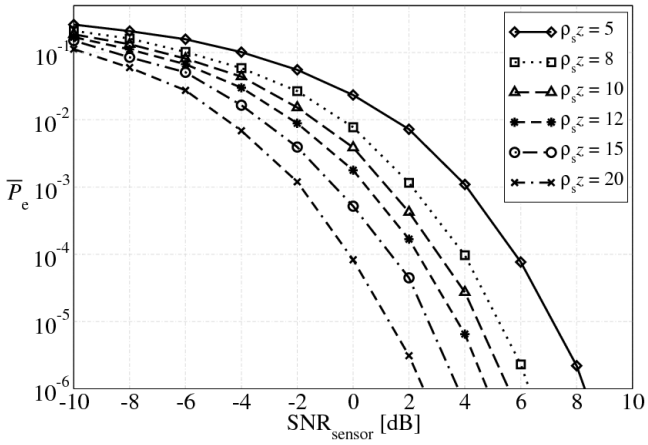

Figure 5.4: Probability of decision error, as a function of the vehicle observation SNR, in a scenario with CHs directly connected with the AP. Different values of $\rho_s z$ are considered.

vehicles and the AP—for instance, in Figure 5.2 (a) $n_h = 2$, whereas in Figure 5.2 (b) $n_h = 4$ (in general $n_h = n_c + 1$).

From our results, however, the performance with the majority-like fusion rule considered above are poor, since the information fusion is performed only on two binary data. In fact, a decision in favor of H_1 is taken if at least one of the two CHs are in favor of H_1. However, if H_0 is the true phenomenon status and observations are noisy, the decision rule is biased towards H_1 and errors may still happen. In order to obtain significant performance, we consider a majority-like fusion rule biased in favor of H_0, i.e., a decision in favor of H_1 is taken only if both CHs' decisions are in favor of H_1. In Figure 5.5, the probability of decision error, as a function of the vehicle observation SNR, in a scenario with CHs connected with the AP through multi-hop communications considering the new decision rule. Different values of $\rho_s z$ are considered. In a scenario with equal a priori probability of the phenomenon (case (a) with $p_0 = 0.5$), the performance drastically worsens with respect to the case with direct communications between the CHs and the AP (Figure 5.4). This is due to the fact that, when the number of hops increases, the number of information

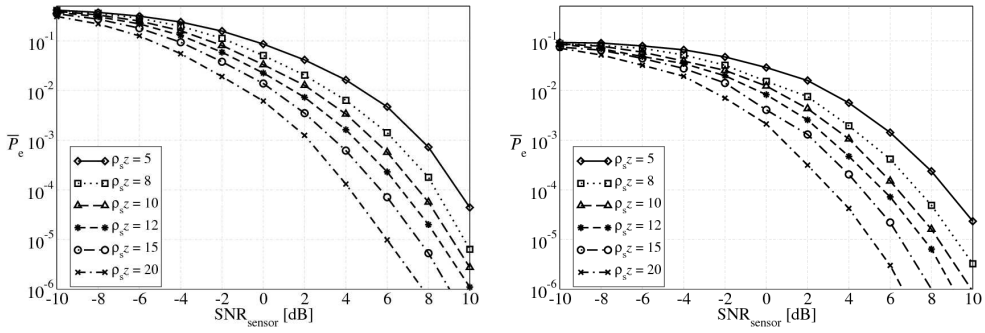

(a) (b)

Figure 5.5: Probability of decision error, as a function of the vehicle observation SNR, in a scenario with CHs connected with the AP through multi-hop communications and different values of $\rho_s z$ are considered. In case (a), $p_0 = 0.5$, whereas in case (b) $p_0 = 0.9$.

fusions also increases and, therefore, the amount of information transferred among the network reduces. This has been also previously observed in [82]. Since, however, this fusion rule is biased in favor of H_0, the performance improves when the observed phenomenon is rare. This can be observed in Figure 5.5 (b), where the probability of decision error is shown in the case with $p_0 = 0.9$ and $p_1 = 1 - p_0 = 0.1$.

In order to improve the performance of the multi-hop topologies, we also consider another (soft output-based) fusion rule. Denote as $n_{\mathrm{d},1}^{(j)}$ the exact number of decision in favor of H_1 at the j-th cluster ($j = 1, \ldots, n_{\mathrm{c}}$). Similarly, $n_{\mathrm{d},0}^{(j)} = d_{\mathrm{c}}^{(j)} - n_{\mathrm{d},1}^{(j)}$ is the number of decision in favor of H_0 in the j-th cluster. At this point, one can consider the following log-likelihood ratio (LLR):

$$\mathscr{L}_j \triangleq \ln \frac{n_{\mathrm{d},1}^{(j)} / d_{\mathrm{c}}^{(j)}}{n_{\mathrm{d},0}^{(j)} / d_{\mathrm{c}}^{(j)}} = \ln \frac{n_{\mathrm{d},1}^{(j)}}{n_{\mathrm{d},0}^{(j)}}$$

which corresponds to the logarithm of the ratio between the probability that the decision of the CH is in favor of H_1 and the probability that the decision of the CH is in favor of H_0: $\mathscr{L}_j > 0$ if the hypothesis H_1 is more likely, and viceversa if $\mathscr{L}_j < 0$.

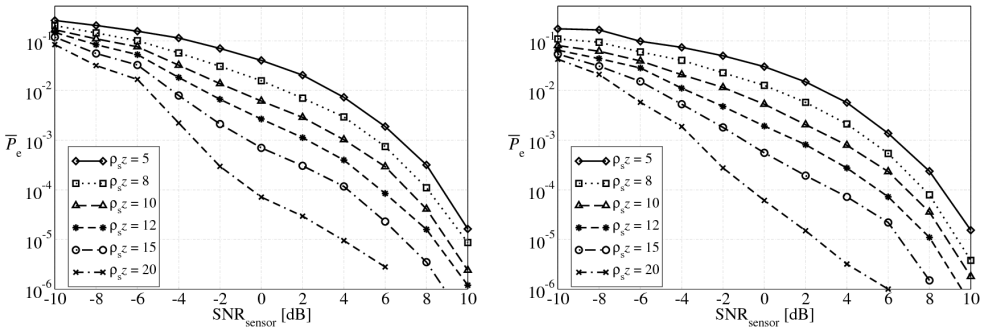

(a) (b)

Figure 5.6: Probability of decision error, as a function of the vehicle observation SNR, for the same scenario of Figure 5.5 and LLR-based fusion rule.

Since each CH receives the LLR from the $(j-1)$-th cluster[3], denoted as $\mathscr{L}_{j-1}^{\text{UP}}$, the fusion rule at the j-th cluster becomes

$$\mathscr{L}_j^{\text{UP}} = \mathscr{L}_{j-1}^{\text{UP}} + \mathscr{L}_{j-1}.$$

Note that in this case, each CH should transmit a real number (instead of a bit) and, therefore, the energy consumption of this scheme is higher than in the presence of simple majority-like fusion rule. Finally, the AP decides with the following rule:

$$\widehat{H} = \begin{cases} H_0 & \text{if } \mathscr{L}_{n_c}^{\text{UP}} < 0 \\ H_1 & \text{if } \mathscr{L}_{n_c}^{\text{UP}} \leq 0. \end{cases}$$

In Figure 5.6, the probability of decision error is shown, as a function of the vehicle observation SNR, for the same scenario of Figure 5.5 and LLR-based fusion rule. One should observe a performance improvement with respect to the majority-like fusion rule, both in a scenario with $p = 0.5$ and with $p = 0.9$. This should be expected, since more information is transferred across the network (each CH transmits a real number instead of a single bit). However, this comes at the price of a larger energy consumption.

[3]We are implicitly assuming that, when $j = 1$, no LLR from previous CH is received.

5.5 Impact of Mobility on Decentralized Detection

In this section, we investigate the impact of mobility on the performance of the proposed vehicular decentralized detection schemes. More precisely, we assume that each cluster breaks when at least one of its vehicles disappears.

In order to characterize the impact of mobility on the cluster lifetime we have performed simulation analysis using the VanetMobiSim mobility simulator, employing the basic IDM model, presented in Section 2.2.1. Using VanetMobiSim we have analyzed two scenarios, an urban-like and a highway-style scenario. The former is characterized by lower speeds ($[v^{\min} = 5, v^{\max} = 20]$ m/s), while the latter has much higher speeds ($[v^{\min} = 20, v^{\max} = 35]$ m/s). In both cases we have simulated the behavior of hundreds of vehicles in stationary condition for a sufficiently long time. In the urban scenario we have obtained an average speed $\overline{v} = 12.4$ m/s and a standard deviation $\sigma_v = 3.97$ m/s, while the highway scenario we have obtained $\overline{v} = 29.52$ m/s and $\sigma_v = 4.37$ m/s.

Let us consider a generic cluster composed by an average number of nodes, denoted as $\overline{d}_{\mathrm{c}}$. In particular, $\overline{d}_{\mathrm{c}}$ can be computed from the PMFs in Figure 5.3 and it can be shown that $\overline{d}_{\mathrm{c}} \simeq \rho_{\mathrm{s}} z$. Assuming that the vehicles are randomly deployed in a cluster of length $2z$, it can be shown that they are, on average, equally spaced by $2z/\overline{d}_{\mathrm{c}}$. The cluster lifetime is theoretically infinite if all nodes are moving at the same average speed. In order to analyze the impact of speed, let us assume that all nodes in the cluster are moving at the same average speed $\overline{v}$, with the exception of one node.

At this point, the minimum cluster lifetime is obtained when the vehicle with different speed is the last in the cluster (with respect to the direction of movement) and is moving with speed $v = \overline{v} - \sigma_v$. The cluster will die when the relative distance, with respect to the next vehicle, is $2z/\overline{d}_{\mathrm{c}}$. Therefore, one can write

$$T_{\mathrm{cl}}^{\min} = \frac{2z}{\overline{d}_{\mathrm{c}} \sigma_v}.$$

The maximum cluster lifetime is obtained, instead, when the last node in the cluster is moving with a speed $v = \overline{v} + \sigma_v$ and the distance to be covered to exit the cluster is

equal to $2z - 2z/\overline{d}_{\mathrm{c}}$. Therefore, one can write

$$T_{\mathrm{cl}}^{\max} = \frac{2z - \frac{2z}{\overline{d}_{\mathrm{c}}}}{\sigma_v} = \frac{2z\left(1 - \frac{1}{\overline{d}_{\mathrm{c}}}\right)}{\sigma_v}.$$

The average cluster lifetime can be simply defined as

$$\overline{T}_{\mathrm{cl}} \triangleq \frac{T_{\mathrm{cl}}^{\max} + T_{\mathrm{cl}}^{\min}}{2} = \frac{2z\left(2 - \frac{1}{\overline{d}_{\mathrm{c}}}\right)}{2\sigma_v} = \frac{z}{\sigma_v}\left(2 - \frac{1}{\overline{d}_{\mathrm{c}}}\right).$$

Assuming that data are collected with observation rate R_{b}, the amount of data which can be, on average, collected during the cluster lifetime is

$$N_{\mathrm{data}} = \overline{T}_{\mathrm{cl}} R_{\mathrm{b}} = \frac{R_{\mathrm{b}} z}{\sigma_v}\left(2 - \frac{1}{\overline{d}_{\mathrm{c}}}\right).$$

Finally, one can define the throughput per VANET lifetime as

$$S \triangleq N_{\mathrm{data}}\left(1 - P_{\mathrm{e}}\right) \tag{5.5}$$

where P_{e} is a function of the observation noise, as shown in Section 5.4.

In Figure 5.7, the throughput per VANET lifetime is shown, as a function of $\rho_{\mathrm{s}} z$, for different mobility scenarios (different σ_v) and fusion rules. The vehicle observation SNR is set to 0 dB: however, it can be shown that the vehicle observation SNR has a limited impact (only for very small values of $\rho_{\mathrm{s}} z$, where $S \simeq 0$). In the case with direct communications between the CHs and the AP, the "classical" majority-like fusion rule is considered, whereas the LLR-based fusion rule is considered in the presence of multi-hop communications between the CHs and the AP. One should observe that, for a fixed value of σ_v, the performance is the same regardless of the fusion rule. This is due to the fact that the probability of decision error has the same order of magnitude and, therefore, its contribution in (5.5) is negligible with respect to N_{data}. Moreover, the throughput in the presence of high mobility (large σ_v) is lower than that in the presence of low mobility (small σ_v). This is due to the fact that in the latter case the average cluster lifetime is larger and, therefore, a greater amount of information can be transferred by the network.

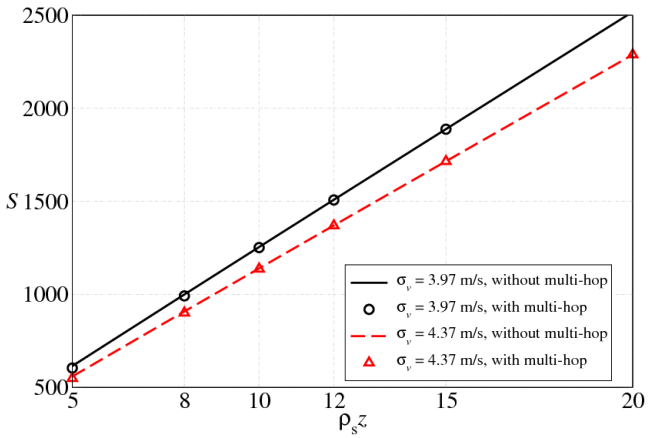

Figure 5.7: Throughput, as a function of $\rho_s z$, for different mobility scenarios (different σ_v) and fusion rules. The sensor SNR is set to 0 dB.

5.6 Concluding Remarks

In this chapter, we have analyzed the performance of vehicular decentralized detection schemes, when a spatially constant phenomenon of interest is observed by a VANET. By using a novel clustering broadcast protocol in a downlink phase, data collection and fusion has been concentrated in the uplink phase. Various clustered VANET topologies have been considered, together with various fusion rules. The performance of the proposed vehicular distributed detection has been analyzed in terms of probability of error on the phenomenon estimate. Unlike clustered sensor networks, where the clustering structure is a design aspect, the proposed vehicular distributed detection schemes exploit the natural formation of ephemeral vehicle clusters. By taking into account a cluster lifetime, our results show clearly that the maximum amount of data collectible during a VANET lifetime is more affected by the node mobility level than by the specific clustering structure.

Chapter 6

Silencing Irresponsible Forwarding

6.1 Introduction

In this chapter, we present an improvement of the IF protocol, the Silencing Irresponsible Forwarding (SIF) protocol, that offers a greater efficiency (e.g., a smaller number of retransmissions), without penalizing the performance in terms of latency and reachability. This improvement is achieved by simply imposing that the winner of a broadcast contention silences the other contenders, restarting a new transmission domain. As a by-product, thanks to this innovation, the SIF protocol can be more easily analyzed then IF, and therefore we will also provide a complete, even if approximated, analytical model. The SIF protocol is presented in two slightly different versions, improperly denoted as “persistent SIF” (pSIF) and “non persistent SIF”(npSIF).

The remainder of this chapter is organized as follows. In Section 6.2 the SIF protocol is accurately described, while in Section 6.3 we present an analytical framework of the SIF protocol. The performance of the SIF protocol in realistic IEEE 802.11p multi-hop linear networks is investigated in Section 6.4. Differently from the rest of the thesis, in this case we have considered the IEEE 802.11p protocol. Finally,

conclusions are drawn in Section 6.5.

6.2 The SIF Protocol

Since directly derived from IF, we will describe of SIF with respect to the reference scenario presented in Section 3.2. As shown in Chapter 3 it is quite challenging to mathematically characterize the performance of the IF protocol. This happens because both he number of retransmissions in a given transmission domain, and the position itself of the retransmitter, is stochastic. A more "mathematical friendly" protocol could be obtained by forcing to have a single retransmitting node in every transmission domain. This can be obtained by imposing the following rules. Let assume that the node k belongs to 1-th transmission domain of a certain frame. As usual, the source belongs at the 0-th transmission domain. Then suppose that the i-th node receives a copy of the frame from the node k, then, it schedules a retransmission according to the standard IF policy, since $d_i > d_k$.[1] Before to effectively transmits, the node k receives another copy of the same frame from the node j, then it behaves as follows:

- if $d_k < d_i < d_j$, the node i shall abort its current transmission attempt of the frame, and renouncing to any future retrials;
- if $d_k < d_j < d_i$, the node i shall abort the current transmission attempt, but it shall immediately triggers a new transmission attempt;
- if $d_j < d_k < d_i$, the node shall ignore the transmission from the node j.

In other words, when a transmission lead to some benefit in terms of the network coverage, the surrounding nodes shall abort they attempts, and verify if they have the requisites in terms of distance, for participating to the successive transmission attempts. Consequently, every successful transmission is like a *renewal* in a Renewal Process, and thus, the transmission domains are statically identical. We note that differently from the IF protocol, a node could belong to consecutive transmission

[1] As in Chapter 3, d_i denotes the distance between the i-th node and the source.

domains. This condition is verified when in a transmission domain is not selected the node with the maximum additional coverage (the furthest node from the source).

We now provide a more detailed description of the operations of the SIF protocol, by considering the first transmission domain for sake of simplicity.

1. The source sends a new frame.
2. The nodes $i \in \{1, N_z\}$ with a distance $d_i <\leq z$ receive the packet, and constituted the 1-th transmission domain.
3. Every node in the 1-th transmission domain probabilistically decides if transmit, according to its probability threshold p_i, computed by replacing d and ρ_s^v in equation (3.3), with respectively, d_i and ρ_s^i, where the latter denotes the local density of node i.
4. The potential forwarders compete for obtaining the channel access, by generating a random slotted waiting time $T_w(i) \geq 0$.
5. The waiting time counters are continuously decreased by all the nodes, until one of the reaches 0, say the k-th timer, $T_w(k) = 0$.
6. The k-th node, the winner of the contention, finally sends the packet.
7. The remaining N_z-1 nodes decode the packet, reset their timer, and discard the potentially queued packet.
8. The whole process (from step 1) is restarted at the 2-th transmission domain, wherein the node k acts as the source.

In order to employ the silencing technique (steps [4-6]), the SIF protocol shall interact with the underlying MAC layer, mainly for being able to abort previously scheduled packet transmissions. For this reason, while the IF protocol is relatively independent from the underlying layer, the SIF protocol is heavily coupled with it. We assume of using the IEEE 802.11p protocol described in Section 2.4, ed in particular the DCF mechanism for accessing the channel. When used coupled with the IEEE 802.11

protocol, the management of the random wait required at step 4 can happen in two different manners: (i) the random waiting time $T_w(i)$ is superimposed on top of the backoff mechanism of the MAC layer, and managed by the network layer; (ii) the waiting time coincides with the random backoff wait of the CSMA/CA mechanism. When adopting the first approach, we denote the protocol as "non-persistent SIF" (npSIF), since the node send the packet at the MAC layer only after winning the contention at the network layer. For the opposite reason, we denote the protocol as persistent SIF' (pSIF) when it adopts the second approach, sending immediately the frame at the MAC layer. For sake of simplicity we assume that the Slot Time is the same in both cases and identical to which of the underlying backoff mechanism (defined as T_{SLOT} in Section 1.3). In the pSIF protocol, $T_w(i) \in [0, \text{CW}_{\text{min}}]$, while in the npSIF protocol $T_w(i) \in [0, \text{CW}^{\text{SIF}}]$, where CW^{SIF} is set independently from CW_{min}.

6.3 Silencing Irresponsible Forwarding: Analysis

In this section we present an analytical framework for characterizing the performance of the SIF protocol. More precisely the model focus on the persistent variant of SIF. We want obtain a closed-form expression of the principal metrics of a multi-hop broadcast protocols, namely, the reachability, the transmission efficiency, and the end-to-end delay. In order to achieve this results, it is necessary to compute some auxiliary parameters, such as the probability of successful retransmission within a transmission domain, the average delay within a transmission domain, and the average number of hops, required for reach the rightmost end of the network. Because of the lack of space, we only present the main ideas behind the analysis and the more important results, but we omit most of the details that can be found in [117].

6.3.1 Theoretical Background

Coherently with the reference scenario described in Section 3.2, the nodes are positioned on a line of length $\ell_{\text{norm}}z$, according to a Poisson distribution with parameter ρ_{s}. Since the transmission domains are homogeneous it is sufficient to model a single

transmission domain for capturing the global behavior of the protocol. The number of nodes in a given transmission domain is given by a random variable $N_{\mathrm{P}} \in \{0,1,2,...\}$ with Probability Mass Function (PMF) $p_{N_{\mathrm{P}}}(k,\rho_{\mathrm{s}}z) = \frac{\exp^{-\rho_{\mathrm{s}}z}(\rho_{\mathrm{s}}z)^k}{k!}$ with average value $\overline{N_{\mathrm{P}}} = \rho_{\mathrm{s}}z = N_{\mathrm{z}}$. We denote the position of the i-node with the symbol R_i.

According to this (exact) model, the problem of computing the successful transmission probability of a transmission domain is quite complex, since it jointly depends by the number of nodes in a transmission domain, and in turns by the their positions, requiring a high number of conditioning, and thus of integrations, since the Poisson distribution can assume infinite values. In order to reduce the complexity of the problem, we adopt a strong, but well justified simplification, based on an approximated form of the total probability theorem. More precisely, we assume that, once conditioning on having a fixed number of nodes in a transmission domain (n), the position of the j-th node, with $j \in \{1,2,\ldots,n\}$ is deterministic and coincident with their average value.

This strong assumption can be motivated by the characteristics of the Poisson points process. In fact, it can be shown that, if one generates k Poisson points conditioning to the fact of lying in a finite interval, as happens in the finite interval $[0,z]$, then the marginal PDF of the position of the j-th node is the following:

$$f_{\mathrm{R}_j}^{(k)}(r_j) = \begin{cases} \frac{n!}{z^n}\frac{(z-r_j)^{n-j}\,r_j^{j-1}}{(n-j)!\,(j-1)!} & r_j \in (0,z) \quad j = 1,...,n \\ 0 & \text{otherwise}. \end{cases} \tag{6.1}$$

while, the average position of the j-th node can be expressed as:

$$\overline{\mathrm{R}_j}^{(n} = \int_0^z r_j \frac{n!}{z^n}\frac{(z-r_i)^{n-j}\,r_j^{j-1}}{(n-j)!\,(j-1)!}\,dr_j = j\frac{z}{n+1} \quad j = 1,...,n. \tag{6.2}$$

From equation (6.2) it emerges clearly that the n nodes are (jointly) uniformly distributed in the interval $[0,z]$.

In order to exploit this characteristic, we partition the linear space $[0,z]$ in N^{int} sub-intervals of length $\frac{z}{N^{\mathrm{int}}}$. Thus, the i-th interval is defined as $\mathrm{I}_i = [\frac{(i-i)z}{N^{\mathrm{int}}}, \frac{iz}{N^{\mathrm{int}}}]$, $i = 1,2,\ldots,N^{\mathrm{int}}$. The number of the considered interval is a design parameter.[2] Every

[2] After some numerical test, we observed that the value $N^{\mathrm{int}} = 100$ is a good tradeoff between precision and computation time.

sub-interval can contain zero, one, or more nodes, than it can be viewed as a virtual node. Consequently, it is possible to associate a transmission probability to the generic interval I_i, defined as $p_{\mathrm{rtx}}^{\mathrm{eq}}(i), i = 1,\ldots,N^{\mathrm{int}}$. Once fixed the number of nodes, the transmission probability of the i-th interval is given by the sum of the probability of retransmission of all nodes within the i-th interval. Since we are considering average positions, a node belong to the i-th interval if its average position is in that interval. We define as $p_{\mathrm{rtx}}^{(m)}(j)$ the probability of retransmission of the j-th node, given that: (i) there are exactly m nodes in the interval $[0,z]$; (ii) the node j is collocated within the interval I_i. Using the (approximated) total probability theorem, $p_{\mathrm{rtx}}^{\mathrm{eq}}(i)$ can be expressed as follows:

$$\begin{aligned} p_{\mathrm{rtx}}^{\mathrm{eq}}(i) &= \sum_{m=1}^{N_{\mathrm{C}}} \left(p_{\mathrm{rtx}}^{\mathrm{eq}}(i)|N_{\mathrm{P}}^{\mathrm{norm}}=m\right) \underbrace{P(N_{\mathrm{P}}^{\mathrm{norm}}=k)}_{p_{N_{\mathrm{P}}^{\mathrm{norm}}}(m,\rho_{\mathrm{s}}z)} \\ &= \sum_{m=1}^{N_{\mathrm{C}}} \sum_{j=1}^{k} p_{\mathrm{rtx}}^{(m)}(j)\ f(i,j,m)\ p_{N_{\mathrm{P}}^{\mathrm{norm}}}(m,\rho_{\mathrm{s}}z) \qquad i=1,\ldots,N^{\mathrm{int}} \end{aligned} \quad , \tag{6.3}$$

where $f(i,j,m)$ is an indicator function defined as follows:

$$f(i,j,m) = \begin{cases} 1 & \overline{\mathrm{R}_j}^{(m)} \in \mathrm{I}_i \\ 0 & \overline{\mathrm{R}_j}^{(m)} \notin \mathrm{I}_i. \end{cases} \tag{6.4}$$

The probability $p_{\mathrm{rtx}}^{\mathrm{eq}}(i)$ is now function of $p_{\mathrm{rtx}}^{(m)}(j)$, but the latter can be easily computed by some combinatorics, since it is relative to a deterministic-like scenario, with m nodes uniformly positioned in $[0,z]$.

In particular, $p_{\mathrm{rtx}}^{(m)}(j)$ depends on two elements: (i) the probability p_j, given by equation (3.3), that the node j will be designated by the IF procedure; (ii) the probabiliy that the j wins the contention among a set of m contending nodes, denoted with $q^{(m)}(j)$.

We now derive the latter by considering a simplified contention mechanism. In particular, we assume that the j-th node will successfully conclude the contention, only and only if is generates the smallest slotted waiting time $T_w(j) \in [0,\mathrm{CW}_{\mathrm{SIF}}]$, while the other $m-1$ node generate a strictly grater value. This is an approximation,

since the node j could win the contentions also choosing a value of $T_w(j)$ greater then the minimum. The probability that the node j wins the contention among m nodes can be express as follows:

$$\begin{aligned} q^{(m)}(j) = q^{(m)} &= \frac{1}{\mathrm{CW}_{\mathrm{SIF}}^{m}}[(\mathrm{CW}_{\mathrm{SIF}}-1)^{m-1}+(\mathrm{CW}_{\mathrm{SIF}}-2)^{m-1}+...+1] \\ &= \frac{1}{\mathrm{CW}_{\mathrm{SIF}}^{m}} \sum_{i=1}^{\mathrm{CW}_{\mathrm{SIF}}-1} i^{m-1} \qquad j=1,2,\ldots,m \end{aligned} \tag{6.5}$$

It is straightforward to observe that the equation (6.5) is the same for every node $j \in \{1,2,\ldots,m\}$.

Finally, after some combinatorics that can be found in [117], we can express the transmission probabiliy $p_{\mathrm{rtx}}^{(m)}(j)$ as:

$$p_{\mathrm{rtx}}^{(m)}(j) = p_j \sum_{n=1}^{m} q^{(n)} p_{V_j^{(m)}}(n-1), \tag{6.6}$$

where $V_j^{(m)} \in \{0,\ldots,m-1\}$ is a discrete random variable defined as:

$$V_i^{(m)} = \{\text{the number of nodes competing with the node } i \text{ given } m \text{ nodes}\}.$$

The PMF of $V_i^{(m)}$ is given by:

$$\mathrm{P}(V_j^{(m)}=v) = \sum_{\substack{i_1=1 \\ i_1\neq j}}^{m} \sum_{\substack{i_2=i_1+1 \\ i_2\neq j}}^{m} \cdots \sum_{\substack{i_v=i_{v-1}+1 \\ i_v\neq j}}^{m} \left(\left(\prod_{s\in\{i_1,i_2,\ldots,i_v\}} p_s \right) \left(\prod_{\substack{t=1 \\ t\notin\{i_1,i_2,\ldots,i_v\}}}^{m} \bar{p_t} \right) \right)$$

At this point, by using (6.6) in equation (6.3), it is possible to obtain a closed-form expression of $p_{\mathrm{rtx}}^{\mathrm{eq}}(i)$, that is the probabiliy of successfully transmission of the interval I_i.

Now we can observe that sum of all the i-th successfully transmission probability ($i \in \{1,2,\ldots,N^{\mathrm{int}}\}$) corresponds to the to the success probabiliy of the whole transmission domain:

$$p_{\mathrm{succ}} = \sum_{i=1}^{N^{\mathrm{int}}} p_{\mathrm{rtx}}^{\mathrm{eq}}(i). \tag{6.7}$$

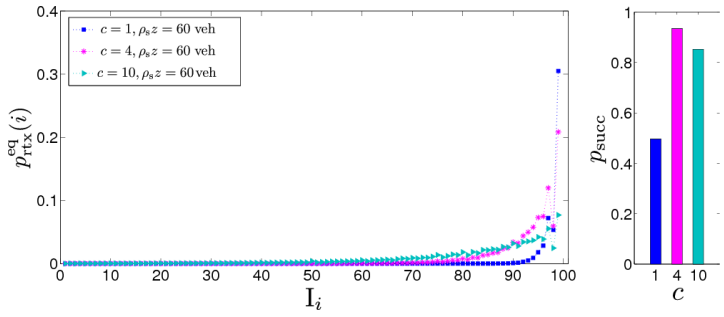

Figure 6.1: On the left side, $p^{eq}_{rtx}(i)$ as a function of the interval index; on the right side, p_{succ} in the first transmission domain. In both cases, $\rho_s z = 60$, and 3 values of c are considered, 1, 4, and 10.

We can also observe that (6.7) coincides with the average number of transmissions in the first transmission domain $\mathbb{E}[M_1]$, and it is the equivalent of equation (3.6).

In Figure 6.1 we shown, on the left side, $p^{eq}_{rtx}(i)$ as a function of the interval index, obtained with $\rho_s z = 60$ and 3 values of c, namely, 1, 4, and 10. We can observe that most of the contribution to p_{succ} come from the the intervals with the higher indexes have the major contribute to p_{succ}. On the right side of Figure 6.1 we observe that p_{succ} exhibits a maximum with $c = 4$, while the performance with $c = 10$ are limited by the excess of contention, while with $c = 1$ the forwarding mechanism is too feeble.

Finally, we recall that the analytical derivation has been further extended in [117], in order to derive the relevant metrics introduced in Section 3.5.1, namely, RE, TE, and D. Even if we have omitted the analytical details, in Figure 6.2 we shown the behavior of the principal metrics as a function of c, and different $\rho_s z$ values, namely, 4, 8, 12, 16, and 20 veh, according to the theoretical framework. From Figure 6.2 it is possible to draw the following observations:

- There is an optimal value of c offering the maximum value of RE. This value is a function of $\rho_s z$, but for all the considered values, lies in the interval $c^* \in [3,4]$. In particular, the optimal value of c is a decreasing function of $\rho_s z$.

- Similarly, also the TE exhibits a peaky trend, denoting he presence of optimal

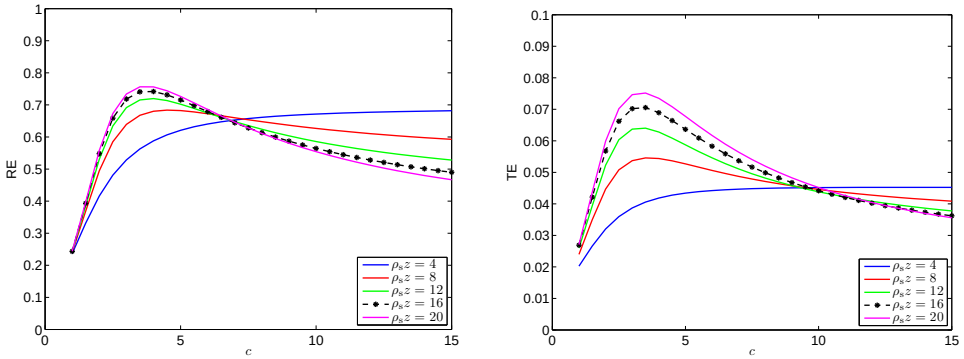

(a) RE (b) TE

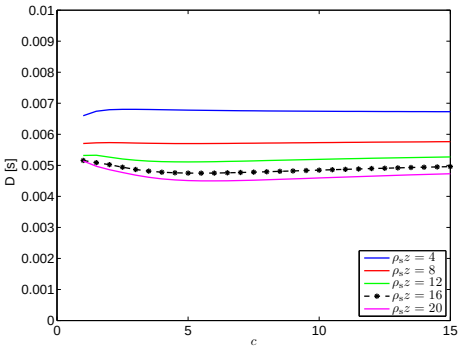

(c) D

Figure 6.2: (a) RE, (b) TE, and (c) end-to-end delay, as a function of c, obtained with the analytical model of the pSIF protocol, with several $\rho_s z$ values, namely, 4, 8, 12, 16, and 20 veh.

Table 6.1: Main IEEE 802.11p network simulation parameters for SIF.

λ	$\{0.1, 100\}$ pck/s
ρ_s	0.02 veh/m
z	$\{200, 400, 600, 600, 1000\}$ m
ℓ_{norm}	8
Packet Size	300 bytes
Carrier Freq.	5.9 GHz
Data rate	3 Mbps
CW_{min}	31

values of c in roughly the same interval $c^* \in [3, 4]$.

- On the opposite hand, the delay is independent from c, and more surprisingly it decreases with increasing value of $\rho_s z$.

6.4 SIF in IEEE 802.11p Networks

6.4.1 Simulation Setup

We now investigate the performance of the SIF protocol in IEEE 802.11p networks, by a comparison with the IF and the flooding protocol. The simulation setup was identical to which adopted for evaluating the performance of IF, with a major exception: the use of the IEEE 802.11p standard instead of the IEEE 802.11b. Since that the IEEE 802.11p module in ns-2.34 does not support the EDCA mechanism, we have employed the DCF mechanism, by setting $\text{CW}_{\text{min}} = 31$. The relevant parameters of the IEEE 802.11p network and of the SIF protocols are listed in Table 6.1. Both Friis and Nakagami channel models are used. The parameters of the Nakagami probability density function has been previously discussed and defined in Section 2.3. Due to the different path-loss attenuation factor used in Section 2.3, we compare the two models by imposing the same (average) transmission range. Thus, the nodes will use different values of transmit power. Obviously, by considering the same level trans-

mission power the Nakagami will exhibit poorer performance with respect to the the deterministic Friis model.

As usual, we consider a linear topology with $\ell_{\text{norm}} = 8$, where the source node is placed at the leftmost vertex. In each topology the source generated a finite number of $N_{\text{p}} = 1000$ packets according to a Poisson process with parameter λ (dimension: [pck/s]). Each packet a fixed small size PS $= 300$ bytes, since alert messages typically carries a small amount of information. The data rate is set to 3 Mbit/s. Two values of λ are considered. The first, $\lambda = 0.1$ pck/s, leads to a very small traffic load of only 0.24 Kbits/s, while the second value, $\lambda = 100$ pck/s determines a high traffic load of 240 Kbits/s, roughly one tenth of the theoretical available data-rate of 3 Mbit/s.

6.4.2 Performance Analysis

First of all, we want to assess the validity of the theoretical framework presented in Section 6.3, with respect to the simulation results. While we have presented a unique framework for both the pSIF and npSIF protocols, they will be separately analyzed here. In Figure 6.3 are shown the RE, and the TE, as a function of c, obtained with the pSIF and npSIF protocols by setting $\rho_{\text{s}}z = 12, 16, \text{and} 20$ veh. We do not show the delay, since in the simulations it has denoted the same constant behavior of Figure 6.2 (c). By comparing Figure 6.2 and Figure 6.3 it emerges a clear lack of agreement between the theoretical and simulative analysis. In particular, differently from Figure 6.2 (a), the RE at low intensity load, is substantially independent from the value of $\rho_{\text{s}}z$, moreover it exhibits a monotonic behavior, without any evidence of the presence of peaks, and much greater values. This mismatching can be motivated by the assumptions at the basis the theoretical model. In fact, the latter does not model the backoff-freezing and, it under-estimate the success probability, since it does not consider the event in which a node can transmit even if it has not chose the smaller waiting time. On the other hand, in the case of TE there is a good matching between simulation and analysis, both in terms of shape and absolute values. In fact, in Figure 6.3 (b) all the TE curves exhibit a peak at $c = 2$, furthermore, as in Figure 6.2 (b), greater values of $\rho_{\text{s}}z$ determine better TE values. Unfortunately, the

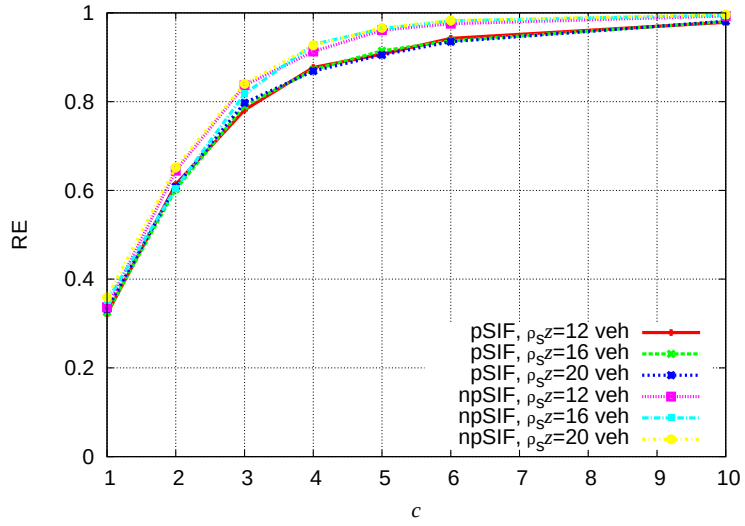

(a) RE

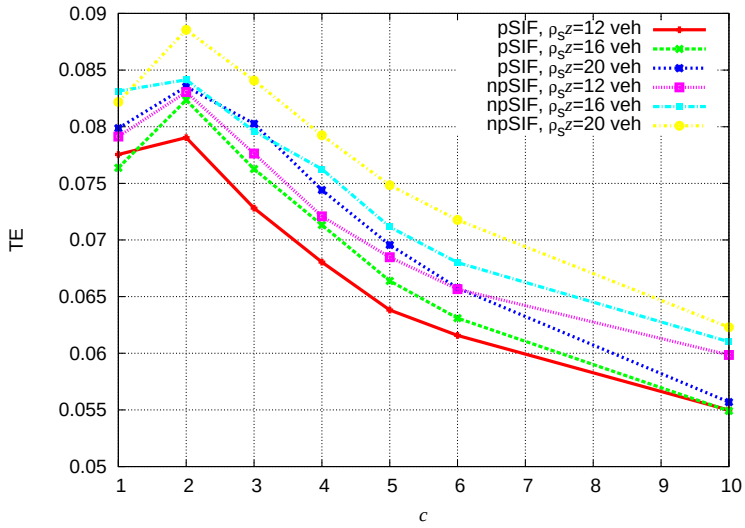

(b) TE

Figure 6.3: (a) RE, and (b) TE, as a function of c, obtained by using the Friis propagation model, with several $\rho_S z$ values, namely, 4, 8, 12, 16, and 20 veh.

peak of the TE at $c = 2$ is not very useful, since it leads to a too small RE. The maximum RE, can be achieved by both pSIF and npSIF by settings $c = 10$. However, if we compare Figure 6.3 (a) and Figure 6.3 (b), it seems that the gain in terms of RE, is more significant than the loss in terms of TE which remains good. As a final remark, we observe that in low-traffic condition, the pSIF and the npSIF variations have roughly the same performance, even if npSIF is slightly more efficient.

In Figure 6.4, we compare the performance of several protocols, including, IF, pSIF, npSIF, and flooding, by considering two different values of λ (0.1 and 100 pck/s), $\rho_s z = 20$ veh, and $c = 5$.

Although in low traffic conditions all the protocols achieve a RE > 0.95, only the flooding reaches the maximum value RE=1, thanks to its exaggerated number of retransmissions, as proved by the smallest value of TE. On the contrary, both pSIF and npSIM are able to conjugate a high reachability with a high efficiency, and they leave behind the FLOOD by a factor 20 in terms of TE. As expected the IF protocol exhibits an intermediate behavior. In high traffic condition, pSIF and npSIF maintains the leadership both in terms of RE and TE, while the IF and the flooding protocol are affected by network congestion. Quite surprisingly, the FLOOD denotes a behavior totally different from the other protocols. In particular, it has a small but constant progression, and it is able to overcome the SIF protocols in the nearby of the 16-th hop. This strange behavior, was already emphasized needs of the double number of hops for obtains a value of RE greater then the SIF protocols. As emphasized in Section 2.4, it is mostly due to the interference management mechanism adopted by the IEEE 802.11p module of ns-2. In order of obtain a greater understanding of this phenomenon, in Figure 6.5 we represent D and the average number of hops (denoted as H), as a function of $\rho_s z$. From that figure we appreciate that the number of hops, and of course the delay, of the flooding protocol explodes with $\rho_s z$. Despite of this the flooding protocol is still able a high value of RE. On the opposite hand, we observe that both the IF and the SIF protocol, show a constant delay and a quasi-constant number of hops, still proving the capacity of that protocols of exploiting the vehicular density, instead of being damaged from it.

Finally, in Figure 6.6 we show the results in terms of RE and TE, obtained using

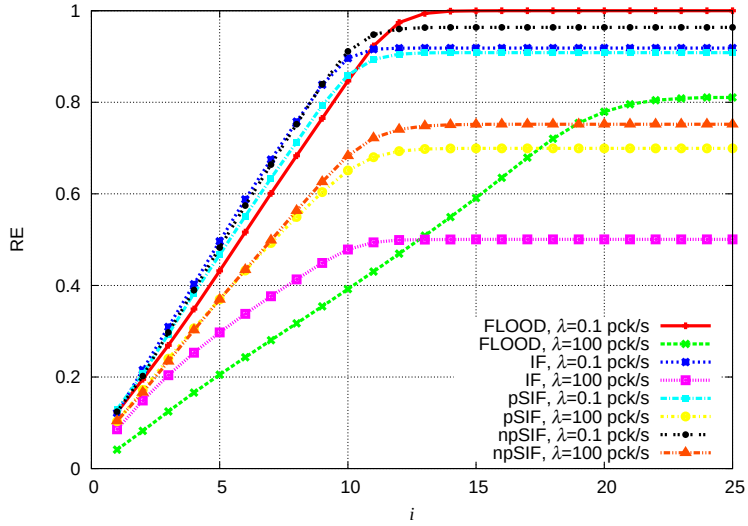

(a) RE

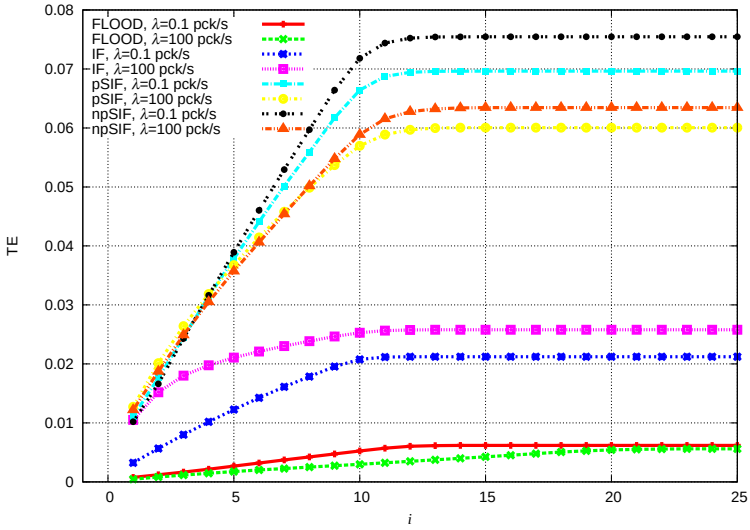

(b) TE

Figure 6.4: (a) RE, and (b) TE, as a function of the Hop Index (i), obtained by using the Friis propagation model, $\rho_s z = 20$ veh, and $c = 5$. Several protocols are considered, namely, IF, flooding, pSIF, and npSIF, and two different values of λ (0.1 and 100 pck/s).

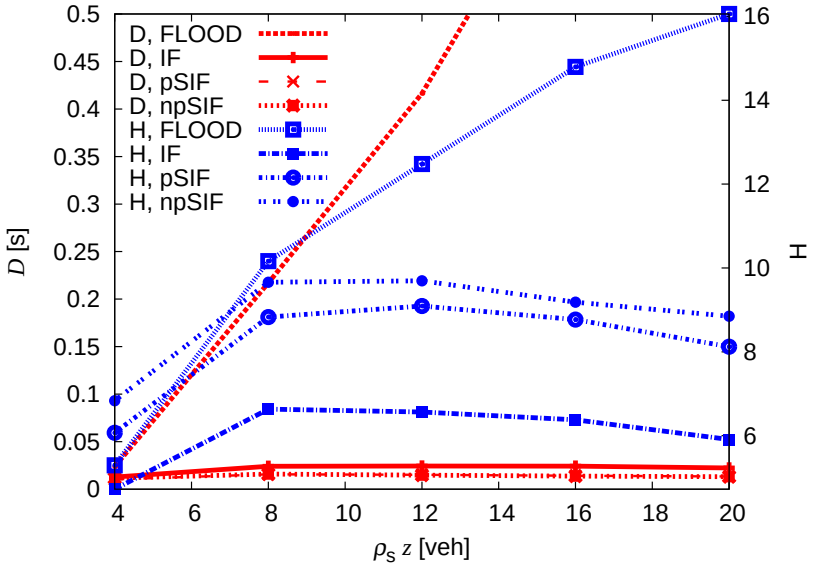

Figure 6.5: D (left axis), and H (right axis) as a function of $\rho_s z$, obtained by using the Friis propagation models. Several protocols are considered, namely, IF, flooding, pSIF, and npSIF. A single value of $\lambda = 100$ pck/s, and a single value of $c = 5$ are considered.

the Nakagami propagation model, after having imposed the same (average) values of transmission range listed in Table 6.1. Hence, in this case the transmit power of the nodes is generally different from which used in Friis propagation conditions. By comparing Figure 6.6 with Figure 6.4, one can observe that, differently from one will expect, the presence of fading does not degrade the performance. Indeed, the presence of Nakagami fading lead to some smaller but significant advantages to in terms of RE. This results can be interpreted as follows. Because of the presence of fading, nobody in the transmission range of the transmitter can be sure of correctly receive the packet. From a communication point of view represents a problem only when there are few nodes in the transmission domain. But in the other cases, it is practically impossible that all the nodes in a transmission domain experiences severe fading at the same time, being the fading realizations uncorrelated. Furthermore, in the presence of fading the effective transmission range is stochastic, and hence there is a non-null probability of selecting a node, whose distance is greater than the average transmission range z used in equation 3.3, thus yielding to a broadcast probability equal to 1. Since this event is rare, it does not leads to congestion, but, on the other hand, when this event happens, it represents an improvement with respect to th expected forwarding range of the process.

6.5 Concluding Remarks

In this chapter, we have proposed an improved probabilistic-based rebroadcast schemes, denoted as Silenced Irresponsible Forwarding, based on the IF protocol introduced in Chapter 3. Although the SIF protocol can be implemented in two different ways, the persistent SIF and the not persistent SIF, these two variants have led to very similar performance in the considered scenarios. The SIF protocols share the same benefit of IF, namely, the decentralized nature, the low-latency, and the absence of overhead, but they offers superior performance, both on saturated (as expected), than in non-saturated conditions. In this chapter we have also shown that, by using the average transmission range of the Nakagami propagation model, in equation 3.3, the IF-derived protocols maintains the same performance level experience in a deter-

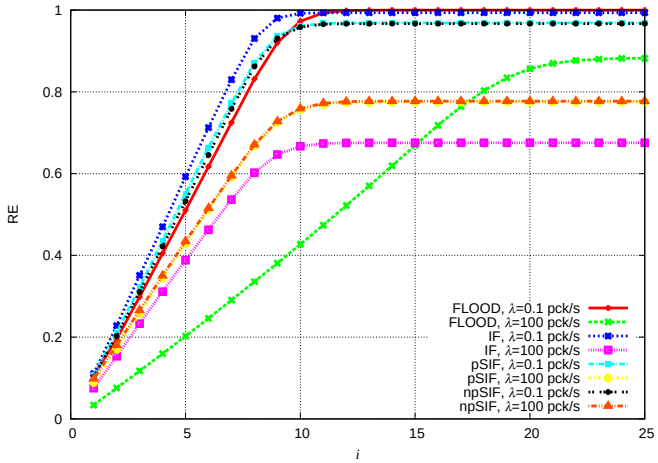

(a) RE

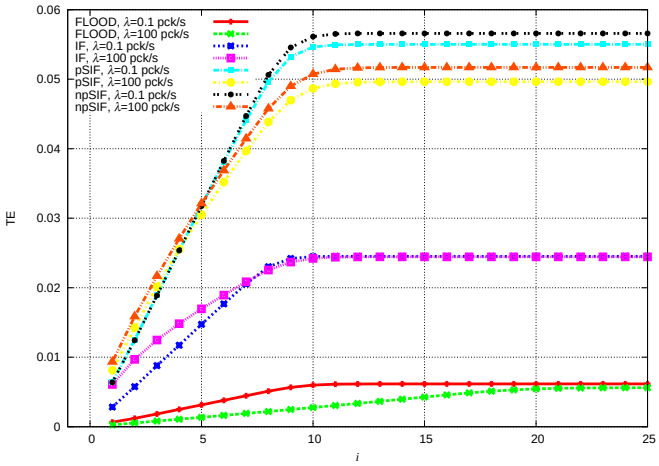

(b) TE

Figure 6.6: (a) RE, and (b) TE, as a function of the Hop Index (i), obtained by adopting the Nakagami propagation model, $\rho_s z = 20$ veh, and $c = 5$. Several protocols are considered, namely, IF, flooding, pSIF, and npSIF, and two different values of λ (0.1 and 100 pck/s).

ministic propagation channel. For this reason, these protocols can be used either in presence of deterministic or stochastic propagation condition.

Chapter 7

Concluding Remarks and Future Work

In this thesis, we have examined the problem of broadcasting information in VANETs by means of multihop protocols. The principal contribution of this work, is the proposal of a family of broadcasting techniques, that can be efficiently employed in various scenarios, including V2V communications, data dissemination, and data collection applications.

First, we have proposed a new probabilistic-based broadcasting scheme, denoted as Irresponsible Forwarding (IF), which takes the statistical distribution of the nodes into consideration. The idea of this rebroadcast paradigm is the following. Once a node receives a packet, it evaluates the presence of other nearby nodes in an average statistical sense. Should there likely be another node close to itself which can rebroadcast the packet more efficiently, the former node will “irresponsibly” choose not to rebroadcast. The main advantages of the IF protocol with respect to solutions present in the literature, are its inherently distributed nature, the low-latency, and the absence of overhead, since auxiliary supporting packets are not needed. Furthermore, since the statical distribution of the nodes is taken into account, by the IF protocol, it works independently from the vehicle density on a network.

The proposed IF protocol has been tested in both V2V and I2V scenarios. In the

former, the IF protocol has been used in safety-related applications (e.g., the dissemination of short alert-messages), with strict reliability and low-latency requirements. In the latter, IF has been employed in a radically different context, which of disseminating information from a fixed Road Side Unit to the vehicles transiting in its proximity, by means of multihop broadcast communications. In order to evaluate the impact of the mobility, these simulative analysis have been conducted in several vehicular environments, namely, highway and urban roads with traffic junctions. From this investigations we have obtained three main results: (i) the vehicles' mobility does not affect significantly the performance of the applications targeted by our tests; (ii) the IF protocol is not affected by the presence of severe fading in the wireless channel; (ii) even if characterized by a very-small latency, the IF protocol cannot guarantee a satisfactory efficiency and reliability.

On the basis of the scarce performance shown by the IF protocol in realistic scenarios, we have presented an improvement of the IF protocol, the Silencing Irresponsible Forwarding (SIF) protocol, able to guarantee a greater efficiency (e.g., a smaller number of retransmissions), without penalizing the reachability, and with a comparable latency. This improvement has been achieved by adding a silencing feature to the IF protocol. More precisely, the winner of a broadcast contention silences the other contenders, triggering a new contention phase. While SIF has been a big step toward optimality, the main problem, which of analytically derive the optimal broadcast strategy, is still open. In fact, our attempt of modeling the behavior of an apparently simple protocol as SIF, is resulted in an approximated model, not able to capture the whole complexity of the system. For this reason, in future research we will search alternatives method for address this challenge.

Finally, we have exploited the probabilistic-concept behind the IF protocol, to develop a novel decentralized clustering protocol, denoted as Cluster-Head Election IF (CHE-IF). This protocol combine the probabilistic nature of IF, with suitable control packets, in order to exploit the natural formation of ephemeral vehicle clusters in VANETs. CHE-IF is a general purpose protocol that can be used by different applications, as a showcase, we have presented a vehicular decentralized detection scheme for I2V networks. This solution is based on tho distinct phases: the creation, during a

downlink phase, of a clustered VANET topology from an Access Point (AP) through the CHE-IF protocol. This clustered topology is then exploited, during an uplink phase, to collect information from the vehicles and perform distributed detection.

Appendix A

Average Number of Retransmissions in the IF Protocol

Since N_z has a Poisson distribution with parameter $\rho_s z$, by applying the law of total probability and observing that $\mathbb{E}[M_1|N_z = 0] = 0$, the average number in (3.4) can be rewritten as follows:

$$\begin{aligned}
\mathbb{E}[M_1] &= \sum_{n=1}^{\infty} \mathbb{E}[M_1|N_z = n]P\{N_z = n\} \\
&= \sum_{n=1}^{\infty} \mathbb{E}\left[\sum_{i=1}^{N_z} V_i|N_z = n\right] P\{N_z = n\} \\
&= \sum_{n=1}^{\infty} \sum_{i=1}^{n} \mathbb{E}[V_i|N_z = n]P\{N_z = n\} \\
&= \sum_{n=1}^{\infty} \frac{(\rho_s z)^n}{n!} e^{-\rho_s z} \sum_{i=1}^{n} \mathbb{E}[V_i] \qquad \text{(A.1)}
\end{aligned}$$

where, in the passage between the third and fourth lines, we have used the fact that V_i is independent of N_z.[1] Since V_i is a Bernoulli random variable, it is immediate to conclude that

$$\mathbb{E}[V_i] = P\{V_i = 1\}$$

[1] Note that V_i is independent of N_z since the i^{th} vehicle is, by its very definition, one of the N_z vehicles in $(0, z)$. Therefore, conditioning is superfluous.

where $P\{V_i = 1\}$ is the probability of rebroadcasting of vehicle i. This probability depends on the distance D_i of this vehicle from the origin. In particular, by definition it follows that

$$P\{V_i = 1 | D_i = \lambda\} = e^{-\frac{\rho_s(z-\lambda)}{c}}$$

i.e., $P\{V_i = 1|D_i = \lambda\}$ is the probability of rebroadcasting for a vehicle placed at distance $\lambda \in (0,z)$ from the origin. By applying the total probability theorem, one can conclude that:

$$\begin{aligned} P\{V_i = 1\} &= \int_0^z P\{V_i = 1|D_i = \lambda\}\, f_{D_i}(\lambda)\,\mathrm{d}\lambda \\ &= \int_0^z e^{-\frac{\rho_s(z-\lambda)}{c}}\, f_{D_i}(\lambda)\,\mathrm{d}\lambda \end{aligned} \tag{A.2}$$

where $f_{D_i}(\cdot)$ is the PDF of the distance D_i, a random variable that can be expressed by:

$$D_i = Y_1 + Y_2 + \cdots + Y_i$$

where Y_j is the distance from the $(j-1)^{\text{th}}$ vehicle to the j^{th} vehicle ($j = 1,\ldots,i$). *If* $\{Y_j\}$ are independent and identically distributed random variables with exponential distribution with mean $1/\rho_s$, one can conclude that D_i has an Erlang distribution with parameters i and ρ_s, i.e., [118]

$$f_{D_i-\text{Erlang}}(\lambda) = \frac{\rho_s e^{-\rho_s\lambda}(\rho_s\lambda)^{i-1}}{(i-1)!}U(\lambda)$$

where $U(\lambda)$ is the unit-step function. However, in our scenario we know, by definition, that the i^{th} vehicle is in $(0,z)$. Therefore, the PDF of its distance D_i from the origin can be written as:

$$\begin{aligned} f_{D_i}(\lambda) &= f_{D_i-\text{Erlang}}(\lambda|D_i \le z) \\ &= \begin{cases} \dfrac{f_{D_i-\text{Erlang}}(\lambda)}{F_{D_i-\text{Erlang}}(z)} & 0 \le \lambda \le z \\ 0 & \text{otherwise.} \end{cases} \end{aligned} \tag{A.3}$$

where $F_{D_i-\text{Erlang}}(z)$ is the cumulative distribution function (CDF) of an Erlang PDF with parameters i and ρ_s. In particular, it can be shown that [119]:

$$F_{D_i-\text{Erlang}}(z) = \frac{\gamma(i,\rho_s z)}{(i-1)!}$$

where γ is the lower incomplete gamma function:

$$\gamma(i,x) \triangleq \int_0^x t^{i-1} e^{-t}\,\mathrm{d}t.$$

From (A.3), the PDF of D_i can be finally expressed as follows:

$$f_{D_i}(\lambda) = \frac{\rho_s e^{-\rho_s\lambda}(\rho_s\lambda)^{i-1}}{\gamma(i,\rho_s z)}[U(\lambda) - U(\lambda - z)]. \tag{A.4}$$

Substituting the PDF (A.4) into (A.2), one obtains:

$$\begin{aligned} P\{V_i = 1\} &= \int_0^z e^{-\frac{\rho_s(z-\lambda)}{c}} \frac{\rho_s e^{-\rho_s\lambda}(\rho_s\lambda)^{i-1}}{\gamma(i,\rho_s z)}\,\mathrm{d}\lambda \\ &= \frac{\rho_s^i e^{-\frac{\rho_s z}{c}}}{\gamma(i,\rho_s z)} \int_0^z e^{-\rho_s(1-\frac{1}{c})\lambda}\lambda^{i-1}\,\mathrm{d}\lambda. \end{aligned} \tag{A.5}$$

At this point, the final integral expression in (A.5) can be evaluated distinguishing between the cases with $c = 1$ and $c > 1$, respectively.

- If $c = 1$, (A.5) reduces to the following:

$$P\{V_i = 1\} = \frac{\rho_s^i e^{-\rho_s z}}{\gamma(i,\rho_s z)} \int_0^z \lambda^{i-1}\,\mathrm{d}\lambda = \frac{(\rho_s z)^i e^{-\rho_s z}}{i\,\gamma(i,\rho_s z)}. \tag{A.6}$$

  Since it can be shown, through integration by parts, that

$$\gamma(i,x) = (i-1)!\left[1 - e^{-x}\sum_{j=0}^{i-1}\frac{x^j}{j!}\right]$$

  the final expression (A.6) can be rewritten as follows:

$$P\{V_i = 1\} = \frac{(\rho_s z)^i e^{-\rho_s z}}{i!\left[1 - e^{-\rho_s z}\sum_{j=0}^{i-1}\frac{(\rho_s z)^j}{j!}\right]}. \tag{A.7}$$

- If $c > 1$, considering $t = \rho_s(1-\frac{1}{c})\lambda$, one obtains:

$$\begin{aligned} P\{V_i = 1\} &= \frac{\rho_s^i e^{-\frac{\rho_s z}{c}}}{\gamma(i,\rho_s z)} \frac{1}{\rho_s^i (1-\frac{1}{c})^i} \\ &\quad \cdot \underbrace{\int_0^{\rho_s z(1-\frac{1}{c})} e^{-t} t^{i-1}\,\mathrm{d}t}_{\gamma(i,\rho_s z\left(1-\frac{1}{c}\right))} \\ &= \left(\frac{c}{c-1}\right)^i e^{-\frac{\rho_s z}{c}} \frac{\gamma(i,\rho_s' z)}{\gamma(i,\rho_s z)} \\ &= \left(\frac{c}{c-1}\right)^i e^{-\frac{\rho_s z}{c}} \frac{1-e^{-\rho_s' z}\sum_{j=0}^{i-1}\frac{(\rho_s' z)^j}{j!}}{1-e^{-\rho_s z}\sum_{j=0}^{i-1}\frac{(\rho_s z)^j}{j!}} \end{aligned} \tag{A.8}$$

  where $\rho_s' = \rho_s\left(1-\frac{1}{c}\right)$.

Finally, using expressions (A.7) and (A.8), in the cases with $c = 1$ and $c > 1$, respectively, for $\mathbb{E}[V_i] = P\{V_i = 1\}$ into (A.1), the average number of vehicles which rebroadcast in $(0,z)$ can be expressed as follows:

$$\mathbb{E}[M_1] = \begin{cases} \sum_{n=1}^{\infty} \frac{(\rho_s z)^n e^{-\rho_s z}}{n!} \sum_{i=1}^{n} \frac{(\rho_s z)^i e^{-\rho_s z}}{i!} \\ \quad \cdot \frac{1}{1-e^{-\rho_s z}\sum_{j=0}^{i-1}\frac{(\rho_s z)^j}{j!}} \\ \qquad \text{if } c = 1 \\ \sum_{n=1}^{\infty} \frac{(\rho_s z)^n e^{-\rho_s z}}{n!} \sum_{i=1}^{n} \left(\frac{c}{c-1}\right)^i e^{-\frac{\rho_s z}{c}} \\ \quad \cdot \frac{1-e^{-\rho_s' z}\sum_{j=0}^{i-1}\frac{(\rho_s' z)^j}{j!}}{1-e^{-\rho_s z}\sum_{j=0}^{i-1}\frac{(\rho_s z)^j}{j!}} \\ \qquad \text{if } c > 1 \end{cases}$$

which corresponds to (3.5).

If $c \gg 1$, it follows that $\rho_s' \simeq \rho_s$ and, from (A.8) (second line), $P\{V_i = 1\}$ can be approximated as

$$P\{V_i = 1\} \simeq e^{-\frac{\rho_s z}{c}} \tag{A.9}$$

where we have used also the fact that $[c/(c-1)]^i \simeq 1$. Substituting (A.9) into (A.1), it can be easily shown that the average number of vehicles which rebroadcast in $(0,z)$ is approximated by the following simple expression:

$$\mathbb{E}[M_1] \simeq \rho_s z\, e^{-\frac{\rho_s z}{c}} \tag{A.10}$$

which corresponds to (3.6).

If, besides the fact that $c \gg 1$, it also holds that $c \gg \rho_s z$, then from (3.6) it follows that $\mathbb{E}[M_1] \simeq \rho_s z$, i.e., the average number of vehicles which rebroadcast in $(0,z)$ is *equal* to the average number of vehicles in $(0,z)$. In other words, *on average* all vehicles in $(0,z)$ rebroadcast. This is intuitive, since for $c \gg \max\{1, \rho_s z\}$ the probability of retransmission is approximately equal to 1 for each vehicle in $(0,z)$.

Bibliography

[1] R. Bishop, “A survey of intelligent vehicle applications worldwide,” in *Proc. of IEEE Symp. on Intelligent Vehicles (*IV 2000*)*, Dearborn, MI, USA, October 2000, pp. 25 –30.

[2] L. Figueiredo, I. Jesus, J. Machado, J. Ferreira, and J. Martins de Carvalho, “Towards the development of intelligent transportation systems,” in *Proc. of IEEE Conf. on Intelligent Transportation Systems*, Oakland, CA , USA, October 2001, pp. 1206–1211.

[3] F. Qu, F.-Y. Wang, and L. Yang, “Intelligent transportation spaces: vehicles, traffic, communications, and beyond,” *IEEE Commun. Mag.*, vol. 48, no. 11, pp. 136 –142, November 2010.

[4] H. Hartenstein and K. Laberteaux, *VANET Vehicular Applications and Inter-Networking Technologies*. Wiley Press, 2010.

[5] “Advanced Safety Vehicle Program,” *Ministry of Land, Infrastructure, Transport and Tourism, Japan*, 2010, `http://www.mlit.go.jp`.

[6] “IntelliDrive: Safer, Smarter, Greener,” *Federal Highway Administration, Public Roads*, vol. 74, no. 1, pp. 18–22, 2010.

[7] “Car-to-Car Communication Consortium,” Website: `http://www.car-2-car.org/`.

[8] "Towards Europe-wide Safer, Cleaner and Efficient Mobility: The First Intelligent Car Report," *Communication from the Commission to the European Parliament, the Council, the European Economic and Social Committee and the Committee of the Regions*, pp. 1–11, July 2007.

[9] "European Telecommunications Standards Institute," Website: `http://www.etsi.org/`.

[10] T. Willke, P. Tientrakool, and N. Maxemchuk, "A survey of inter-vehicle communication protocols and their applications," *Communications Surveys Tutorials, IEEE*, vol. 11, no. 2, pp. 3 –20, June 2009.

[11] U. Lee, E. Magistretti, M. Gerla, P. Bellavista, and A. Corradi, "Dissemination and harvesting of urban data using vehicular sensing platforms," *IEEE Trans. Veh. Technol.*, vol. 58, no. 2, pp. 882 –901, February 2009.

[12] S. Kato, S. Tsugawa, K. Tokuda, T. Matsui, and H. Fujii, "Vehicle control algorithms for cooperative driving with automated vehicles and intervehicle communications," *IEEE Trans. Intelligent Transportation Systems*, vol. 3, no. 3, pp. 155 – 161, September 2002.

[13] A. Broggi, "VisLab's Vehicles Just Reached Siberia: Driverless! Now Kazakhstan and Then China until Shanghai [ITS Events]," *Intelligent Transportation Systems Magazine, IEEE*, vol. 2, no. 3, pp. 43–44, 2010.

[14] R. Chen, W.-L. Jin, and A. Regan, "Broadcasting safety information in vehicular networks: issues and approaches," *Network, IEEE*, vol. 24, no. 1, pp. 20 –25, January 2010.

[15] K. Lee, S. Lee, R. Cheung, U. Lee, and M. Gerla, "First experience with CarTorrent in a real vehicular ad hoc network testbed," in *Proc. of IEEE Intl. Conf. on Mobile Networking for Vehicular Environments (*MOVE*)*. Los Angeles, CA, USA: IEEE, May 2007, pp. 109–114.

[16] M. Amadeo, C. Campolo, and A. Molinaro, "Enhancing IEEE 802.11 p/WAVE to provide infotainment applications in VANETs," *Ad Hoc Networks, Elsevier*, 2010, in press.

[17] "Communications Access for Land Mobiles (CALM)," *ISO TC204 WG16*, Website: `http://www.calm.hu/`.

[18] "3GPP," *3rd Generation Partnership Project*, Website: http://www.3gpp.org.

[19] Insitute of Electrical and Electronics Engineers, "IEEE Std 802.16TM-2009. Part 16: Air Interface for Broadband Wireless Access Systems," 2009.

[20] "IEEE Standard for Information technology–Telecommunications and information exchange between systems–Local and metropolitan area networks–Specific requirements Part 11: Wireless LAN Medium Access Control (MAC) and Physical Layer (PHY) Specifications Amendment 6: Wireless Access in Vehicular Environments," *IEEE Std 802.11p-2010 (Amendment to IEEE Std 802.11-2007)*, pp. 1 –51, July 2010.

[21] Insitute of Electrical and Electronics Engineers, "IEEE 1609-2006. IEEE Trial-Use Standard for Wireless Access in Vehicular Environments (WAVE)," 2006.

[22] G. Korkmaz, E. Ekici, F. Özgüner, and U. Özgüner, "Urban multi-hop broadcast protocol for inter-vehicle communication systems," in *Proc. of ACM Intl. Workshop on Vehicular ad hoc networks (*VANET*)*. Philadelphia, PA, USA: ACM, October 2004, pp. 76–85.

[23] C. Toh, *Ad Hoc Wireless Networks: Protocols and Systems*. Upper Saddle River, NJ, USA: Prentice Hall, 2001.

[24] O. K. Tonguz and G. Ferrari, *Ad Hoc Wireless Networks: A Communication-Theoretic Perspective*. Chichester, UK: John Wiley & Sons, Inc., 2006.

[25] M. Gast, *802.11 Wireless Networks: The Definitive Guide, Second Edition*. O'Reilly Media, 2005.

[26] Insitute of Electrical and Electronics Engineers, "IEEE Std 802.11TM-2007. Part 11: Wireless LAN Medium Access Control (MAC) and Physical Layer (PHY) specifications," 2007.

[27] "IEEE Standard for Information technology–Part 11: Wireless LAN Medium Access Control (MAC) and Physical Layer (PHY) specifications Amendment 5: Enhancementss for Higher Throughput," *IEEE Std 802.11n-2009*, pp. 1–211, July 2005.

[28] "IEEE Standard for Information technology–Part 11: Wireless LAN Medium Access Control (MAC) and Physical Layer (PHY) specifications Amendment 8: Medium Access Control (MAC) Quality of Service Enhancements," *IEEE Std 802.11e-2005*, pp. 1–211, July 2005.

[29] H. Zimmermann, "OSI reference model–The ISO model of architecture for open systems interconnection," *IEEE Trans. Commun.*, vol. 28, no. 4, pp. 425–432, 2002.

[30] R. Uzcategui and G. Acosta-Marum, "WAVE: a tutorial," *IEEE Commun. Mag.*, vol. 47, no. 5, pp. 126–133, 2009.

[31] Insitute of Electrical and Electronics Engineers, "IEEE 1609.1-2006. IEEE Trial-Use Standard for Wireless Access in Vehicular Environments (WAVE) - Resource Manager," 2006.

[32] E. Kaplan and C. Hegarty, *Understanding GPS: principles and applications*. Artech House Publishers, 2006.

[33] Insitute of Electrical and Electronics Engineers, "IEEE 1609.2-2006. IEEE Trial-Use Standard for Wireless Access in Vehicular Environments (WAVE) - Security Services for Applications and Management Messages," 2006.

[34] ——, "IEEE 1609.3-2010. IEEE Draft Standard for Wireless Access in Vehicular Environments (WAVE) - Networking Services," 2010.

[35] " RFC 2460 Internet Protocol, Version 6 (IPv6) Specification," *The Internet Engineering Task Force (IETF)*.

[36] Insitute of Electrical and Electronics Engineers, "IEEE 1609.4-2010. IEEE Draft Standard for Wireless Access in Vehicular Environments (WAVE) - Multi-Channel Operation," 2010.

[37] D. Jiang and L. Delgrossi, "IEEE 802.11 p: Towards an international standard for wireless access in vehicular environments," in *Proc. IEEE Vehicular Tech. Conf.* (VTC) Spring, Marina Bay, Singapore, May 2008, pp. 2036–2040.

[38] "European profile standard for the physical and medium access control layer of Intelligent Transport Systems operating in the 5 GHz frequency band," *ETSI ES 202 663 V1.1.0*, pp. 1–27, January 2010.

[39] F. Martinez, C. Toh, J. Cano, C. Calafate, and P. Manzoni, "A survey and comparative study of simulators for vehicular ad hoc networks (VANETs)," *John Wiley & Sons Wireless Communications and Mobile Computing*, November 2009.

[40] J. Harri, F. Filali, and C. Bonnet, "Mobility models for vehicular ad hoc networks: a survey and taxonomy," *Communications Surveys & Tutorials, IEEE*, vol. 11, no. 4, pp. 19–41, 2009.

[41] M. Fiore and J. Härri, "The networking shape of vehicular mobility," in *Proc. on ACM Intl. Symp. on Mobile ad hoc networking and computing (MobiHoc)*. New York, NY, USA: ACM, 2008, pp. 261–272.

[42] O. Tonguz, W. Viriyasitavat, and F. Bai, "Modeling urban traffic: a cellular automata approach," *IEEE Commun. Mag.*, vol. 47, no. 5, pp. 142–150, 2009.

[43] F. Legendre, V. Borrel, M. de Amorim, and S. Fdida, "Modeling mobility with behavioral rules: the case of incident and emergency situations," *Springer Technologies for Advanced Heterogeneous Networks II*, pp. 186–205, 2006.

[44] "SUMO Project, 2010," Website: `http://sourceforge.net/projects/sumo/`.

[45] "VanetMobiSim Project," Website: `http://vanet.eurecom.fr/`.

[46] "FreeSim, 2010," Website: `http://www.freewaysimulator.com/`.

[47] F. Martinez, J. Cano, C. Calafate, and P. Manzoni, "Citymob: a mobility model pattern generator for VANETs," in *Proc. IEEE International Conf. on Commun. Workshops* (ICC). Beijingm, China: IEEE, May 2008, pp. 370–374.

[48] "Network Simulator 2 (ns-2)," Available at: `http://isi.edu/nsnam/ns/`.

[49] "OMNeT++," Available at: `http://www.omnetpp.org/`.

[50] R. Mangharam, D. Weller, D. Stancil, R. Rajkumar, and J. Parikh, "GrooveSim: a topography-accurate simulator for geographic routing in vehicular networks," in *Proc. of ACM Intl. Workshop on Vehicular ad hoc networks (*VANET*)*. Cologne, Germany: ACM, September 2005, pp. 59–68.

[51] "NCTUns 5.0," Available at: `http://nsl10.csie.nctu.edu.tw//`.

[52] "Traffic and Network Simulation Environment (TraNS)," Available at: `http://lca.epfl.ch/projects/trans/`.

[53] C. Sommer, R. German, and F. Dressler, "Bidirectionally Coupled Network and Road Traffic Simulation for Improved IVC Analysis (PDF)," *IEEE Transactions on Mobile Computing*, vol. 10, no. 1, pp. 3–15, January 2011.

[54] N. Wisitpongphan, O. Tonguz, J. Parikh, P. Mudalige, F. Bai, and V. Sadekar, "Broadcast storm mitigation techniques in vehicular ad hoc networks," *IEEE Wireless Commun. Mag.*, vol. 14, no. 6, pp. 84–94, 2007.

[55] F. Li and Y. Wang, "Routing in vehicular ad hoc networks: A survey," *IEEE Magazine on Vehicular Technology*, vol. 2, no. 2, pp. 12–22, June 2007.

[56] S. Ni, Y. Tseng, Y. Chen, and J. Sheu, "The broadcast storm problem in a mobile ad hoc network," in *Proc. ACM Intern. Conf. on Mobile Comput. and Networking* (MOBICOM), Seattle, Washington, USA, August 1999, pp. 151–162.

[57] B. Das and V. Bharghavan, "Routing in ad-hoc networks using minimum connected dominating sets," in *Proc. IEEE International Conf. on Commun.* (ICC), vol. 1, Montreal, QC, Canada, June 1997, pp. 376–380.

[58] H. Lim and C. Kim, "Flooding in wireless ad hoc networks," *Computer Communications*, vol. 24, no. 3-4, pp. 353–363, 2001.

[59] S. Guha and S. Khuller, "Approximation algorithms for connected dominating sets," *Algorithmica, Springer*, vol. 20, no. 4, pp. 374–387, 1998.

[60] L. Bononi and M. D. Felice, "A cross layered MAC and clustering scheme for efficient broadcast in VANETs," in *Proc. Int. Conference on Mobile Ad-hoc and Sensor Systems* (MASS), Montreal, QC, Canada, Oct. 2007, pp. 1–8.

[61] Z. Wang, L. Liu, M. Zhou, and N. Ansari, "A position-based clustering technique for ad hoc intervehicle communication," *IEEE Transactions on Systems, Man, and Cybernetics, Part C: Applications and Reviews*, vol. 38, no. 2, pp. 201–208, March 2008.

[62] Y. Tseng, S. Ni, and E. Shih, "Adaptive approaches to relieving broadcast storms in a wireless multihop mobile ad hoc network," *IEEE Trans. Comput.*, pp. 545–557, March 2003.

[63] M. Kihl, M. Sichitiu, and H. P. Joshi, "Design and evaluation of two geocast protocols for vehicular ad-hoc networks," *Journal of Internet Engineering, Klidarithmos Press*, vol. 2, no. 1, pp. 127–135, June 2008.

[64] M. Zorzi and R. Rao, "Geographic random forwarding (GeRaF) for ad hoc and sensor networks: energy and latency performance," *IEEE Trans. Mobile Comput.*, vol. 2, no. 4, pp. 349–365, October-December 2003.

[65] M. Torrent-Moreno, J. Mittag, P. Santi, and H. Hartenstein, "Vehicle-to-vehicle communication: Fair transmit power control for safety-critical information," *IEEE Trans. Veh. Technol.*, vol. 58, no. 7, pp. 3684–3707, September 2009.

[66] Y. Sasson, C. Cavin, and A. Schiper, "Probabilistic broadcast for flooding in wireless mobile ad hoc networks," in *Proc. IEEE Wireless Commmunications and Networking Conference* (WCNC), New Orleans, LA, USA, March 2003, pp. 1124–1130.

[67] H. Alshaer and E. Horlait, "An optimized adaptive broadcast scheme for inter-vehicle communication," in *Proc. IEEE Vehicular Tech. Conf.* (VTC), Stockholm, Sweden, May 2005, pp. 2840–2844.

[68] Z. J. Haas, J. Y. Halpern, and L. Li, "Gossip-based ad hoc routing," *IEEE/ACM Trans. Networking*, vol. 14, no. 3, pp. 479–491, June 2006.

[69] I. A. Khan, A. Javaid, and H. L. Qian, "Distance-based dynamically adjusted probabilistic forwarding for wireless mobile ad hoc networks," in *Proc. IFIP Intl. Conf. on Wireless and Optical Communications Networks* (WOCN), Surabaya, Indonesia, May 2008, pp. 1–6.

[70] J. Cartigny and D. Simplot, "Border node retransmission based probabilistic broadcast protocols in ad-hoc networks," *Telecommunication Systems Journal, Springer*, vol. 22, no. 1-4, pp. 189–204, January 2003.

[71] A. M. Hanashi, A. Siddique, I. Awan, and M. Woodward, "Performance evaluation of dynamic probabilistic broadcasting for flooding in mobile ad hoc networks," *Simulation Modelling Practice and Theory, Elsevier*, vol. 17, no. 2, pp. 364 – 375, February 2009.

[72] G. Korkmaz, E. Ekici, and F. Ozguner, "Black-burst-based multihop broadcast protocols for vehicular networks," *IEEE Trans. Veh. Technol.*, vol. 56, no. 5, pp. 3159–3167, September 2007.

[73] J. Sobrinho and A. Krishnakumar, "Quality-of-service in ad hoc carrier sense multiple access wireless networks," *IEEE J. Select. Areas Commun.*, vol. 17, no. 8, pp. 1353–1368, 2002.

[74] E. Fasolo, A. Zanella, and M. Zorzi, in *Proc. IEEE International Conf. on Commun.* (ICC), vol. 9, Istanbul, Turkey, June 2006, pp. 3960 –3965.

[75] J. Sahoo, E. Wu, P. Sahu, and M. Gerla, "Bpab: Binary partition assisted emergency broadcast protocol for vehicular ad hoc networks," in *Proc. of Intl. Conference on Computer Communications and Networks (*ICCCN*)*, August 2009, pp. 1 –6.

[76] U. Lee and M. Gerla, "A survey of urban vehicular sensing platforms," *Computer Networks, Elsevier*, vol. 54, no. 4, pp. 527–544, 2010.

[77] U. Lee, B. Zhou, M. Gerla, E. Magistretti, P. Bellavista, and A. Corradi, "Mobeyes: smart mobs for urban monitoring with a vehicular sensor network," *Wireless Communications, IEEE*, vol. 13, no. 5, pp. 52 –57, October 2006.

[78] B. Hull, V. Bychkovsky, Y. Zhang, K. Chen, M. Goraczko, A. Miu, E. Shih, H. Balakrishnan, and S. Madden, "CarTel: a distributed mobile sensor computing system," in *Int. Conf. on Embedded Networked Sensor Systems (*SenSys*)*, Boulder, Colorado, USA, November 2006, pp. 125–138.

[79] P. Mohan, V. N. Padmanabhan, and R. Ramjee, "Nericell: rich monitoring of road and traffic conditions using mobile smartphones," in *Int. Conf. on Embedded Networked Sensor Systems (*SenSys*)*, Raleigh, NC, USA, November 2008, pp. 323–336.

[80] C. R. Lin and M. Gerla, "Adaptive clustering for mobile wireless networks," *IEEE Journal on Selected Areas in Communications*, vol. 15, no. 7, pp. 1265–1275, September 1997.

[81] J. F. Chamberland and V. V. Veeravalli, "Decentralized detection in sensor networks," *IEEE Trans. Signal Processing*, vol. 51, no. 2, pp. 407–416, February 2003.

[82] G. Ferrari, M. Martalò, and R. Pagliari, "Decentralized detection in clustered sensor networks," *IEEE Trans. Aerosp. Electron. Syst.*, to appear, 2010. Available: http://www.tlc.unipr.it/martalo/privfold/preprint.pdf.

[83] M. Martalò, C. Buratti, G. Ferrari, and R. Verdone, "Decentralized detection in IEEE 802.15.4 wireless sensor networks," *Journal on Wireless Communications and Networking, EURASIP*, vol. 2010, 10 pages, 2010, doi=10.1155/2010/174063.

[84] S. Busanelli, G. Ferrari, and S. Panichpapiboon, "Cluster-based irresponsible forwarding," in *The Internet of Things, 20th Tyrrhenian International Workshop on Digital Communications, Springer*, G. M. D. Giusto, A. Iera and L. Atzori, Eds., September 2009.

[85] L. Breslau, D. Estrin, K. Fall, S. Floyd, J. Heidemann, A. Helmy, P. Huang, S. McCanne, K. Varadhan, Y. Xu, and H. Yu, "Advances in network simulation," *IEEE Computer*, vol. 33, no. 5, pp. 59 –67, May 2000.

[86] I. Purushothaman, S. Roy, and D. Denial, "IEEE 802.11 implementation issues/bugs in ns2," Tech. Rep., 2006, available at `http://ee.washington.edu/research/funlab`.

[87] F. Schmidt-Eisenlohr, J. Letamendia-Murua, M. Torrent-Moreno, and H. Hartenstein, "Bug Fixes on the IEEE 802.11 DCF module of the Network Simulator ns-2.28," Tech. Rep., 2006, available at `http://dsn.tm.uni-karlsruhe.de/`.

[88] J. Tian, J. Hahner, C. Becker, I. Stepanov, and K. Rothermel, "Graph-based mobility model for mobile ad hoc network simulation," in *Proc. IEEE Annual Simulation Symposium*. San Diego, CA, USA: IEEE, April 2002, pp. 337–344, available at `http://canu.informatik.uni-stuttgart.de/mobisim/`.

[89] A. H. M. Treiber and D. Helbing, *Traffic and Granular Flow '99*. Springer-Verlag, 2006, ch. "Microscopic Simulation of Congested Traffic", pp. 365–376, Eds.:D. Helbing, H. J. Herrmann, M. Schreckenberg, and D. E. Wolf.

[90] A. Kesting, M. Treiber, and D. Helbing, "General lane-changing model MOBIL for car-following models," *Transportation Research Record: Journal of the Transportation Research Board*, vol. 1999, no. -1, pp. 86–94, 2007.

[91] S. Krauss, P. Wagner, and C. Gawron, "Metastable states in a microscopic model of traffic flow," *Physical Review E, APS*, vol. 55, no. 5, pp. 5597–5602, 1997.

[92] M. Treiber, A. Hennecke, and D. Helbing, "Congested traffic states in empirical observations and microscopic simulations," *Phys. Rev. E*, vol. 62, no. 2, pp. 1805–1824, August 2000.

[93] M. Fiore, J. Harri, F. Filali, and C. Bonnet, "Understanding vehicular mobility in network simulation," in *Proc. Int. Conference on Mobile Ad-hoc and Sensor Systems* (MASS). Pisa, Italy: IEEE, October 2007, pp. 1–6.

[94] A. Molisch, F. Tufvesson, J. Karedal, and C. Mecklenbrauker, "Propagation aspects of vehicle-to-vehicle communications - an overview," in *Proc. on IEEE Radio and Wireless Symposium (*RWS), January 2009, pp. 179 –182.

[95] I. Ivan, P. Besnier, X. Bunlon, L. Le Danvic, and M. Crussiere, "Influence of propagation channel modeling on V2X physical layer performance," in *Proc. on IEEE European Conference onAntennas and Propagation (*EuCAP*)*. IEEE, April 2010, pp. 1–5.

[96] D. Matolak and Q. Wu, "Vehicle-to-vehicle channels: Are we done yet?" in *Proc. IEEE Global Telecommun. Conf.* (GLOBECOM), Honolulu, HA, USA, December 2009, pp. 1 –6.

[97] G. Acosta-Marum and M. Ingram, "Six time-and frequency-selective empirical channel models for vehicular wireless LANs," *Vehicular Technology Magazine, IEEE*, vol. 2, no. 4, pp. 4–11, 2008.

[98] I. Sen and D. Matolak, "Vehicle-vehicle channel models for the 5-GHz band," *IEEE Trans. Intelligent Transportation Systems*, vol. 9, no. 2, pp. 235–245, 2008.

[99] A. Paier, J. Karedal, N. Czink, H. Hofstetter, C. Dumard, T. Zemen, F. Tufvesson, A. Molisch, and C. Mecklenbrauker, "Car-to-car radio channel measurements at 5 GHz: Pathloss, power-delay profile, and delay-Doppler spectrum," in *Proc. IEEE Intl. Symposium on Wireless Communication Systems (*ISWCS*)*. IEEE, October 2007, pp. 224–228.

[100] P. Paschalidis, A. Kortke, K. Mahler, M. Peter, M. Wisotzki, and W. Keusgen, "Wideband car-to-car mimo radio channel measurements at 5.7 ghz in typical communication scenarios," in *Proc. IEEE Vehicular Tech. Conf.* (VTC) Fall, September 2009, pp. 1 –5.

[101] T. S. Rappaport, *Wireless Communications. Principles & Pratice*, 2nd Edition. Uper Saddle River, NJ, USA: Prentice-Hall, 2002.

[102] J. Parsons, *The mobile radio propagation channel*. Wiley Online Library, 1992, vol. 67.

[103] A. Goldsmith, *Wireless communications*. Cambridge Univ Pr, 2005.

[104] S. Busanelli, G. Ferrari, and V. A. Giorgio, "On the Effects of Mobility for Efficient Broadcast Data Dissemination in I2V Networks," in *Proc. SWiM Workshop IEEE Global Telecommun. Conf.* (GLOBECOM), Miami, FL, USA, December 2010.

[105] F. K. Karnadi, Z. H. Mo, and K. C. Lan, "Rapid generation of realistic mobility models for VANET," in *Proc. IEEE Wireless Commmunications and Networking Conference* (WCNC), Hong Kong, China, March 2007, pp. 2506–2511.

[106] F. Ye, R. Yim, J. Zhang, and S. Roy, "Congestion Control to Achieve Optimal Broadcast Efficiency in VANETs," in *Proc. IEEE International Conf. on Commun.* (ICC). Cape Town, South Africa: IEEE, May 2010, pp. 1–5.

[107] M. Torrent-Moreno, F. Schmidt-Eisenlohr, H. Fubler, and H. Hartenstein, "Effects of a realistic channel model on packet forwarding in vehicular ad hoc networks," in *Proc. IEEE Wireless Commmunications and Networking Conference* (WCNC), vol. 1, Las Vegas, NV, USA, April, pp. 385–391.

[108] V. Taliwal, D. Jiang, H. Mangold, C. Chen, and R. Sengupta, "Empirical determination of channel characteristics for DSRC vehicle-to-vehicle communication," in *Proc. of ACM Intl. Workshop on Vehicular ad hoc networks (*VANET*)*. Philadelphia, PA, USA: ACM, October 2004, p. 88.

[109] J. Yin, G. Holland, T. ElBatt, F. Bai, and H. Krishnan, "DSRC Channel Fading Analysis from Empirical Measurement," in *Intl. Conf. on Communications and Networking in China, 2006. (*ChinaCom*)*, Beijing, China, October 2006, pp. 1 –5.

[110] L. Cheng, B. Henty, D. Stancil, F. Bai, and P. Mudalige, "Mobile vehicle-to-vehicle narrow-band channel measurement and characterization of the 5.9 GHz dedicated short range communication (DSRC) frequency band," *IEEE J. Select. Areas Commun.*, vol. 25, no. 8, pp. 1501–1516, 2007.

[111] Q. Wu, D. Matolak, and I. Sen, "5-ghz-band vehicle-to-vehicle channels: Models for multiple values of channel bandwidth," *IEEE Trans. Veh. Technol.*, vol. 59, no. 5, pp. 2620 –2625, June 2010.

[112] D. Matolak, I. Sen, and W. Xiong, "Generation of multivariate Weibull random variates," *Communications, IET*, vol. 2, no. 4, pp. 523–527, 2008.

[113] Q. Chen, F. Schmidt-Eisenlohr, D. Jiang, M. Torrent-Moreno, L. Delgrossi, and H. Hartenstein, "Overhaul of IEEE 802.11 modeling and simulation in ns-2," in *Proc. of the ACM Symposium on Modeling, Analysis, and Simulation of Wireless and Mobile Systems* (MSWiM), Chania, Crete Island, Greece, October 2007, pp. 159–168.

[114] R. Oliveira, L. Bernardo, and P. Pinto, "The influence of broadcast traffic on IEEE 802.11 DCF networks," *Computer Communications, Elsevier*, vol. 32, no. 2, pp. 439–452, 2009.

[115] N. Wisitpongphan, F. Bai, P. Mudalige, V. Sadekar, and O. K. Tonguz, "Routing in sparse vehicular ad hoc wireless networks," *IEEE J. Select. Areas Commun.*, vol. 25, no. 8, pp. 1538–1556, October 2007.

[116] M. Fiore, J. Härri, F. Filali, and C. Bonnet, "Vehicular mobility simulation for VANETs," in *Proc. of SCS Annual Simulation Symposium* (ANSS), Norfolk, VA, USA, March 2007, pp. 301–309.

[117] S. Busanelli, S. Panichpapiboon, G. Ferrari, and R. Gruppini, "Irresponsible Forwarding in Linear Vehicular Ad-hoc Networks - Part I: Analytical Framework," *IEEE Trans. Intelligent Transportation Systems*, January 2011, submitted, available upon request.

[118] A. Papoulis and S. U. Pillai, *Probability, Random Variables and Stochastic Processes*, 4th ed. New York, NY, USA: McGraw-Hill, 2002.

[119] M. Abramowitz and I. A. Stegun, Eds., *Handbook of Mathematical Functions*. New York, NY, USA: Dover, 1972.

Acknowledgments

It is a pleasure to thank those who made this thesis possible. First and foremost I want to to express my deep and sincere gratitude to my advisor Prof. Gianluigi Ferrari. During these years Gianluigi has been a guide, and a teacher. His support was constant, and he had played a fundamental role in orientating my efforts in the right direction. Under his supervision the quality of my work has constantly improved.

I would like also to thank my colleagues at WASN Lab for the (few) sleepless nights we were working together before deadlines, and for all the fun we have had. Marco and Paolo have always been an example to follow, and I have often relied on their support and advises. I hope to could playing the same positive role for the new colleagues at WASN Lab: Guy, Giovanni, Vito, and Matteo. Furthermore, some of them have also played a significant role in the realization of this thesis. Hence, I wish express my gratitude to Marco for his contribution to Chapter 5, to Vito for his assistance in the simulative analysis, and to Roberto for his contribution to Chapter 6.

I wish to express my thanks to Prof. Sooksan Panichpapiboon from the King Mongkut's Institute of Technology Ladkraban, since part of the material presented in Chapter 3 has been obtained with his help.

I would like to thank Dr. Isabelle Icart for hosting me during my 6-month internship at Thales Communications, that has been an extremely interesting experience, also for the precious presence of Dr. Christophe Le Martret that has always believed in me, also during though moments. I also thanks Antonio, David, Erwan, Vanessa, Cecile, Benjamin, and all the guys of the lab, that have introduced by to the secret of

the French language, through a method based on “pot", appetizers, and coffee breaks.

I gratefully acknowledge the funding sources that made my Ph.D. work possible. I was funded by the CNIT Consortium, by the Spinner Consortium, and by Thales Communications during my stage at Colombes. I therefore thanks Mrs. Martine Jacquet (Thales), Savino (CNIT), and Giorgia (Spinner) for assisting me in the eternal fight against bureaucracy.

All the work during the last years was impossible to be finished without coffee and tea breaks, therefore I thanks Tommy, Donato, Michele, Nicola, Alicia, and all the colleagues of Pal. 2, for having reserved the right attention for this important task. With Muzzo, Fabio, Loso, and Giova, I have shared thousands of kilometer, words, and laughs, the best way to start and finish a workday, and I thanks them for this. I would like to express a warm thanks to Sara, Kathrin, Leopold, Henry, Erik, KGB, Sylvain, and all the numerous one-night friends that have make unforgivable my lovely staying in Paris.

The Ph.D period has been plenty of work, deadlines and hard times, during which your friends are authorized to forgive you. Fortunately, they have not. Therefore, I have a never-ending list of persons to say ”thanks“, starting from Doffele, Scioscia, Fastix, Teddy, Elisir, Lela, Izka, Roger, Mimmo, Milo, to end with the Piccolo Sistina members and with the fool volleyball-mates.

Last but not least, this thesis is dedicated to my parents (Leardo and Vanda) and my brother (Mauro), for their unconditioned support, and for having sustained and encouraged every my decision.